THE UNIVERSITY
of EDINBURGH

Measurements of redox potential during apoptosis

Anna-Maria Maciejuk

Thesis presented for the degree of

Doctor of Philosophy,

The University of Edinburgh

2017

Declaration of Authorship

I declare that this thesis is my own composition; that the work, which is described has been carried out by me, unless otherwise stated; and that it has not been submitted in any previous application for a higher degree.

This thesis describes the results of research carried out in the School of Chemistry and Queen's Medical Research Institute, University of Edinburgh, under the supervision of Dr Colin J. Campbell and Professor Christopher D. Gregory.

Anna-Maria Maciejuk

University of Edinburgh

February 2017

Signed: _____

Abstract

Consensus opinion suggests that apoptosis occurs when the intracellular redox potential reaches its oxidative range, i.e. when the balance between oxidants and reductants is disturbed. An understanding of the links between redox potential and the induction of apoptosis in cells could improve our understanding of the process and help to predict therapeutic responses.

This study investigates the changes in redox potential at distinct stages of apoptosis induced in the human cervical cancer cell line, HeLa. Stages of the apoptotic process were defined by loss of mitochondrial membrane polarisation ($\Delta\Psi m$), membrane phosphatidyl serine exposure, caspase-3 activation, and nuclear fragmentation. To measure real-time redox potential change in apoptotic cells two independent methods were used: (1) expression of redox-responsive green fluorescent protein (roGFP2) measured by flow cytometry and (2) redox-responsive nanosensors detected by surface enhanced Raman spectroscopy (SERS).

roGFP2 measurements showed that HeLa cells demonstrate a shift towards an oxidative redox state during the later stages of apoptosis and this was preceded by loss of $\Delta\Psi m$. The relationship between these two events was investigated by transient inhibition of mitochondrial permeability transition pore opening using the inhibitor bongkrekic acid (BKA) pre-treatment.

At the cell population level, transient exclusion of the mitochondrial contribution delayed two key events of apoptosis in the first two hours measured by nuclear fragmentation and loss of $\Delta\Psi m$. However, BKA treatment did not affect redox potential, reported by roGFP2, when compared with controls. Therefore, this suggests that mitochondria do not contribute towards the overall redox potential change in apoptosis.

To gain insight into the significance of redox change at the earliest stages of apoptosis, single cell studies were performed. SERS, employing simultaneous redox potential and intracellular pH measurements using two synthetic nanosensors AQ-NS and MBA-NS,

showed that BKA pre-treatment resulted in increased alkalinity and the cells were consequently protected from induction of apoptosis in the first thirty minutes of the kinase inhibitor staurosporine treatment.

Measurements with SERS nanosensors allowed for adjustment for pH, which provides a clearer insight into redox potential dynamics, with consideration of the environment, and accurate quantitative assessment of redox at early stages of apoptosis.

Together these data suggest that while roGFP2 is a valid method to use at a population level, SERS is a more sensitive method for measuring the redox potential of the cell at the early stages of apoptosis.

Lay summary

Cancer is characterised by established hallmarks including abnormal cell growth, altered metabolism, and evasion of apoptosis. Apoptosis is a form of programmed cell death, meaning that it is an active process, which is characterised by a sequence of subcellular events eventually leading to cell death. Many cancer treatments aim to induce cancer cell apoptosis in order to halt or reverse tumour growth. However, our understanding of some of the apoptosis-associated events is incomplete. One of these events is a change in the so-called redox potential, which defines the chemical state of molecules within the cell. Understanding the dynamics of the redox-potential throughout the process of cell death could help define new treatment strategies.

The aim of this study was to characterise the intracellular redox potential change throughout apoptosis and relate it to other, well-defined events happening during this process. However, current redox potential detection methods are limited in their specificity and sensitivity, measuring only one out of many redox couples. With recent advancements in nanotechnology, our group developed a range of redox sensitive nanosensors. These sensors are able to pick up changes in the redox potential of all redox couples present within the cells, giving a better measurement of the overall redox potential than previous technologies.

Using these nanosensors, which proved non-toxic to the cell type used in this study, the time course of redox potential and pH changes following the induction of apoptosis could be assessed. It could also be established that the modulation of another subcellular event associated with cell death beneficially altered the overall redox potential and coincided with a delay in cell death. Whether changes in the redox potential themselves are able to drive or inhibit the progression of apoptosis, remains to be determined. However, the nanosensors tested in this thesis offer the ideal tool for further studies in this direction.

Acknowledgements

aka the place in the thesis, where things become sentimental after the time takes its deep breath.

I would like to thank my supervisors, Dr Colin J. Campbell and Professor Christopher D. Gregory for the opportunity to work on such exciting project and for their patience and support. I was very lucky to have such great mentors throughout this scientific journey.

I am grateful to members of the Campbell and Gregory labs for their expertise. I am extremely thankful to Dr Kate Fisher and Dr Lauren Jamieson from the Campbell group for their help with MatLab and setting up initial SERS experiments; Dr John Pound and Dr Margaret Paterson for training me in flow cytometry; Dr Catriona Ford, the Queen of Western Blotting, for teaching me this laborious craft. However, I think I was a good apprentice (see my blots in Chapter 4). I would like to thank Menglu (Lily) Wang for providing purified roGFP2 used in this study.

Finally, I would like to thank my wonderful Mom and Dad, and Brother for their patience driven to extremes at times, their invaluable understanding and support.

I reserve extra-special thanks to Dr Dmitrijs for his generosity with time and his kindness, and all those interesting, motivating, and thought-provoking facts about a whole array of things! I'd like to thank Dr Sophie for her contagious enthusiasm, Dr Jorine who is now using the apop-corn-tosis video (if interested you can email me to get access to it!) that I have made for her to use in lectures to inspire the next generation of open-minded scientists; Dr Iris, who is an all rounded gem and best flatmate; Dr Eileen for the moral support during the splendid winter days of board games, hot chocolate and keeping me in check when things got a bit tougher than usual. I am also grateful for the Spectroscopy in a Suitcase scheme, that I have been enjoying running and teaching teachers how to teach spectroscopy to their pupils. Also, all the Cats in the block (Catriona, Catherine, Katherine) for teaching me independence and giving me a comprehensive guide to PyMOL and MatLab.

These were the days of utter joy and pain pleated together like long hair. It made me an absolute all-rounded person and open-minded researcher with expertise in apoptosis and redox potential. The days spent on discussing experiments, strengths and weaknesses of research, inspiring group meetings and meetings after hours with *Hum over Deadpan Plum* also known as *Whine over wine* club, made this experience worthwhile. Thank you everyone whom I have not mentioned by name, but I have kept in my memories, that will sadly fade with time, but since it is written here, the paper will still keep a record.

Contents

List of Figures

List of Equations

List of Tables

Abbreviations

%	Per cent
µg	Microgram
µJ	Micro Joule
µl	Microlitre
·OH	Hydroxyl radical
3D	Three dimensional
AIF	Apoptosis Inducing Factor
ALLN	Calpain inhibitor 1, proteasome inhibitor 1
AMP100	100 µg/ml ampicillin
Apaf-1	Apoptotic peptidase activating factor -1
APO1, CD95	Cluster of differentiation 95
AQ	N-[2-(disulfanyl)ethyl]-9,10-dioxo-9,10-dihydroanthracene-2-c carboxamide (bis-(2-Anthraquinone carboxamide)
ATG 4	Autophagy-related gene 4
ATG 8	Autophagy-related gene 8
ATP	Adenoside triphosphate
AxV	Annexin V (five)
BAD	Bcl-2-associated death promoter
BAK	Bcl-2 homologous antagonist/killer
BAX	Bcl-2-like protein 4
Bcl-2	B-cell lymphoma protein-2
Bcl-xL	B-cell lymphoma-extra large
BH3	Bcl-2 homology domain 3
BKA	Bongkrek acid
BL2	Burkitt’ s lymphoma 2 cell line
BNIP3	BNIP3 BCL2 interacting protein 3
BRCA1	Breast Cancer Gene 1
BSA	Bovine serum albumin
C, Cys	Cysteine

Ca^{2+}	Calcium ions
$CaCl_2$	Calcium chloride
CARD	Caspase Recruitment Domain
CDK1	Cyclin dependent kinase 1
cm	Centimetre
CO_2	Carbon dioxide
CRADD	Death domain-containing protein
Cys	Cysteine
’API	4',6-Diamidino-2-Phenylindole, Dihydrochloride
Ac-DEVD-pNA	Ac-Asp-Glu-Val-Asp-pNA
DFT	Density Functional Theory
dH_2O	Distilled water
DMSO	Dimethyl sulfoxide
DISC	Death-induXXIignallingnaling complex
DNA	Deoxyribonucleic acid
DTT	DL-dithiothreitol, trans-4,5-dihydroxy-1,2-dithiane
E.coli	*Escherichia coli*
E2F	E2 factor
EDTA	Ethylenediaminetetraacetic acid
eGFP	Enhanced Green Fluorescence Protein
E_i	Half wave potential
EMEM	Earl’s Modified Eagle Medium
E^{θ}	Standard electrode potential
F	Faraday constant
FACS	Fluorescence Assisted Cell Sorting
FADD	Fas-associated death domain
Fas	Type-II transmembrane protein
FBS	Foetal bovine serum
FITC	Fluorescein isothiocyanate
fM	Femtomole
g	Gram

G0/G1	Gap0/Gap1 resting phase of the cell cycle
G2-M	Gap 2/Meiosis phase of the cell cycle
GFP	Green Fluorescent Protein
Gly	Glycine
GPX	Glutathione peroxidase
Grx-1	Glutaredoxin -1 Glutathione reductase –1
GSH	Glutathione
GSSG	Glutathione disulfide
H_2O_2	Hydrogen peroxide
HEPES	N-2-Hydroxyethylpiperazine-N'-2-Ethanesulfonic Acid
HIF1	Hypoxia inducing factor 1
HPLC	High Performance Liquid Chromatography
HRP	Horse Radish Peroxidase
IL-7	Interleukin - 7
IR	Infrared spectrometry
JC-1	1H-Benzimidazolium, 5,6-dichloro-2-[3-(5,6-dichloro-1,3-diethyl-1,3-dihydro-2H-benzimidazol-2-ylidene)-1-propenyl]-1,3-diethyl-, iodide
JK	Kilo Joule
K	Kelvin
K, Lys	Lysine
kDa	Kilo dalton
LA	DL-6,8-thioctic acid/DL-α-lipoic acid
LB broth	Lysogeny broth
M	Molar
MBA	4-mercaptobenzoic acid
MC	Mitotic catastrophe
MES	2-(N-morpholino)ethanesulfonic acid
mg	Milligram
mJ/cm^2	Millijoule per centimetre squared

ml	Millilitre
mM	Millimolar
mm^2	Millimetre squared
MnSOD	Manganese superoxide dismutase
MOMP	Mitochondrial outer membrane permeabilisation
MPTP	Mitochondrial permeability transition pore
mV	Millivolts
MWCO	Molecular weight cut-off
n	Number of electrons involved in the reaction
Na^+	Sodium ions
NaCl	Sodium chloride
$NADH/NAD^+$	Nicotinamide adenine dinucleotide
$NADP^+/NADPH$	Nicotinamide adenine dinucleotide phosphate
NEM	N-Ethylmaleimide
NFκB	Nuclear factor κB
NHE	Normal hydrogen electrode
NHS	N-hydroxysuccinimide
NIR	Near infrared
nm	Nanometre
nM	Nanomolar
NOX	NADPH oxidases
NOXA	Phorbol-12-myristate-13-acetate-induced protein 1
NQ	1,8-diaza-4,5-dithian-1,8-di(2-chloro-[1,4]-naphthoquinone-3-yl)octane
Nrf2	Nuclear factor (erythroid-derived 2)-like 2
NS	Gold nanoshells
O	Oxidised
$O_2^{\cdot-}$	Superoxide anion
^oC	Celsius degree
OD_{600}	Optical density at 600 nm
p53	Protein 53

PARP	Poly (ADP-ribose) polymerase
PBS	Phosphate buffered saline
PerCP Cy 5.5	Peridinin-chlorophyll-protein Complex: CY5.5 Conjugate
pH	Potential of hydrogen
pH_e	Extracellular potential of hydrogen
pH_i	Intracellular potential of hydrogen
PI	Propidium iodide
pO_2	Partial pressure of oxygen
Pro	Proline
Prx	Peroxiredoxins
PS	Phosphatidyl serine
PtdIns3K	Class III phosphatidylinositol 3-kinase
PUMA	p53 upregulated modulator of apoptosis
PVDF	Polyvinylidene difluoride
Q	ratio of products to substrates of the reaction
Q, Gln	Glutamine
R	Universal gas constant
R, Arg	Arginine
R, red	Reduced
RIP1	Receptor interacting protein 1
RNA	Ribonucleic acid
RNase A	Ribonuclease A
RNS	Reactive nitrogen species
roGFP1	Reduction-oxidation green fluorescent protein 1
roGFP2	Reduction-oxidation green fluorescent protein 2
ROS	Reactive oxygen species
RPM	Rotor per minute
s	Second
S, Ser	Serine
S phase	Synthesis phase of the cell cycle
SD	Standard deviation

SDS-PAGE	Sodium Dodecyl Sulphate-polyacrylamide gel electrophoresis
SEM	Standard error of the mean
SERS	Surface enhanced Raman spectroscopy
SQSTM1	Protein p62/sequestosome 1
STS	Staurosporine
T	Temperature
T, Thr	Theorine
tBid	Truncated p15 BH3-interacting domain death agonist
TEM	Transmission electron microscopy
TMRE	Tetramethylrhodamine ethyl ester, perchlorate
TMRM	Tetramethylrhodamine, methyl ester, perchlorate
TNFR	Tumour necrosis factor receptor
TNFR1	Necrosis factor receptor 1
TNF-α	Tumour necrosis factor alpha
TRAIL	TNF-related apoptosis-inducing ligand
Tris Base	2-Amino-2-(hydroxymethyl)-1,3-propanediol
Tris HCl	Tris hydrochloride
$Trx(SH)_2$	Reduced thioredoxin
TrxSS	Oxidised thioredoxin
UV-B	Ultraviolet B radiation
V	Volt
Wt GFP	Wild type Green Fluorescence Protein
CuZnSOD	Copper-zinc superoxide dismutase
z-VAD.fmk	N-benzyloxycarbonyl-Val-Ala-Asp-fluoromethylketone Pan-Caspase Inhibitor
ΔG°	Gibbs change in free energy
Δ	Delta
Ψ_m	Mitochondrial electrochemical gradient

Chapter 1

Introduction

1.1 Role of redox potential in cellular homeostasis

Cellular homeostasis is maintained by a range of processes that rely on the energy that comes from electron transfer between oxidizable organic molecules to oxygen. Despite the fact that oxygen is essential for living, it is highly reactive and its interactions with biological molecules can give rise to products that, if in excess, have a deleterious effect on the body. A delicate balance of forces between anti-oxidants and oxidants is essential for maintaining the health of the cell.

A range of processes rely on the energy that comes from the electron transfer between redox couples. This movement of electrons is predetermined by the specific combination of donors and acceptors of a reaction. The redox potential of the biological environment is therefore defined as a measure of the oxidative and reductive ability of the environment and is measured in millivolts (mV).

Redox regulation of biological systems is of interest since hypoxia or oxidative damage plays an important role in normal physiology as well as a role in diseases such as cancer [1], cystic fibrosis [2] atherosclerosis [3], or ischaemic and reperfusion damage [4].

1.2 Intracellular redox state and cellular processes

Oxidative damage can be caused by reactive oxygen species (ROS) (e.g. superoxide anion ($O_2^{\cdot-}$), hydrogen peroxide (H_2O_2) and hydroxyl radical ($\cdot OH$) produced in the extracellular environment or internally as byproducts of metabolic pathways (Figures 1.1 and 1.2). Not all ROS act in the same way, and their damaging or messaging properties may solely depend on the quantity within the intracellular environment and therefore they may have a dual role in the fate of the cell.

In small quantities these molecules serve as messengers that can reversibly modify proteins and therefore regulate their activity. However, if in excess their toxicity lies in their powerful oxidising properties [5, 6] (Figure 1.1). One of the examples of oxidative stress is lipid peroxidation of fatty acids present in cellular membranes. Reaction between unsaturated fatty acid and free radical occurs by a radical capturing a hydrogen moienty from an unsaturated carbon to form water. An unpaired electron is prone to capture an oxygen resulting in peroxy radical formation. It is important therefore to maintain an equitable balance between oxidants and antioxidants (Figure 1.2).

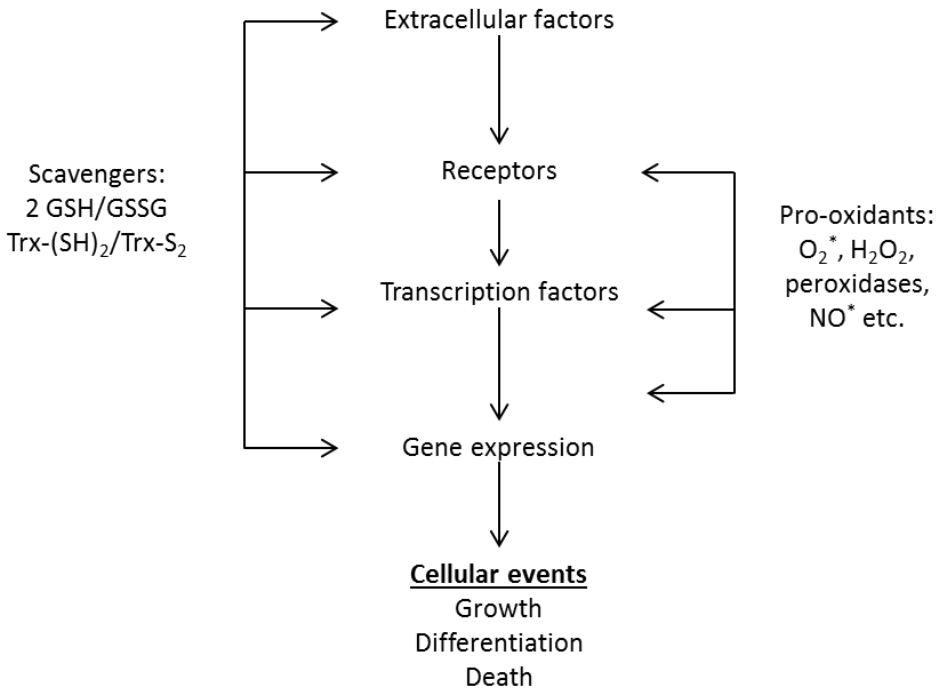

Figure 1.1 Redox regulation of cellular systems. Scavengers and pro-oxidants control of protein function directly by thiol regulation of key proteins regulating cellular responses [7]. Scavenger redox couples: glutathione and glutathione disulphide (GSH/GSSG); reduced and oxidised thioredoxin protein (Trx-$(SH)_2$./Trx-S_2.

The redox system comprises of redox couples that are the driving force for the maintenance of the redox status within the cell. These include regulation of GSH/GSSG, thioredoxins, NAD(P)H/$NAD(P)^+$ and ROS. Quantitatively, the redox environment can be described as follows [8]:

$$\text{redox environment} = \sum_{i=1}^{n\,(\text{couple})} E_i \times [\text{reduced species}]_i$$

where E_i is the half wave potential for a redox couple and $[\text{reduced species}]_i$ is the concentration of the reduced species in the environment. The flow of electrons between species is related to the Gibbs change in free energy ($\Delta G°$) by

$$\Delta G° = -nFE$$

Compounds involved can donate electrons, so called reductants, and oxidants can easily take up electrons thus oxidising other compounds. It has been problematic to quantify the values of intracellular oxidised and reduced species in biological systems as redox couples are never in equilibrium as this would indicate that the system is non-viable. For example, the ratio of the concentration of reduced NADPH to oxidised $NADP^+$ is 100:1 while for NADH:NAD^+, with similar redox potential, the ratio is 30:70 [8].

The oxidised and reduced forms of the same molecule form redox couples (Table 1.1). Redox reactions are often a consecutive chain of interaction of redox active moieties. A list of biological redox potentials is shown in Table 1.1.

Redox couple	**Standard redox potential**
$NADH/NAD^+$	-320 mV
$NADPH/NADP^+$	-324 mV
$Trx(SH)_2/TrxSS$	-292 mV
GSH/GSSG	-240 mV

Table 1.1 Standard redox potentials of common redox pairs at 310 K [8].

1.2.1 Nernst Equation

The redox potential of the cell can be quantified by using the Nernst equation (Equation 1). This is widely used in electrochemistry to define the potential of the half-cell under non-standard conditions,

$$E = E^{\theta} - \frac{RT}{nF}\ln Q$$

Equation 1: Nernst equation

where E is a potential measured under standard conditions (298 K (25 ^{o}C), 1 M concentration of substrates and pH 0) in (V); E^{θ} - is the standard half wave potential for [9, 10] a particular redox couple (V); R - is the universal gas constant (R=8.314472(15) JK^{-1} mol^{-1}); T - is the temperature (K); n – is the number of electrons involved in the reaction; F – is the Faraday constant ($9.65(24)x10^{4}$ C mol^{-1}); Q is the ratio of products to substrates of the reaction.

Redox couples are linked to each other and therefore the redox state of the environment is a reflection of the status of these couples and this defines an overall redox potential. For example, the ratio of the oxidised to reduced form of glutathione allows definition of the environment as reducing or oxidising. The standard redox potential at pH 7 for glutathione is estimated to be -240 mV [8][8] at 298.15 K (25 ^{o}C) and the change in redox potential would be as follows:

$$GSSG + 2H^{+} + 2e^{-} \rightleftharpoons 2\,GSH$$

$$\Delta E = -240 - \frac{59.1}{2}\log\left(\frac{[GSH]^{2}}{[GSSG][H^{+}]^{2}}\right)\ mV$$

To apply the Nernst equation in biological systems, one has to adjust the temperature value, normally to 310 K (37 ^{o}C) and the pH to 7.2, so-called physiological conditions. However, pH may vary between different subcellular compartments for example the mitochondria or cytoplasm, and thus it is important to measure the pH and redox potential simultaneously throughout biological processes and different compartments. When applied to biological systems, measuring electrical activity by using the ratio of oxidised to reduced species under physiological conditions, of the local environment assumes a pH of 7.2 [8].

1.2.2 Antioxidant system

Cells have a range of molecules that act as scavengers for harmful radicals and these are in the form of antioxidant enzymes (e.g. superoxide dismutase, catalases, peroxidases) [6] or non-enzymatic antioxidants: glutathione, or ubiquitous proteins such as thioredoxins. The main role of these molecules is to convert superoxide to hydrogen peroxide and ultimately neutralise it to water (Figure 1.2).

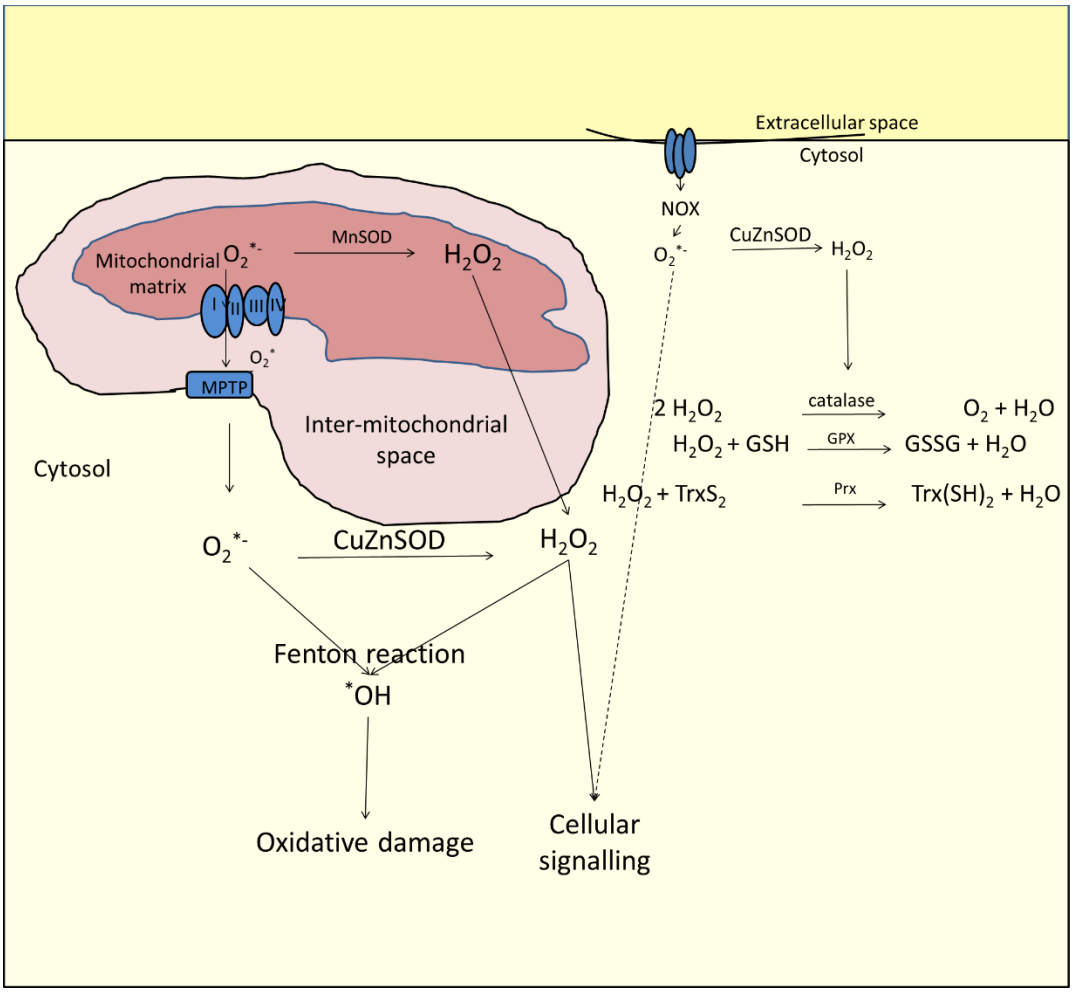

Figure 1.2 Mechanisms of ROS generation and detoxification. Modified from [6]. Two compartments are shown here: Cytosol and mitochondria. Generated in the inner membrane of the mitochondria as a by-product, superoxide, is released into the mitochondrial matrix or cytosol via the mitochondrial permeability transition pore (MPTP). Alternatively, superoxide is also generated through NADPH oxidases (NOX) in response to growth factor receptors. Superoxide dismutase enzymes (SOD) reduce superoxide to hydrogen peroxide. Both hydrogen peroxide and superoxide radical contribute to cellular signalling. However, if in excess it is balanced out by the antioxidant system in the cytosol (including catalase, glutathione peroxidase, peroxiredoxins) which reduce it further to water.

The superoxide radical is one of the electron transport chain byproducts at the inner mitochondrial membrane, which is then released into the mitochondrial matrix or cytosol. It is usually reduced to hydrogen peroxide (H_2O_2) by superoxide dismutases. It can also be generated through NADPH oxidases (NOX) in the cytosol. It is reduced to H_2O_2 by cytosolic systems serving as antioxidants (peroxiredoxins (Prx); glutathione peroxidase (GPX), and catalase). In low concentrations it contributes to intracellular signalling [11].

1.2.3 Glutathione/glutathione disulfide

Glutathione (gamma-glutamyl-cysteinyl-glycine) is the most abundant non-protein thiol redox buffer in the cell [12] . Glutathione is a tripeptide, synthesised from glutamate and cysteine by gamma-glutamylcysteine synthetase. It results in the formation of gamma-glutamylcysteine and glycine is added by GSH synthetase.

Depletion of free cysteines or gamma glutamyl cysteine sensitises cells to cell death [4, 13]. Studies on several cancer types in leukaemia [14], lymphoma [15]and hepatic cancers [16] have reported that these cells have higher intracellular GSH content than healthy cells.

It can be found in two forms: (1) reduced (GSH), a monomer with the free thiol group, and (2) oxidised (GSSG) dimer formed via a disulfide bond (Figure 1.3), however its innate form is reduced and acts as an electron donor. Glutathione therefore acts as a guard to maintain the reduced intracellular environment. Depletion of the intracellular GSH pool has been shown to induce cell death pathways[17].

Glutathione can become oxidised, forming intermolecular disulfide bonds, thus protecting the cell from oxidative and nitrosative stress. Its concentration ranges from 1 to 11 mM [18]. The ratio of the oxidised to reduced form of glutathione allows definition of the environment as reducing or oxidising.

Glutathione is a reserve form of cysteine for the cell [19], which plays a crucial role in regulatory aspects. It is a major intracellular reducing agent and free radical scavenger. It also participates in amino acid transport [2, 18-21].

A.

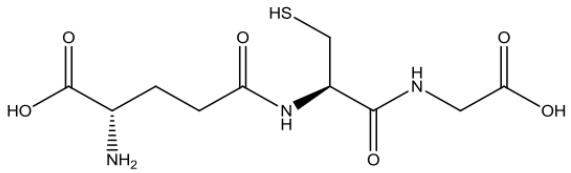

B.

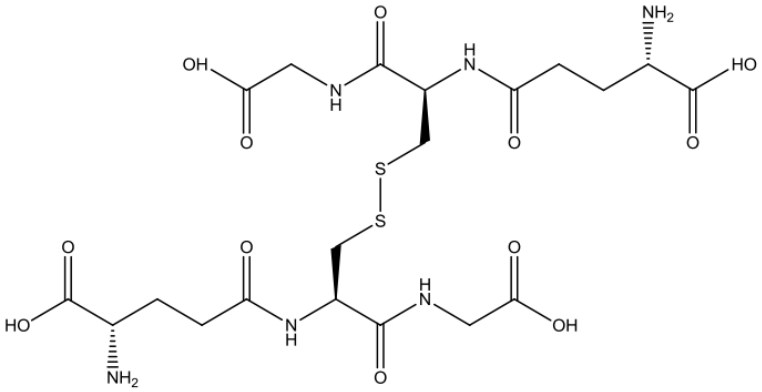

Figure 1.3 Glutathione (A) and glutathione disulfide (B).

In addition to its thiol-redox control, glutathione contributes to iron-sulphur cluster (ISC) maturation. Kumar et al. challenged the field by reporting that during redox stress high glutathione levels is linked to its involvement in iron metabolism, and that the thiol-redox maintenance is dependent on iron metabolism [22].

Glutathione is soluble and as a redox-wise regulatory buffer, its redox state is compartmentalised between cell structures such as the cytoplasm, mitochondria, endoplasmic reticulum and nucleus[23]. Glutathione is actively transferred by groups of enzymes called glutathione S-transferases (GST). The companion redox systems to GSH/GSSG are thioredoxins [12, 24].

1.2.3.1 Thioredoxins

Thioredoxins are small proteins that have cysteine residues in a sequence, Cys-Gly-Pro-Cys at a conserved active site at the N-terminus of an α helix near the central portion of a β sheet [25][23]. Upon oxidation these cysteines form intramolecular disulfide bonds. Thioredoxin reductase enzymes transform oxidised thioredoxin back to its reduced form using NADPH as an electron donor (Figure 1.4) [8].

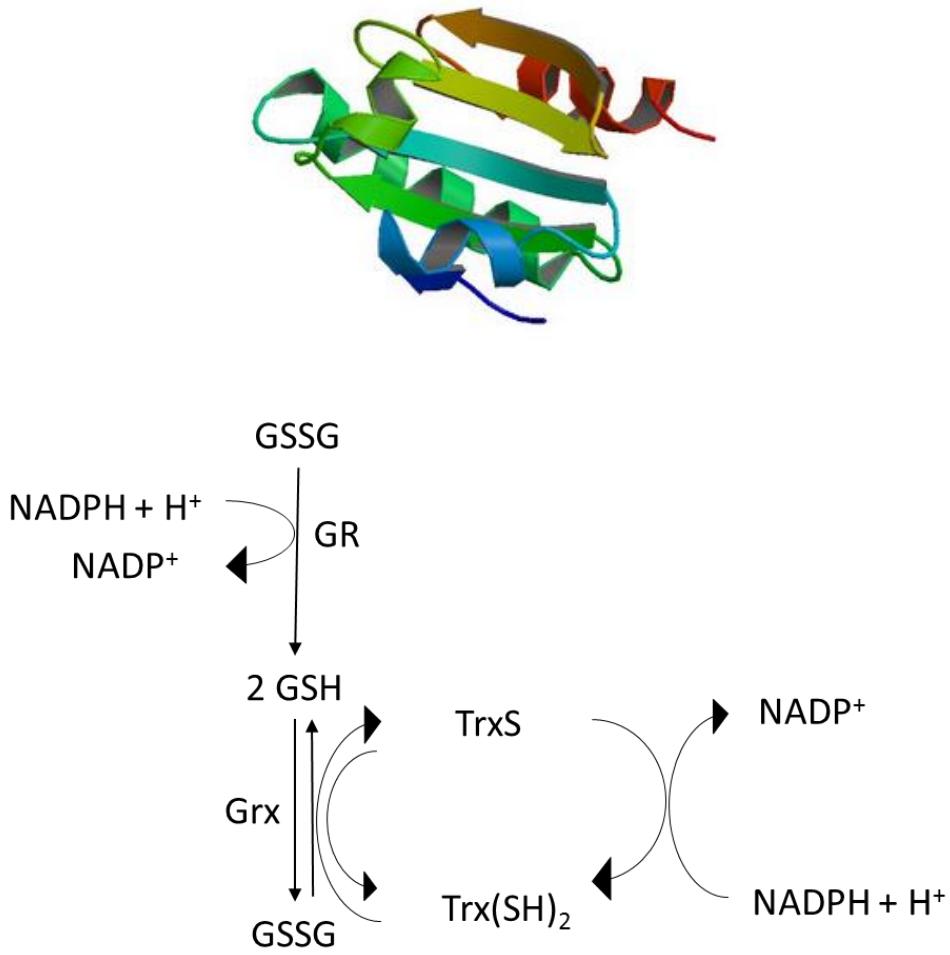

Figure 1.4: Crystal Structure of human Thioredoxin-2 . PDB ID 1THX. B. NADPH-dependent renewal of GSH by glutathione reduxtase GR, Grx) and by Thioredoxin (reduxed form $TrxSH_2$ and oxidised TrxS) and Thioredoxin reductase (Trx).

1.2.3.2 Nicotinamide adenine dinucleotide and nicotinamide adenine dinucleotide phosphate

The glutathione buffer system is tightly connected to thioredoxin proteins by a common substrate nicotinamide adenine dinucleotide (NAD^+/NADH) and nicotinamide adenine dinucleotide phosphate ($NADP^+$/NADPH). This provides a reductive driving force, which enables it to act effectively as a scavenger of free radicals, ROS, and reactive nitrogen species (RNS). NADPH is a derivative of NADH and is necessary in the phosphogluconate pathway (secondary route for glucose oxidation). NADPH functions as an electron donor in reductive reactions,

while NAD^+ plays a major role in oxidative reactions and is an electron acceptor. These two redox couples are not in equilibrium with each other to allow functioning of these couples **[26]**.

1.3 Redox compartmentalisation and regulation of cellular processes within the cell

Steady-state redox potentials differ between cell compartments, reflecting local functions. For example, mitochondria are structures that maintain one of the most reducing environments in the cell [26]. Mitochondria are the primary site of ROS generation in the cell [27] (Figure 1.5). They produce free electrons via the citric acid cycle which reduces NAD^+ to NADH and this serves as an electron donor in the mitochondrial electron transport chain to release ATP into the cytoplasm.

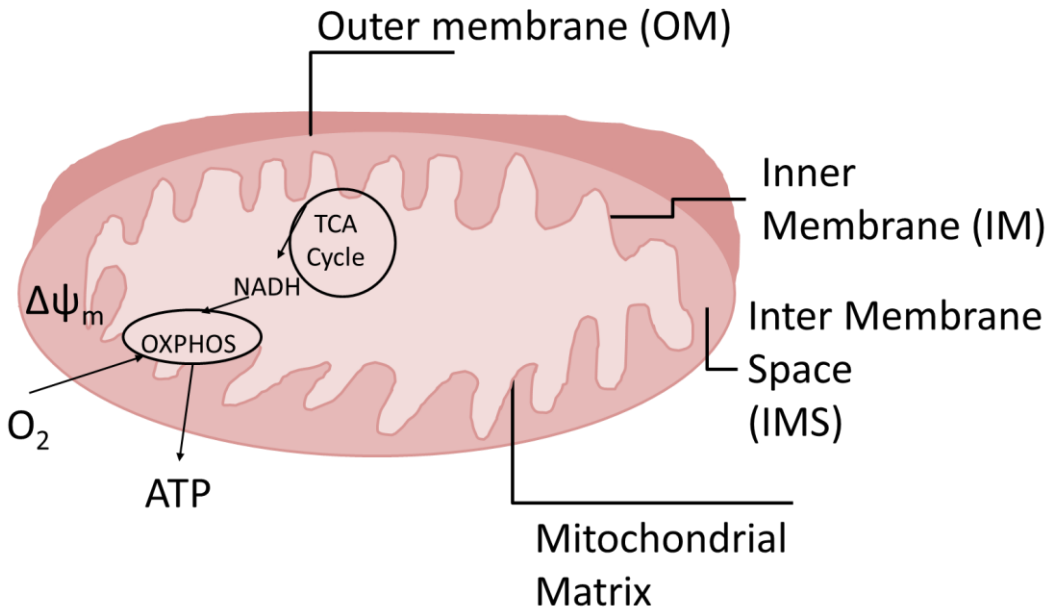

Figure 1.5 A representation of mitochondria and processes involved in the energy production (enzymes of the tricarboxylic acid (TCA) cycle and oxidative phosphorylation (OXPHOS) and its byproducts ROS.

The cytosol is both structurally and functionally important as typically most redox couples are found here, serving as buffering systems for the organelles. Cytoplasmic redox potential determined from GSH/GSSG couples varies between -260 mV to -170 mV, depending on the activity of the cell [28]. Redox potentials for common couples among different organelles are given in Table 1.2. Studies attempted to

distinguish potentials of those couples, however, the values are mostly from studies in which cell lysates were used for measuring the concentration of particular couples, therefore this may not reflect a true redox potential status of the intracellular environment of the cell [26].

On the opposite scale of redox potentials, due to the function, the endoplasmic reticulum maintains a fairly oxidizing environment to provide milieu favouring disulfide formation to ensure correct folding of proteins [29].

	Mitochondrion	**Cytoplasm**	**Nucleus**	**Endoplasmic Reticulum**
GSH/GSSG	-300	-260 to -170		-150
Trx1(SH)2/SS		-280	-300	
NADPH/NADP+	-405	-393		
NADH/NAD+		-250		
CySH/CySS	-360	-160		

Table 1.2: Distributions of redox couples and their steady state potentials (mV) in different compartments of the cell. Adapted from [26]. Adapted from Kemp *et al*. Steady-state redox potentials are said to vary between cell compartments. From various studies on GSH/GSSG in the cytoplasm, it has been concluded that reductive potential range promotes proliferation and are more reducing to ones of non-proliferating cells. Due to a loss of GSH cell's environment becomes more oxidative. It has been also shown that cytoplasmic Trx-1 is more reduced than GSH; however it becomes oxidised at the terminal stages of apoptosis.

The current consensus is that an individual cell has five choices: to divide, differentiate, undergo senescence, commit suicide or remain unchanged [30]. Each one of these choices is crucial for the maintenance of tissue homeostasis. Reactive oxygen species are capable of damaging all groups of biological macromolecules [31]. However, in recent years it has become apparent that the redox status of certain molecules contributes towards signalling of various cellular responses from proliferation, through differentiation, to cell death [32].

It has been shown that when cells are in a reductive environment, such as a hypoxic stem cell niche, the cells are mostly in a proliferative state (in active cell cycle); cells in a normoxic environment tend to initiate pathways which promote differentiation.

In line with this, a more oxidative environment promotes cell death (Figure 1.6) [8, 32]. However, the levels of partial oxygen pressure (pO2) may differ between tissues, hence influencing different redox potential and promoting different cell behaviour.

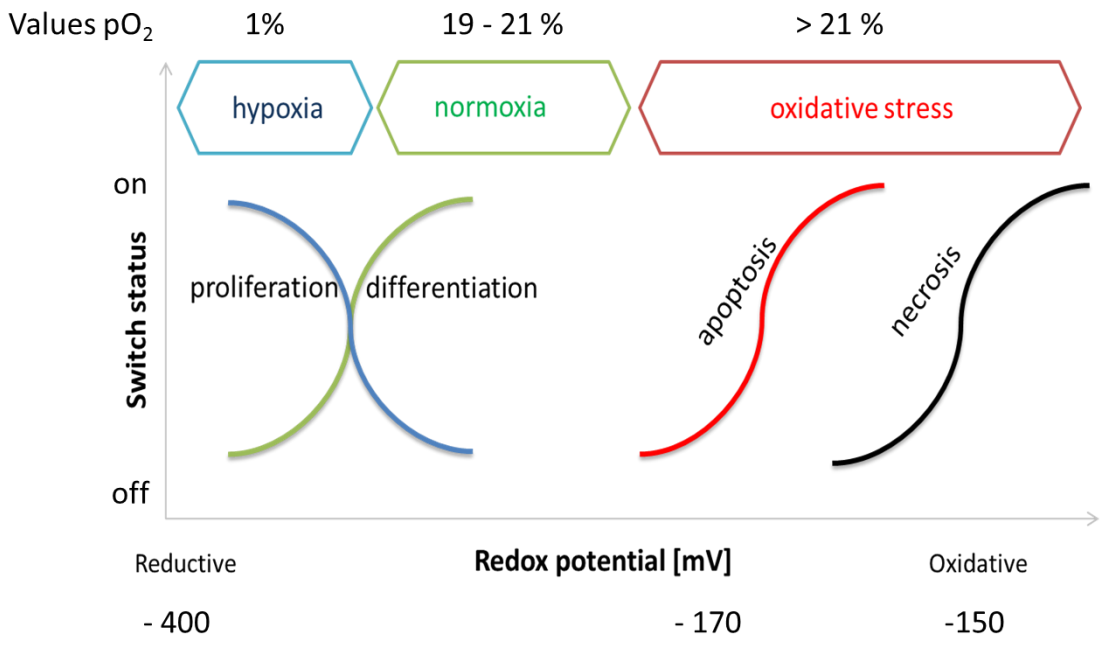

Figure 1.6 Redox environment and switching status of activity. A visual representation of interplay between pO_2, redox potential and cellular fate. More reductive environment in hypoxic regions of the tissue promotes proliferation, progressing though to normoxia promoting differentiation of cells, though to controlled oxidative range of redox potentials initiating single cell demise or multicellular uncontrolled response – necrosis. Modified from [8].

Changes of the reduction potential of the intracellular environment is assumed to correlate with the biological status of the cell and the pO_2 of the tissues [8, 33]. Reductive potentials in hypoxic regions promote proliferation, normoxic regions – differentiation, while more oxidative range promotes apoptosis. This hypotesis can be used to help understanding the redox biochemistry that results from oxidative stress (Figure 1.7). A need for quantitatively measure biology is hypothesised to provide an understanding of the cellular mechanisms associated with mechanisms directing cell signalling that are quintessential to cellular fate.

Although, consistent with the above evidence, the redox potential has been reported to play a role in apoptotic events, there are differences in opinion regarding the relationships between the molecular events which determine the redox potential and those which result in apoptosis [34].

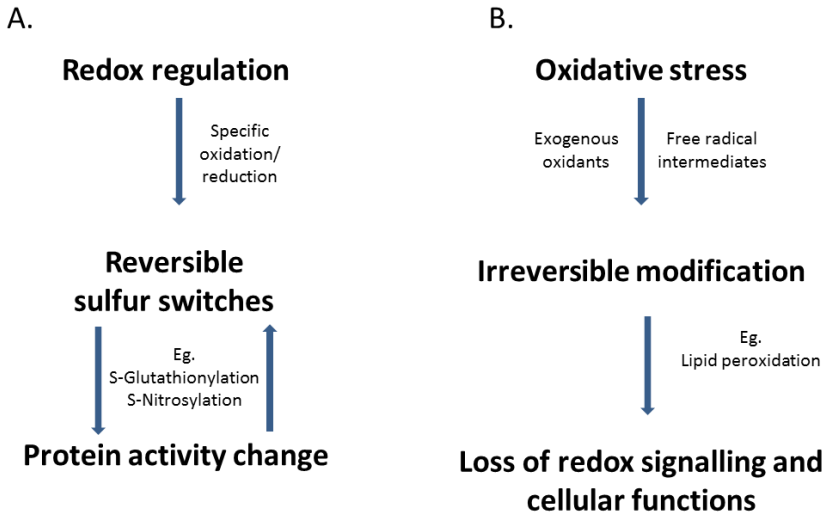

Figure 1.7 Redox regulation versus oxidative stress. A. Redox regulation of proteins is reversible and only appears at specific sites of regulatory proteins changing their activity in a reversible manner. As example, such specific change in stabilisation may happen through S-nitrosylation of HIF-1a subunit, which causes the stabilisation of the subunit and further interaction with HIF-1b subunit [35]. Post-translational S-glutathionylation occurs through the reversible addition of glutathione to cysteines in target proteins, where the modification alters molecular mass, charge, structure, and function. B. Oxidative stress, in contrast, is reported to cause irreversible, uncontrolled changes in macromolecules leading to permanent loss of cellular function and eventually resulting in cell death. Modified from [34].

ROS and GSH/GSSG couple can regulate protein activity by interacting with protein-thiols [34]. Therefore the redox potential of the environment, through thiol/disulfide switching, is driving the redox status of different proteins within the cellular pathways involved in the fate of the cell.

1.4 Oxidative stress and cell death

Vogt is acknowledged to have first described the principles of the morphological features of apoptosis in 1842. The term apoptosis was first used by Kerr *et al.* in 1972 after observation of the process in various tissues. The Greek translation is

from *apo* 'from' + *ptōsis* 'falling, a fall' [36]. Unlike necrosis, which is an uncontrolled cell death of multiple cells in one region, apoptosis has a sequence of pathways that is activated upon intrinsic or extrinsic stimuli.

Apoptosis is a programmed cell death, which is necessary in development and homeostatic maintenance of multicellular organisms [36]. In normal tissues of multicellular organisms, apoptosis is essential for the development (e.g. mammary gland involution) [37] and homeostasis (e.g. epithelial cells after wearing). It is also a defence mechanism against mutations or in immunity[37, 38].

Apoptosis can be triggered by many physiological and pathological stimuli, but the conditions which induce apoptosis can vary between cell types [37]. Despite this, apoptotic events in different cell types and even in cells from different species share common morphological hallmarks.

Cells in early apoptosis exhibit shrinkage and pyknosis (nuclear chromatin condensation). As a consequence of the shrinkage, caused by Na^+ influx to the cell, organelles within the cell are clustered within the reduced volume of the cell [39]. Later on in apoptosis irregular membrane blebbing occurs and, as a consequence, development of apoptotic bodies takes place. These apoptotic bodies may contain fragments of cellular compartments and may also serve as 'eat me' signals to immune cells[38]. During later stages of apoptosis further chromatin condensation is also observed, allowing for easier nuclear fragmentation (Figure 1.8).

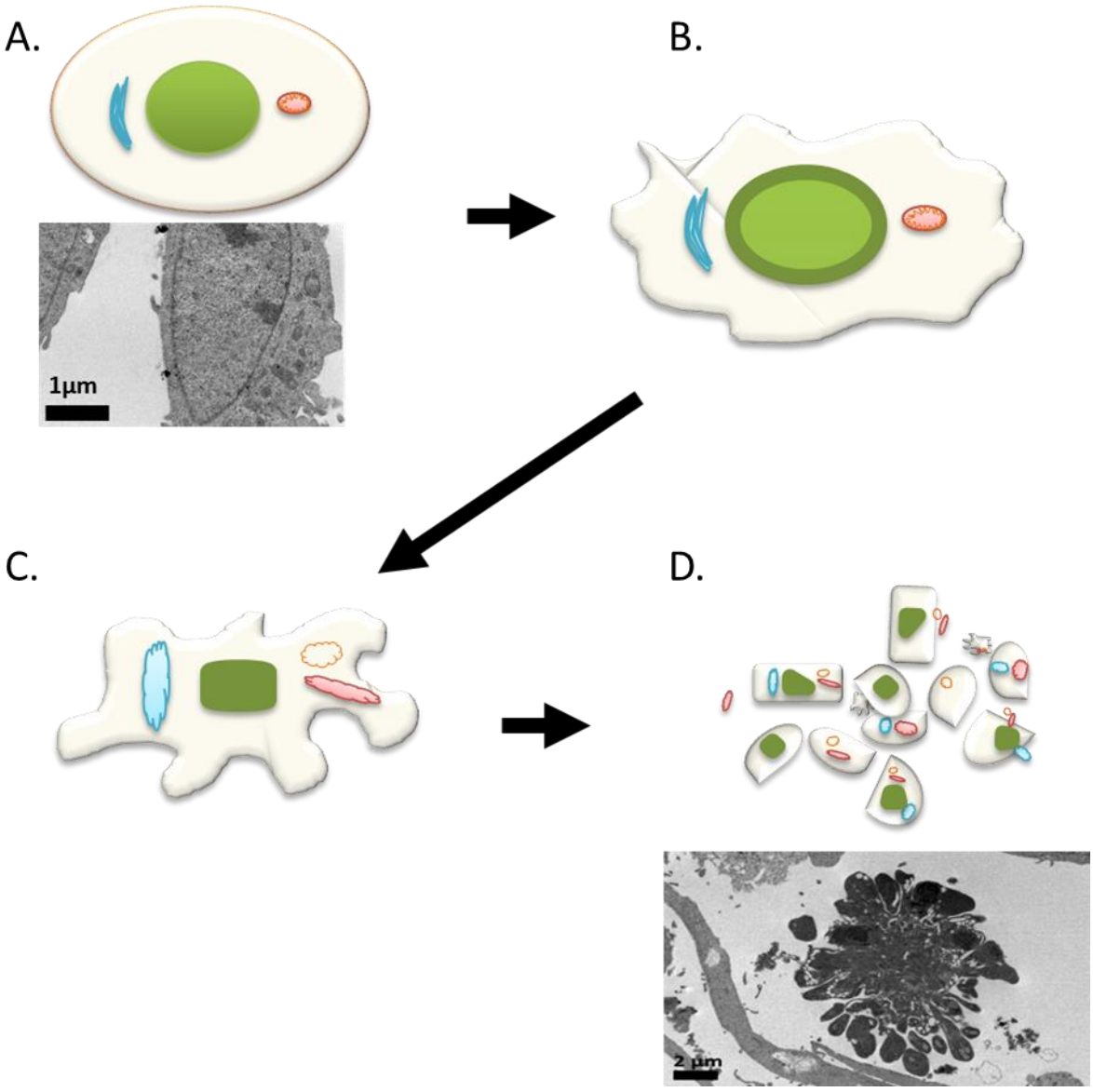

Figure 1.8 A schematic illustration of the apoptotic process supplemented with electron micrographs showing HeLa cell non-apoptotic (in A) and dead cell which has undergone (D.) staurosporine-induced apoptosis. Apoptotic cells are characterised by shrinkage and condensation of genetic material (green nucleus). Breakdown of the cytoskeleton (beige oval) gives rise to membrane blebbing and apoptotic bodies. Mitochondria (pink small ovals) and endoplasmic reticulum (blue banana-shaped structures) are exemplar organelles undergoing structural change throughout apoptosis.

The aforementioned characteristics are a consequence of an organised series of biochemical events. These happen in a distinct sequence:

a. initiation phase induced by either external or internal signals;

b. effector phase, where the cell 'decides' to either undergo

senescence (a slow deterioration) or die;

c. execution phase, where cells are fully committed to cell death and

morphological features are observed.

An apoptotic cell produces a soluble or membrane bound 'find me signal' in the form of ATP, lysophosphatidylcholine, fractalkine/CX3CL1 [40], which attracts phagocytes, enabling removal of the cell from the system.

Apoptosis is said to occur when the redox potential reaches its 'oxidative range' i.e. when the balance between free radicals and scavengers (antioxidants) is disturbed. Distinct cysteine residues of the proteins which are involved in the apoptotic process are being oxidised which in turn activates them (Figure 1.8). Previously, Campbell's group has assembled a map of proteins which contribute to apoptosis and includes all those that are regulated by the redox status [41].

Proteins regulated by the redox potential are hypothesised to be placed within the pathway depending on their redox function. The redox potential of the intracellular environment plays an important role in determining the behaviour of the cell also through switching on or off the proteins that are sensitive to the redox status of the environment such as caspases. On the other hand, the depletion of glutathione, by active transport away from cellular structures, has been reported to contribute towards oxidative stress [42-44]. These two systems, the protein regulation and the regulation by depletion in redox buffers, are interconnected.

Two major pathways can be triggered to commit the cell to programmed cell death, referred to as the extrinsic and intrinsic apoptotic pathways [45] (Figure 1.9). It has been suggested that these two pathways are separate and only one mode of activation can occur in a single cell, however there is evidence that in some cells these two pathways do co-exist and cannot be separated [46]. The redox status of cysteines in the proteins of these pathways is one of the crucial players for execution of apoptosis.

1.4.1 Extrinsic pathway

1.4.1.1 Role of ligand – receptor binding in transducing signals for apoptosis

Apoptosis can be triggered by a 'death ligand' binding to a membrane receptor (extrinsically induced cell death). The tumour necrosis factor receptor (TNFR) family consist of necrosis factor receptor 1 (TNFR1), CD95 (other names Fas, APO1) and TNF-related apoptosis-inducing ligand (TRAIL) receptors. Death ligands include TNF, CD95-ligand and TRAIL. All receptors of this superfamily are trimers, meaning that they undergo conformational change upon ligand binding and trimerise.[47] (Figure 1.9).

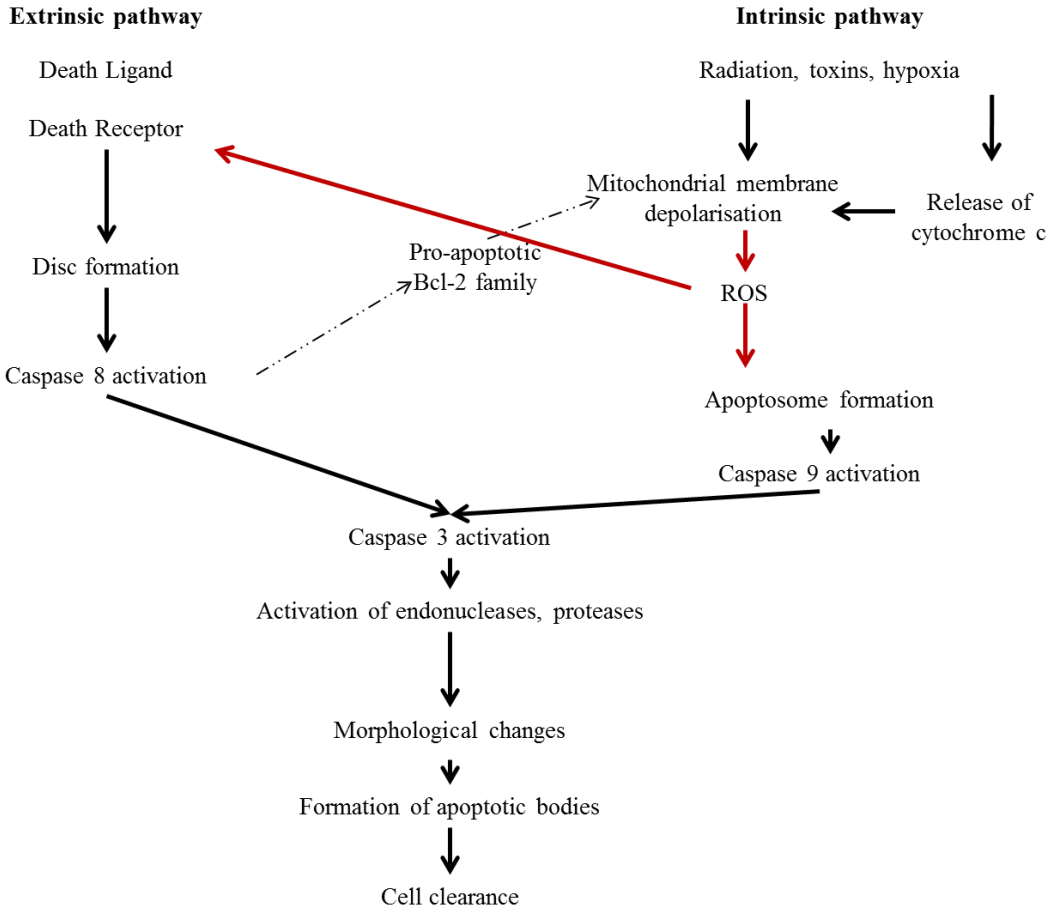

Figure 1.9 Intrinsic and extrinsic apoptotic pathways. Extrinsic pathway activated by external factors, such as injury, is executed by ligand binding to cell membrane receptors, triggering the activation of specific activator caspases. Intrinsic pathway, triggered mainly by damage to mitochondria by radiation, toxins, hypoxia causing membrane depolarisation and release of pro-apoptotic proteins into the cytosol. The two pathways intersect at the activation of executioner caspases (3/7). These caspases are commonly used as markers for apoptosis in research investigation prior to the typical, morphological changes that occur as a consequence at the later stages of apoptotic process.

Upon ligand binding a death receptor exposes a region located in the intracellular space (Figure 1.9). For instance in CD95 the intracellular region contains a death domain that recruits adapter molecules such as Fas-associated death domain (FADD) and procaspase-8 [14, 48][13, 44]. As a consequence a Death-Inducing Signalling Complex (DISC) is formed and a death signal is transferred downstream, leading to activation of initiation caspases, such as caspase-8. This leads to activation of effector caspases-3 and -7 thus initiation of the execution phase of programmed cell death [49].

However, caspase-8 has also been shown to trigger intrinsic apoptosis by cleaving Bid (a member of the B-cell lymphoma protein-2 (Bcl-2) family). The active form of Bid, truncated Bid (tBid), translocates to the mitochondrial membrane facilitating the release of cytochrome c [50][46]. This leads to activation of caspase-9, which forms the apoptosome with other proteins, and ultimately activates executioner caspases-3 and -7 [51].

1.4.2 Intrinsic pathway

The intrinsic pathway (Figure 1.9) can be triggered by genotoxic stress, ionising radiation, DNA damage or nutrient deprivation. It is characterised by mitochondrial outer membrane permeabilisation (MOMP), which results in the release of soluble pro-apoptotic factors including cytochrome c and ROS. This process leads to activation of caspases and a reduction of the primary function of the mitochondria, energy production [52]. The energy production complexes, including complex I, which reside in the mitochondrial membrane, are cleaved by active caspases and mitochondrial function is lost. MOMP is mainly regulated by members of the Bcl-2 family [53].

1.4.2.1 Oxidative stress due to mitochondrial depolarisation

Since mitochondria are the principal sites of cellular respiration, they supply energy for cell functioning. At the same time they are also the main generators of ROS. This makes them an important organelle in the control of redox homeostasis, survival and cell death. Mitochondrial membrane permeabilisation has been considered to be an event which commits the cell to programmed cell death [54].

Mitochondria consist of an inner space, the matrix bound by two membranes, the outer membrane and the inner membrane, which is greatly folded forming cristae. Between the membranes there is a space containing hydrogen ions driven out of the inner membrane from the electron-transport-chain, which is formed by a series of proteins embedded in the membrane. The accumulation of protons in between the outer membrane and inner membrane creates an electrochemical gradient ($\Delta\Psi_m$) across the inner membrane (Figure 1.5).

Mitochondrial permeabilisation is one of the hallmarks of apoptosis [55]. It has been considered as a ‘point of no return’ as once the apoptotic factors, such as cytochrome c and Apoptosis Inducing Factor (AIF), have been released, progression of apoptosis cannot be arrested. Mitochondrial depolarisation is said to occur stepwise and glutathione transport via the outer mitochondrial membrane has been reported [56][52]. Bcl-2 family members regulate the permeability of the outer mitochondrial membrane and this is regulated by interaction between pro- and anti-apoptotic members of the family (Figure 1.10). This interaction of pro-apoptotic Bcl-2 family members causes mitochondrial outer membrane permeabilisation (MOMP) which is considered to be a point of no return and cells’ commitment to apoptosis. [52, 57-59].

Reactive oxygen species, changes in intracellular pH and in calcium concentration can all contribute to the opening of permeability transition pores in the mitochondrial intermembrane space and, as a consequence, have deleterious effects on cellular homeostasis. Depolarisation of the inner membrane is lost, water and other solutes are able to enter the mitochondria causing its membrane to rupture and, as a consequence, the release of pro-apoptotic proteins occurs.

1.4.3 Bcl-2 protein family

Bcl-2 is a proto-oncogene that was first discovered in B-cell lymphoma. There are many Bcl-2 homologs that have pro- or anti-apoptotic functions (Figure 1.10). Bcl-2 family members range in size from 20 to 37 kDa.

a. Anti-apoptotic: Bcl-2 26 kDa; BCL-xL 30 kDa;

b. Pro-apoptotic: BAX 20 kDa; BAK 25 kDa; BAD 23 kDa; NOXA 10 kDa; PUMA 23 kDa; tBID 15.4 kDa; BIM 15 kDa; BIK 20 kDa).

The ratio between pro and anti-apoptotic protein family members determines the fate of the cell [60, 61]. In particular, apoptotic signals are sensed by BH3-only factors, due to their varied distribution and ability to be activated non-redundantly [62].

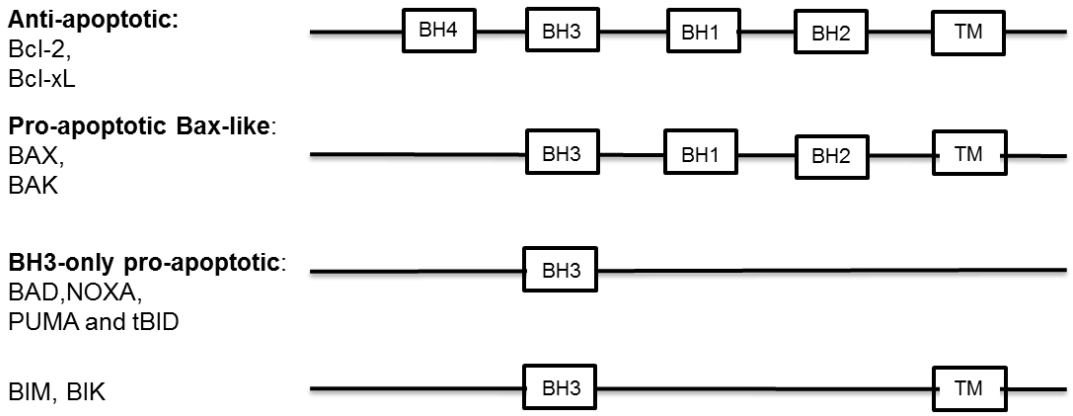

Figure 1.10 Bcl-2 family of proteins. Three subclasses have been identified depending on their function and structure: anti-apoptotic (Bcl-2, Bcl-xL) multidomain pro-apoptotic (BAK, BAX); BH3-domain-only (BAD, NOXA, PUMA, tBID); [62]. BH stands for Bcl-2 homology domain; TM is transmembrane domain at the c-terminus.

It has been reported that Bcl-2 has both pro- and anti-oxidant activity. Hockenbery *et al.* one of the first proposed the model that Bcl-2 functions as an antioxidant thus preventing apoptosis. Specifically, in their study, the Bcl-2 protected cells from hydrogen peroxide induced cell death, and overexpression of Bcl-2 supressed lipid peroxidation [63]. Cells expressing Bcl-2 have an increased pool of GSH and Bcl-2 knockout mice demonstrate higher oxidative stress. It has been suggested that depletion in glutathione influences the decrease in Bcl-2 expression [64, 65]. On the

other hand, Bcl-2 increased intracellular ROS levels suggesting that Bcl-2 also acts as a pro-oxidant [6].

The interaction between Bcl-2 family members is selective and this provides an important mechanistic basis for triggering pro-apoptotic or pro-survival signalling pathways. BAX is expressed in response to stress by a p53-dependent mechanism. In highly oxidative environments, p53, through its transcriptional activity, enhances the expression of pro-apoptotic, especially BH3-domain-only proteins, and therefore promotes the intrinsic apoptotic pathway. [66, 67]

BAX undergoes a conformational change, dimerises, and penetrates the mitochondrial membrane [68]. It has been shown that the depletion of reduced glutathione increases the activation of BAX [2]. Consequently, cytochrome c and procaspase-9 are released from the mitochondria to the cytoplasm and together with APAF-1 form a complex referred to as the apoptosome. This in turn recruits pro-caspases either directly via CARD-domains or indirectly through involvement of additional mediators (CRADD). As a result, the caspase cascade (culminating in cleavage of executioner caspases) is activated and the effector phase in the form of morphological changes can be observed (Figure 1.9).

1.4.4 Cytochrome c release from mitochondria

Cytochrome c is a protein that in its pro-form, apo-cytochrome c, is synthesised in the cytosol and transported to the mitochondrial intermembrane space where it is converted to holocytochrome c by addition of a haem group by haem lyase. Cytochrome c can act as an antioxidant and has ROS scavenging function [69]. Upon disruption of the mitochondrial membrane, release of cytochrome c occurs and this results in increased levels of superoxide due to interruption of the electron transport chain.

The oxidation state of cytochrome c is regulated by conformational change and this is thought to be critical for its binding to apoptotic peptidase activating factor (Apaf-1)[70], whereas the reduced form of cytochrome c has lower affinity for Apaf-1 and thus promotes survival. Therefore, it is important to distinguish between the oxidised and reduced forms of cytochrome c [70] (Figure1.11). Oxidised cytochrome

c promotes binding to Apaf-1, allowing for oligomerisation and formation of a structure called the apoptosome. [71] The disulfide-mediated interaction with Apaf-1 results in caspase 9 activation [72].

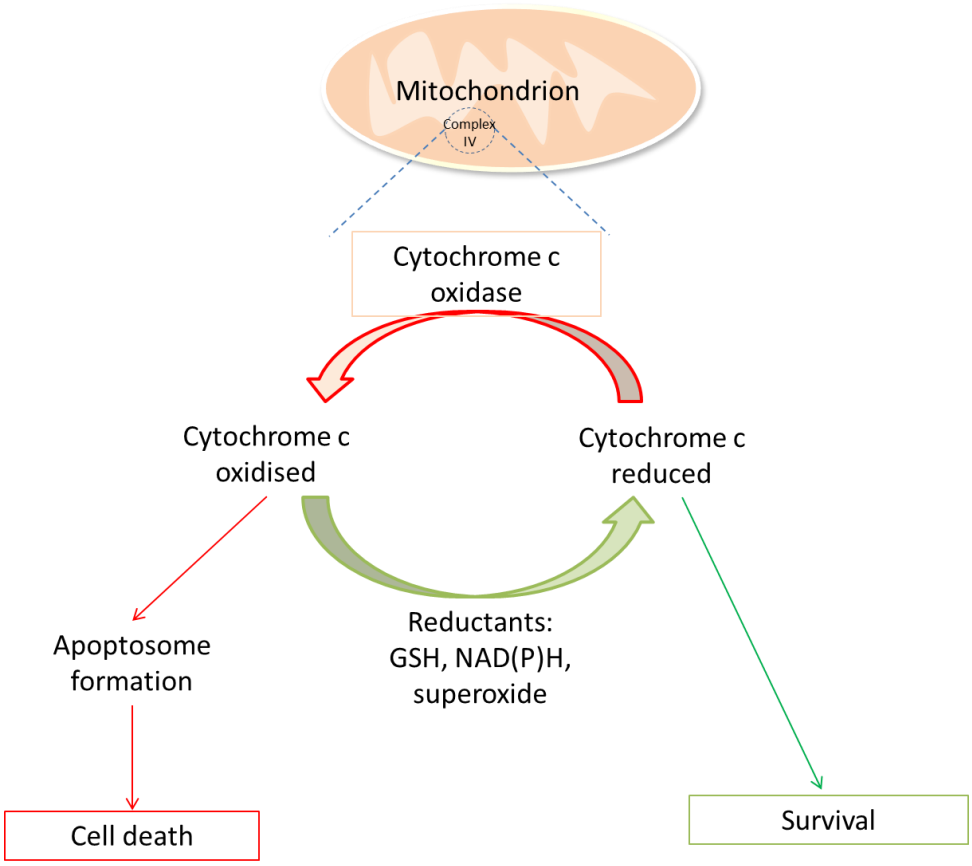

Figure 1.11 Redox state of cytochrome c and mediation of cell fate. Modified from [70]

It has been shown that ligand binding of cytochrome c does not affect its ability to accept or transfer electrons [73]. These have been reported to be independent functions as mutation of lysine 72 has been shown to impair apoptosome formation, but not activity of cytochrome c in the electron transport chain [74].

1.4.5 Caspases

Both extrinsic and intrinsic pathways require the activation of caspases (cysteine proteases cleaving substrates after aspartic acid residues), another critical group of proteins orchestrating apoptosis. To date, we distinguish three different subclasses of mammalian caspases:

- activators of apoptosis (caspases -2, -4, -8, -9),
- executioners of apoptosis (caspases -3, -6, -7).
- mediators of the inflammatory response (caspases -1, -5).

Caspases exist in cells in their pro-form which renders the enzyme inactive [75]. Procaspases are built from three regions: pro-domain, large subunit (p20), and small subunit (p10). The activation of caspase is initiated either by self-processing or by proteolytic processing by other caspases.

Interestingly, activator caspases are specifically recruited to different sites of cell death – caspase-8 is recruited by death-receptor signalling; caspase-2 facilitates genotoxic stress-mediated death; caspase-4 is involved in facilitating ER-stress-mediated death [62]. Most importantly the major executor caspase is caspase-3. The cysteine in the caspase active site is sensitive to oxidation or to thiol alkylation. Caspase activity can also be reversibly modulated by S-nitrosylation. [76] Circu *et al.* also reported that staurosporine activates caspase-3 independently, to some degree, of caspase-8 and -9 and this is also associated with temporal GSH efflux from the cell.

1.5 Cancer and evasion of apoptosis

One of the fundamental hallmarks of cancer is its ability to evade cell death [77, 78]. Some cancer cells are deficient in or express a mutant form of tumour suppressor gene p53 which is a transcription factor for many proteins involved in apoptosis. Thus, p53 mutation may increase the activity of anti-apoptotic proteins and similarly decrease the activity of pro-apoptotic proteins[79]. This could result in preventing the release of cytochrome c from mitochondria and inhibition of caspases. It is postulated that cancer cells maintain a more reducing environment due to their higher metabolic rate [79]. This could affect the redox potential of the cell, making it more reducing. p53 plays a crucial role in cell fate, there are other p53-independent mechanisms that cancer cells use to promote tumour growth via mutation of these genes (so called proto-oncogenes). Proto-oncogenes are involved in cell proliferation such as (growth factor receptors, signal-transduction proteins, or transcription factors).

1.6 Redox regulation and other forms of cell death

1.6.1 Necrosis

In contrast to apoptosis, necrosis is an uncontrolled cell death due to disease, extrinsic or bioenergetic stimuli. Necrosis is characterised by distinct morphological features such as loss of cellular membrane integrity (organelles rupture, ion pumps/channels lose function) and consequently the cell swells and the plasma membrane ruptures. Often an inflammatory response occurs in the surrounding tissue. These features are due to mitochondrial dysfunction (ROS production, failure of Ca^{2+} homeostasis), ATP depletion (bioenergetic catastrophe), perinuclear clustering of mitochondria and activation of proteases. Unlike apoptosis, during tissue injury necrosis can be observed in many cells in the same region and it has been proposed that it occurs in a more oxidising redox environment (Table 1.3). Necrosis is mediated by several genotoxic factors: ROS, excess of cytosolic calcium, proteases, and pro-inflammatory molecules. Hirsch *et al.* reported that excessive oxidation may cause disruption of enzymatic caspase activity thus shifting the cells' choice from apoptosis to necrosis[80]. Another component that is also capable of initiation of necrosis is the nuclear enzyme PARP. PARP is stimulated by formation of breaks in DNA. PARP destabilizes chromatin allowing access of DNA repair enzymes to the damaged part of DNA. The activation of PARP that leads to necrosis is by depletion of NAD^+, which prevents cells from using glucose as a major metabolic substrate [81]. Interestingly, the inhibition of PARP can promote genomic instability and consequently initiate tumourigenesis; on the other hand, when a cell lacks other components such as BRCA1, inhibition of PARP contributes towards the induction of necrosis (this process is known as synthetic lethality)[82]. Necrosis has recently been identified to be executed by molecular mechanisms and pathways called necroptosis [62].

1.6.2 Ferroptosis

A fairly recently reported form of cell death is ferroptosis, characterised form of cell death by iron-dependent accumulation of lethal lipid ROS. The term ferroptosis was first used in 2012 by Dixon *et al.* [83], where a mass molecule erastin inhibited a cysteine-glutamate antiporter, an essential system providing cystine for the cells in cell culture, and a precursor of glutathione synthesis. It has been described as a regulated form of necrosis, however it is distinct from this type of cell death (Table 1.3). To date, mechanisms involved in this type of cell death remain only partly understood, however ROS and bioenergetic catastrophe is a characteristic of this form of cell death [84]. In particular, the GSH peroxidase 4 (Gpx-4), which works through catalysis of hydrogen peroxide to water using GSH as an essential cofactor, has been shown to be related to ferroptosis as it prevents detrimental phospholipid oxidation [84]. The depletion of GSH pool from the cell, inhibited Gpx-4 thus increasing lipid and cytoplasmic ROS [84].

It has been shown that ferroptotic proteins can be used as a biomarkers or targets to induce cell death in cancer. Recently, Doll *et al.* showed that Acsl4, which is involved in cellular lipid composition, contributes to cellular lipid composition, in particular to the death signals formation by oxidised lipids [85]. This study focused on triple negative breast cancer cells, which are negative for Acsl4, were highly resistant to ferroptotic form of cell death [85]. Thus determination of redox potential status may play here a crucial role in that type of cellular demise, as well as be useful for cancer patient stratification.

1.6.3 Necroptosis

Necrosis as a programmed event can be identified in multiple tissue failure (ischaemia), neurodegeneration and trauma [86]. Necroptosis shares the same morphological features as necrosis, however it is induced by external stimulation of death domain receptors by apoptotic ligands: TNF-α, Fas ligand (FasL) and TRAIL. It is initiated when apoptosis cannot be executed (e.g. during inhibition of caspases)[86] [87].

A family of receptor interacting protein (RIP) kinases has been identified to play crucial roles in regulating cell fate (survival or death). This family consists of seven members, from which RIP1 kinase activation is required to initiate the necroptosis pathway [87]. It has been identified that RIP1 requires uncoupled mitochondria to function (generation of ROS, ATP depletion) [86].

To this date has not been shown *in vivo*, other than in genetically manipulated scenarios that suppress apoptosis. Through the evolution of cancer, tumour cells are known to gain resistance towards apoptotic cell death by acquiring genetic and epigenetic alterations. However, it has been reported that necroptosis has been identified as the potential form of death induction in cancer cells *in vitro [88]*.

Apoptosis	**Necrosis**	**Ferroptosis**
Single cells / small clusters	Population of cells	Single cells/ small clusters
Cell shrinkage	Cell swelling	rounding-up of the cell
GSH-depletion	Excessive ROS production, failure of Ca^{2+} homeostasis Bioenergetic catastrophe	Accumulation of ROS and Iron GSH-depletion due to decrease in cysteine uptake substantial depletion of intracellular ATP
Mitochondrial depolarisation	Perinuclear clustering of mitochondria	Reduction of size in mitochondria, condensed mitochondrial membrane, reduced number of cristiae, outer mitochondrial membrane rupture
Pyknosis and karyorrhexis	Pyknosis, karyolysis	Lack of chromatin condensation, nucleus preserves its size
Intact cell membrane	Disrupted cell membrane	Intact cell membrane
Cytoplasm retained in apoptotic bodies	Cytoplasm leakage	No evidence of plasma membrane blebbing
Absence of inflammation	Inflammatory response in local tissue	Pro-inflammatory

Table 1.3 Contrasting features of apoptosis, necrosis and ferroptosis.

1.6.4 Autophagy

Autophagy, literally self-eating, is an alternative form of pro-survival that is partially mediated by redox signalling [89]. Nutrient deprivation, endoplasmic reticulum stress, ROS and hypoxia are known to induce autophagy. Autophagy can also be induced as a stress response: for example, HIF1 and E2F transcription factors induce BNIP3 which competes with Beclin1 for Bcl-2 (Figure 1.12).

Autophagy has multiple physiological and pathophysiological functions. When a cell encounters an environmental stress such as starvation or infection, autophagy takes place resulting in either (1) adaptive survival in which cells return to normal when conditions improve or (2) cell death. Several studies have shown that oxidative damage associated with mitochondrial dysfunction can trigger autophagy [90].

The blood supply to tumours is poor leading to regions that are poorly perfused with blood – i.e. poor nutrient supply and hypoxia, both of which are key triggers for autophagy. These cells undergo autophagy and in this case, it is a protective mechanism to allow cells to survive stressful conditions (provide cells with key nutrients to survive).

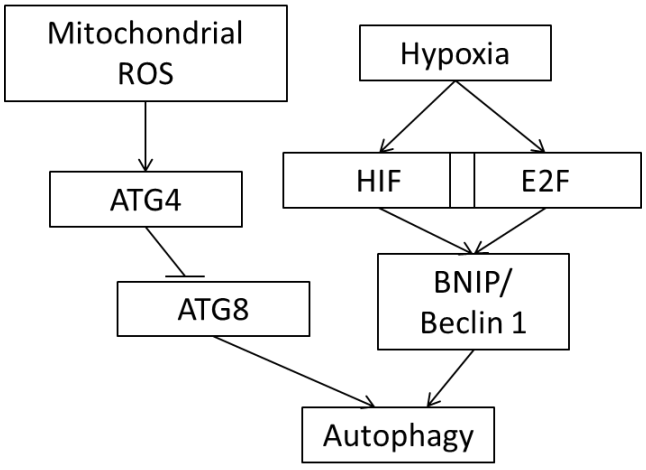

Figure 1.12: Autophagy regulation in response to stress. Autophagy induction by mechanisms sensing hypoxia or oxidative stress. E2F promotes BNIP1. Induction of apoptosis occurs via BNIP3 disruption of the interaction between Bcl-2-Beclin 1; which leads to activation of Beclin1. Adapted from: [91].

In mammals, autophagy acts to clear cytosolic ubiquitinated substrates – this process is selective and is mediated through the mammalian protein p62/sequestosome 1 (SQSTM1). Cargo is recognised through interactions with specific receptor proteins [92]. Autophagosomes emerge from several sites created by the addition of new membranes rather than budding from existing organelles. Next, multiple proteins are recruited to the phagophore. The assembly of the phagophore requires class III phosphatidylinositol 3-kinase (PtdIns3K) complex which includes Beclin 1 – this is regulated by Bcl-2, an anti-apoptotic protein that inhibits autophagy [91]. The small molecules derived from the degradation process are transported back into the cytosol for protein synthesis and maintenance of critical cellular functions under stressful conditions [93].

1.6.5 Mitotic cell death

Mitotic catastrophe (MC) is the delayed death during or after aberrant mitosis [55, 94]. It is not a pure death executioner pathway but an oncosuppressive mechanism that is initiated by perturbations in the mitotic apparatus, initiated during M phase and paralleled by some degree of mitotic arrest. It can ultimately trigger cell death or senescence.

Mitotic catastrophe can be induced by many factors such as: directly by DNA-damaging agents (e.g. ionizing radiation, anticancer drugs), interference with chromosome segregation machinery (microtubule destabilizers).

Morphologically MC hallmarks include the characteristic formation of giant cells with abnormal multiple nuclei. It also displays some apoptotic characteristics such as loss of mitochondrial membrane potential and activation of caspases. Cells undergoing mitotic catastrophe are known to have increased DNA content (tetraploid). It has been reported, that p53 mediates expression of PUMA and BAX that are promoting death of tetraploid cells [95]. Biochemically, following patterns have been identified to execute MC: caspases, release of cytochrome c, chromosomal condensation, DNA degradation.

It has been shown that cells arrested at the G2-M transition or in mitosis might be mediated by CDK1 which is capable of phosphorylation of surviving and therefore induction of apoptotic or anti-apoptotic signals. It has also been reported that CDK1 phosphorylation of Bcl-$_{XL}$ component is inhibiting the induction of cell death. It is also assumed that mitotic catastrophe can be mediated by p53 [94].

MC induction contributes to sensitisation of cancer cells. Since the tumour cells are aneuploid or tetraploid, they are more prone to aberration during mitosis and therefore this can be used as a strategy for selective killing of cancer cells [94].

1.7 Project Aims

The current understanding of redox potential is that it is one of the mediators of the cellular behaviour and fate regulating cysteine switches of proteins.

It is hypothesised that accumulation of harmful radicals and consequent rise in critical threshold of redox potential results in triggering apoptotic pathways [41]. The driving force for this is redox potential and it is also postulated that it is a driving force for the initiation of apoptotic events. The aim of this project is to investigate the redox potential at different stages of apoptosis and to correlate this change with hallmarks of apoptosis. Encompassed in these investigations is the determination of whether the redox potential is the cause or a consequence of the apoptotic process. To date, the redox regulation and oxidative stress in cell death has not been clearly distinguished, due to a complexity of interplay between molecules and its environment as well as lack of sensitive enough methods to capture subtle changes.

The specific aims of the project were:

(1) To establish methodology for investigation of the intracellular redox potential.
(2) To carry out time course measurements of redox potential throughout apoptosis and correlate this with established biochemical markers in single cells at a population level.
(3) To monitor redox potential change in apoptosis at the single cell level in real-time.

Chapter 2 Materials and methods

2.1 Reagents

Reagents and chemicals were purchased from Sigma-Aldrich (Poole, UK) or Thermo Fisher Scientific (UK) unless otherwise stated. Gibco and Invtrogen products were from Thermo Fisher Scientific.

2.2 Cell culture

Immortalised human cervical cancer, HeLa cell line, was obtained from the ATCC and cultured as a monolayer in Earl's Modified Eagle Medium (EMEM) containing 1 mg/ml D-glucose further supplemented with 10 % Foetal Bovine Serum, 1 % L-glutamine. The cells were kept at 37 ^{o}C and 5 % CO_2 in a humidified atmosphere containing 5 % CO_2. Cells were kept below 80 % confluency.

2.3 Apoptosis induction conditions

2.3.1 Staurosporine

Synchronous apoptosis was induced with 1 µM staurosporine (STS) (Invitrogen) as a trigger. A stock of 1 mg/ml STS in DMSO (Sigma Aldrich, St Louis, USA) was kept at -20 ^{o}C. Cells were washed twice with phosphate buffered saline (PBS; GS Chemicals) and serum-free MEM medium, supplemented with 2 mM L-glutamine, 100 U/ml penicillin, 100 µg/ml streptomycin and 1% non-essential amino acids was applied. Staurosporine was added at indicated time points in a reverse time course manner.

2.3.2 UV-B radiation

Ultraviolet-B (UV-B) induced apoptosis was used as an alternative to staurosporine induced apoptosis. 100, 200 or 400 mJ/cm^2 UV-B was used as a trigger.

HeLa cells were seeded at a density of 20,000 per well in six-well plates or 32 mm^2 single petri dishes. 100, 200 or 400 mJ/cm2 UV-B was used as a trigger of apoptosis. The intensity of the UV-B exposure was determined using a UV meter (Scientific Laboratory Suppliers, Ltd.).

Final dose (µJ) / meter reading = time required (s)

Exposed cells were incubated at 37ºC for the indicated time and detached with versene (Gibco, UK), followed by staining, using the methods outlined below.

2.4 Flow cytometry

Ratios for HeLa-roGFP2 cells were obtained on the Attune Acoustic Flow Cytometer (Life Technologies Ltd.). Cells were excited using laser lines at 405 nm (50 milliwatts) and 488 nm (150 milliwatts). Emission filters were 510/30 for both excitation wavelengths.

2.4.1 Annexin V/Propidium Iodide staining

Annexin V and propidium iodide staining of the cells allows for distinction between living cells (double negative), apoptotic (annexin V positive and propidium iodide negative in first instance and then double positive at later stages and death of the cell), necrotic (annexin V negative and propidium iodide positive). More details of the mechanism of work are given in section 4.1.9 of this thesis. The method used was developed by the Gregory Lab Voss *et al. [96]*

Cells were seeded at a density of 200,000 cells per 32 mm^2 single petri-dish. Following the appropriate treatment cells were trypsinised and spun down at 250 x g. Supernatant was removed and cells were washed once in 2 ml PBS and spun down again at 250 x g, then resuspended in 100 µl annexin V (AxV) binding buffer (140 mM NaCl, 10 mM HEPES, 2.5 mM $CaCl_2$) and incubated with 1 µl AnnexinV-FITC (Invitrogen) for 15 minutes at 4 ˚C. Next 300 µl AxV-binding buffer was added and AxV binding was analysed by flow cytometry and compared to unstained controls. 10 µl (20 µg/ml) propidium iodide (Sigma Aldrich) was added 1 minute before analysis.

2.4.2 JC-1 staining

HeLa cells were seeded at a density of 350,000 cells per 60 mm^2 single petri dish. Following staurosporine or UV treatment cells were trypsinised and centrifuged at 400 x g at 20 ºC for 5 minutes. Cells were stained with JC-1 according to the

protocol by Enzo Scientific where the reagent was obtained from (Enzo Scientific). Briefly, cells were washed in 1 ml of 1x assay solution (5 ml assay solution contained: 0.5 ml of 10 x component A, 0.1 ml of 50 x component B and 4.4 ml dH_2O), centrifuged again, then resuspended in 400 µl dual detection reagent (per every 1 x assay solution 10 µl JC-1 was added) and incubated for 15 minutes in the dark. Analysis was performed by flow cytometry (Coulter Epics) and compared to unstained controls.

2.4.3 Tetramethylrhodamine, Methyl Ester, Perchlorate

HeLa cells were seeded at a density of 20,000 cells per well in six-well plates. Following the staurosporine or UV-B treatment cells were detached with EDTA, centrifuged at 150 x g at 20 ^{o}C for 5 minutes, washed with cold PBS and spun again. Supernatant was removed and the cell pellet was resuspended in 100 µL of AxV binding buffer (140 mM NaCl, 10 mM HEPES, 2.5 mM $CaCl_2$) and stained with 20 nM tetramethylrhodamine, methyl ester, perchlorate (TMRM) (Life Technologies) for 30 minutes in the dark at 37˚C. Analysis was performed using flow cytometry (Attune Acoustic Flow Cytometer) and compared to unstained controls.

2.4.4 Caspase -3 and -7 activity staining

HeLa cells were seeded at a density of 20,000 cells per well in six-well plates. Following staurosporine or UV-B treatment, cells were detached with EDTA, centrifuged at 150 x g at 20 ^{o}C for 5 minutes, washed with cold PBS and spun again. Supernatant was removed and the cell pellet was resuspended in 100 µl of AxV binding buffer (140 mM NaCl, 10 mM HEPES, 2.5 mM $CaCl_2$) and stained with 3 µM DEVD caspase-3/7 detection reagent for 30 minutes in the dark at 37 ˚C. Analysis was performed using flow cytometry (Attune Acoustic Flow Cytometer) and compared to unstained controls.

2.4.5 Annexin V-PerCP-Cy5.5 staining

HeLa cells were seeded at a density of 200,000 cells per well in six-well plates. Following staurosporine or UV-B treatment, cells were detached with versene,

centrifuged at 150 x g at 20 ºC for 5 minutes, washed with cold PBS and spun again. Supernatant was removed and the cell pellet was resuspended in 100 µl of AxV binding buffer (140 mM NaCl, 10 mM HEPES, 2.5 mM $CaCl_2$) and stained with Annexin V-PerCP-Cy5.5 (Biolegend, UK) for 30 minutes in the dark at 37˚C. Analysis was performed using flow cytometry (Attune Acoustic Flow Cytometer) and compared to unstained controls.

2.4.6 Cell cycle

Cell cycle phase distribution was analysed using SYTOX Red (Invitrogen, UK). Briefly, asynchronous cells were seeded at a density of approximately 200,000 cells per well in six-well plates and left overnight to allow adherence. Cells were detached with versene into single cell suspension and fixed with ice cold 70 % ethanol and left at -20 ºC overnight. Cells were stained in PBS solution containing 20 µg/ml RNase A and incubated for 30 min at 37 ºC. Prior to analysis, 1.5 µl of SYTOX Red was added and the samples were incubated in the dark at room temperature for 30 minutes. The distribution of the cells in the cell cycle was measured by flow cytometry (Attune Acoustic Flow Cytometer). Flow cytometry analyses were performed using Attune Cytometric Software (Life Technologies, UK).

2.4.7 Bongkrekic acid (BKA) mitochondrial depolarisation

Bongkrekic acid binds to the adenine nucleotide translocase fixing its conformation in matrix state (m-state) preventing mitochondrial depolarisation. Further explanation on BKA binding and function can be found in section 4.1.17. [97]

Cells were plated at a density of 20,000 cells per well in 24-well plates and left overnight to adhere. The following day, cells were washed with PBS and incubated with 100 µM Bongkrekic acid (BKA) for 1.5 hours. Cells were then treated with 1 µM staurosporine in a reverse time course. Cells were detached with versene and stained with TMRM as described previously.

2.4.8 DAPI staining

Cells were seeded in 12-well plates on sterile coverslips in monolayers at a density of 200,000 cells per well and grown for a further 24 hours. Each coverslip was washed

three times with PBS. The cells were permeabilised on the coverslips using 1 % formaldehyde for 30 minutes at a room temperature, followed by washing with PBS. The coverslips were mounted on to slides using DAPI-containing Vectashield hard set mounting medium (Vector Laboratories, Peterborough, UK) in drop-wise manner. Slides were analysed using an inverted fluorescent Zeiss Axiovert 25 microscope (Carl Zeiss Ltd.) and a digital camera (Leica DFC425C).

2.4.9 Hoescht33342 staining

Cells were seeded in 24-well plates on sterile coverslips in monolayers at a density of 200,000 cells per well. Cells on coverslips were washed three times with PBS. The cells were incubated with Hoescht33342 (Thermofisher, UK), an organic compound bisbenzimide, nuclear stain for 10 minutes and analysed using Cytation 3 fluorescence plate reader and imager. Images were processed with ImageJ software.

2.5 Surface Enhanced Raman Spectroscopy

2.5.1 Functionalisation of nanoshells with AQ, NQ, MBA

Surface Enhanced Raman Spectroscopy based method was developed by the Campbell lab. It uses redox-responsive molecules mounted onto the gold-nanospheres that when inserted into the biological cells give a quantitative, real-time reading of the environment the sensor is currently at. More detailed explanations of the sensor structure as well as the background to the method are contained in Chapter 5.

Gold nanoshells (NS) (Nanospectra Biosciences, Inc.) used in this study were characterised by 125 nm silica core and 25 nm gold shell thickness. In-house made bis-(2-anthraquinone carboxamide) (AQ) [98] and 1,8-diaza-4,5-dithia-1,8-di(2-chloro-[1,4]-naphthoquinone-3-yl)octane (NQ) [99] were used for functionalization. *para*-mercapto benzoic acid (MBA) [100] and 1mM AQ (final 1% DMSO) were incubated overnight with NS in the dark at room temperature. NQ nanoparticles were prepared in a 9:1 water:EtOH mixture. The UV-Vis spectra were taken before and after two (AQ-NS, MBA-NS) and three (NQ-NS) washes with deionised water.

2.6 Surface Enhanced Raman Spectra acquisition from nanosensors in cells

2.6.1 Measurements of NQ-NS

HeLa cells were seeded onto a glass coverslip (18 mm in diameter) in 12-well plates at a density of 60,000 cells per well and left to attach overnight. The following day, cells were washed 2 times in PBS and serum-free medium was added. After two hours functionalised NS were added (to a final concentration of 10 fM) and were left overnight for cellular uptake. The next morning cells were washed with PBS to remove unabsorbed NS and the medium was changed to fresh serum-free medium supplemented with 2.5 mM HEPES. Cells were stimulated or unstimulated with 1 µM staurosporine for 2-6 hours incubation.

Spectra were acquired with a Reinshaw inVia Raman microscope Raman spectrometer. A 785 nm diode laser along with a 50x Olympus long working distance objective was used. First an overall map was established. Then a detailed scan was performed with 1x 1mm steps in y- and x-axis. NQNS and AQNS SER spectra were acquired over 30 seconds with 10 % laser power (0.1). For both nanosensors, spectra smoothing and a baseline correction were evaluated using Origin 8.5.1 software.

2.6.2 Measurements of AQ-NS and MBA-NS

HeLa cells were seeded onto a Raman graded glass coverslip (13 and 26 mm in diameter) in 12-well plates at a density of 60,000 and 35,000 cells per well respectively and left to attach overnight. The following day, cells were washed 2 times in PBS and serum-free medium was added. After two hours functionalised NS were added (to a final concentration of 10 fM) and were left overnight for cellular uptake. The next morning cells were washed with PBS to remove non-adsorbed NS and the medium was changed to fresh serum-free medium supplemented with 2.5 mM HEPES. Cells were stimulated or unstimulated with 1 µM staurosporine for the indicated times.

Spectra were acquired with a Reinshaw inVia Raman microscope Raman spectrometer. A 785 nm diode laser along with a 60x Olympus water immersion

objective was used. First an overall map was established. Then a detailed scan was performed with 1 mm by 5 mm steps in y- and x-axis respectively. AQ-NS and MBA-NS SER spectra were acquired over 10 seconds with 50 % laser power. For both nanosensors, spectra smoothing and a baseline correction were evaluated using MatLab R2015b software.

2.7 Transmission Electron Microscopy

Cells were grown in 35 mm^2 petri dish at a density of 350,000 cells and they were treated with nanosensors (NQ-NS, AQ-NS, MBA-NS) using the procedures described in sections 2.7.3 and 2.7.4 of Materials and Methods. Preparation of TEM sections was perfomed by Dr Stephen Mitchell at the University of Edinburgh TEM facility. Briefly, the cells were washed two times with PBS and fixed for 15 minutes in 0.5 % glutaraldehyde in 0.2 M Pipes pH 7.2. The cells were then scraped off and centrifuged for 15 minutes at 10,000 x g followed by fixation for another 30 minutes at room temperature (20 ^oC). Cells were washed three times with 0.1 M sodium cacodylate buffer, and then ultrathin sections were cut and positioned onto a grid. Grids were analysed by transmission electron microscope (CM120 Biotwin, Phillips).

2.8 Whole cell protein extraction

200,000 exponentially growing cells were plated onto 6-well plates and treated with 1 µM staurosporine. At the appropriate time-point cells were washed twice in PBS at room temperature. Cells were resuspended in cold reducing lysis buffer (10 mM HEPES (pH 7.0), 1 mM EDTA (pH 7.4), 1 % triton-x-100). Protease inhibitors were added (10 mM leupeptin, 1 mg/ml pepstatin, 2.3 mg/ml aprotinin, 250 mM ALLN). The plates were incubated on ice on a horizontal shaker for 20 minutes. Cells were scraped off the surface and the suspension was mixed for 30 minutes at 4 ^oC. The cell lysate was centrifuged in a Micro 200R microcentrifuge (Hettich Zentrifugen, Germany) at 14,000 x g at 4 ^oC for 10 minutes. The supernatant was collected, aliquoted, and stored at -20 °C overnight or until required.

2.9 Bradford assay

The protein concentrations of whole cell extracts were determined using a Bradford assay. The Bio-Rad Protein assay reagent (Bio-Rad, Hemel Hempstead, UK) was used to measure the absorbance at an optical density of 595 nm using a plate reader (Whatman, UK). As a reference for calculation of the protein concentration, a series of bovine serum albumin (BSA) concentrations were used.

2.10 Western blotting

Separation of proteins was performed by SDS-polyacrylamide gel electrophoresis (SDS-PAGE). Protein samples were prepared in loading buffer containing NuPAGE LDS Sample Buffer (106 mM Tris HCl, 141 mM Tris Base, 2% LDS, 10% Glycerol, 0.51 mM EDTA, 0.22 mM SERVA Blue G250, 0.175 mM Phenol Red, pH 8.5) and NuPAGE Sample Reducing Agent 50 mM dithiothreitol (DTT), (Novex by Life Technologies, UK) following denaturation at 70 °C for 5 minutes and loading on to a 4-12 % SDS-polyacrylamide gel (NuPAGE, Life Technologies, UK). The SeeBlue Plus2 Prestained Standard (Novex by Life Technologies TM, UK) was used as a protein marker (3-198 kDa fragments). Electrophoresis was performed at 200 V for 35 min in MES SDS Running Buffer (50 MM MES. 50 mM Tris Base, ,0.1 % SDS, 1mM EDTA, pH 7.3) (Novex by Life Technologies, USA). The separated proteins were then transferred onto an Immobilon-FL polyvinylidene difluoride (PVDF) membrane, 0.45 μm pore size (Amersham HybondTM-P, GE Healthcare, CA, USA), at 30 V for 1.5 hours in NuPAGE transfer buffer (25 mM Bicine, 25 mM Bis-Tris (free base), 1 mM EDTA, pH 7.2). The membrane was blocked for 1 hour at room temperature in 5 % dried skimmed milk in PBS containing 0.1% Tween-20.

The primary antibodies were diluted according to Table 2.1 in PBS supplemented with 0.1 % Tween-20 and 5 % dried skimmed milk. Membranes were incubated as indicated in Table 2.1 and after being washed three times in PBS and 0.1 % Tween-20; then incubated for 1 hour with the appropriate secondary antibody diluted according to Table 2.1. The membranes were washed six times in PBS containing 0.1 % Tween-20 and visualised using the chemiluminescence method. Briefly, AmershamTM ECL Detection Reagents were mixed in 1:1 ratio and protein bands

were visualised using Amersham High Performance Chemiluminescence Film (GE Healthcare Ltd., UK). Exposure time is indicated in the figure legends.

Antibody	Reactivity (Isotype)	Clone	Dilution	Incubation time
anti-human caspase 3 (NEB, Cell Signalling Technology, 9662S)	Rabbit (IgG)	Polyclonal	1:2,000	1.5 hours
anti-β-actin Abcam ab6276	Mouse (IgG1)	AC-15	1:10,000	40 minutes
Anti-mouse-HRP GE Healthcare NXA931	Mouse		1:10,000	30 minutes
Anti-rabbit-HRP Sigma A6154	Rabbit		1:5,000	1 hour

Table 2.1: Table shows type of antibody used, dilution and time of incubation.

2.11 Cell proliferation

Cells were plated at a density of 20,000 cells per well in 12-well plates, grown further and counted every 24 hours for 5 days. For counting cells were washed once with PBS, then trypsinised and neutralised with complete MEM medium containing 10 % FBS. They were then diluted in trypan blue 1:1 (v/v) and analysed on a haemocytometer by Olympus Microscope CKX41 (Olympus Optica Ltd., Japan). Each count was performed in duplicate. Each experiment was repeated three times.

2.12 Plasmid transfection

Cells were transfected using FuGENE transfection reagent (Promega, UK) according to the manufacturer's protocol. Briefly, 6 cm^2 dishes containing 300,000 adhered cells were prepared for plasmid transfection. Per plate, 8 µL Fugene 6 was incubated in MEM without FBS for 5 minutes at room temperature. Then 1 µg of relevant

plasmid was added to the diluted Fugene 6 complex and incubated for 15 minutes at room temperature. The Fugene 6-DNA complex was added to the cells in a drop-wise manner. The plates were incubated at 37 °C for 24 hours, the media washed off and replaced with media containing 400 µg/ml selection antibiotic Neomycin (G418, Sigma Aldrich). The cells were harvested at 24 hour post-transfection unless otherwise stated. roGFP positive cells were separated from the negative cells via Fluorescence Assisted Cell Sorting (BD FACS Aria II, BeckmanCoulter).

2.13 DNA purification

Plasmids were purified from 7 ml of transformed bacterial culture using the Qiaprep Miniprep kit (Qiagen, Crawley, UK) according to the manufacturer's protocol. Plasmid DNA concentrations were determined using the NanoDrop ND-1000 Spectrophotometer (software version V3.5.2).

2.14 Statistical analysis

Results are presented as a mean ± standard deviation. Data from at least three independent biological experiments was used. Statistical analysis was performed using student's paired t-test with a two-tailed distribution. Values of $p<0.05$ were considered statistically significant.

2.15 Plasmids

roGFP1 and roGFP2 proteins were generated from the peGFP plasmid containing the roGFP1 or roGFP2 gene insert that was purchased from Remington's Lab at the University of Oregon. [101, 102]

Plasmids pENGFP containing either roGFP1 or roGFP2 were purified from 7 ml of transformed bacterial culture using the Qiaprep Miniprep kit (Qiagen, Crawley, UK) according to the manufacturer's protocol. Plasmid DNA concentrations were determined using the NanoDrop ND-1000 Spectrophotometer (software version V3.5.2) at a wavelength of 230 nm.

2.16 Plasmid and Protein purification

2.16.1 Transformation

Plasmids containing eGFP sequence were centrifuged for 1 minute at 500 x g and inserted into BL21(DE3) competent cells and C2987 cells followed by incubation on ice for 25 minutes, heat shock (42 °C for 40 seconds), and incubation on ice for 2 minutes. 100 µL SOC media was added and samples were further incubated on ice for 1 hour. Cells were streaked onto an agar plate with 100µg/mL Ampicillin (Sigma Aldrich, UK) antibiotic and incubated at 37 °C overnight.

2.16.2 Induction

A single colony from each agar plate was selected and added to separate 250 ml lysogeny broth (LB) containing 100µg/mL ampicillin and incubated overnight at 37^{o}C.

The starter cultures were then diluted to OD_{600} ≈0.1 in LB broth (500 ml) with AMP100 (100 µg/ml). Colonies were kept at 30 ^{o}C until its OD_{600} reached 0.6 ~ 0.8. Samples were induced with 500 µl of IPTG and further incubated for 3 hours followed by centrifugation at 433,664 x g for 10 minutes. Supernatant was then discarded and the pellet was resuspended in PBS and stored at -20 °C.

2.16.3 Recombinant protein purification

Recombinat roGFP2 and eGFP from *E.coli* purification procedure was performed by Menglu (Lily) Wang at the EaStCHEM School of Chemistry, University of Edinburgh.

2.16.4 Cell lysis

Cells were resuspended in 25 ml binding buffer followed by sonication for 15 minutes (30 seconds on/off). After sonication the buffer solution was centrifuged at 108,416 x g for 30 minutes at 4^{o}C. 50 µl of the supernatant was retained and filtered.

2.16.5 Ni resin

3 ml of Ni resin was added to the filtered supernatant and gently spun for 1 hour at 4 ^{o}C. The mixture was injected into the filter cartridge. The mixture was allowed to

flow through, leaving the resin in the filter cartridge. The washing buffer was then added through the resin followed by the elution buffer.

2.16.6 Dialysis

Samples were dialysed at 4 °C for 2 hours using MWCO 8K dialysis tubing.

2.16.7 Gel filtration

The sample volume was decreased to 6 ml by centrifugation. The protein sample (6 ml) was filtered and loaded into a Superdex200 filtration column (GE Healthcare Life Sciences) and pre-equilibrated. (flow rate: 0.7 ml/min, pressure alarm: 0.3 mPa). The eluted samples were collected in fractions which were tracked using 280 nm UV. Protein was stored in 1 ml aliquots at -80 ^{o}C in glycerol until further use.

2.17 roGFP2 protein amine conjugation to N-hydroxycuccinimide (NHS) magnetic beads

2.17.1 Dialysis

roGFP2 protein was thawed on ice following an overnight dialysis in Sodium Phosphate buffer (pH 7.2) at 4 ^{o}C using a 0.5 ml Slide-A-Lyser Dialysis Cassette MWCO 7K (Thermo Fisher Scientific, UK).

2.17.2 Coupling and blocking

Protein and magnetic beads were equilibrated to room temperature. 10 mg/ml beads were placed into the microcentrifuge tube and placed on a magnetic stand; beads were collected and the supernatant discarded. Beads were washed with ice-cold 1 mM hydrochloric acid, the pellet was collected and immediately afterwards, protein was added in a 1:1 (v/v) ratio and the solution was vortexed for 30 seconds and incubated overnight on a vertical rotator at 4 ^{o}C. The following day, the pellet was collected on the magnetic stand and washed with 0.1 M glycine (pH 2.0) and vortexed for 15 seconds. The tube was placed into the magnetic stand and beads were collected. This was repeated twice more, following addition of ultrapure water and vortexing for 15 seconds. Beads were collected on the magnetic stand and resuspended in 3 M ethanolamine (pH 9.0), vortexed for 30 seconds and incubated on a rotator for 2 hours. Next, beads with protein were washed once with purified

water, mixed well, collected on a magnetic stand and washed in sodium phosphate buffer (pH 7.2) three times. For a sodium phosphate buffer pH 7.2 use 280mL of 1 M NaH_2PO_4 with 720ml of 1 M Na_2HPO_4. Beads were resuspended in sodium phosphate buffer (pH 7.2) to a final concentration of 10 mg/ml.

2.17.3 Flow cytometry analysis

All solutions were prepared fresh on the day, degassed with Nitrogen gas and experiments were performed under nitrogen. Titration of proteins on beads was performed in sodium phosphate buffer (pH 7.2) including either of: DL-dithiothreitol/trans-4,5-dihydroxy-1,2-dithiane, DL-6,8-thioctic acid/DL-α-lipoic acid or glutathione/glutathione disulphide at concentrations indicated in the FIGURE legends. Samples were incubated for 2.5 hours at 25 ^{o}C. Data was collected on the Attune acoustic flow cytometer using the high sensitivity setting. Data was analysed with Attune Cytometric Software (Life Technologies, UK).

Chapter 3

Establishing a methodology for the investigation of intracellular redox potential in cells

3.1 Introduction

The first aim of this project was to establish a methodology to measure redox potential in cells undergoing apoptosis in single cells at a synchronised population level so that proposed studies at the individual cell level could be rationalised. Population studies are important since they enable one to determine the percentage of cells moving towards more reductive or oxidative redox potential values, and hence a systemic view of the process can be formed whereas single cell analytical approaches provide a mechanistic view of the process.

In order to best determine the state of the intracellular redox potential in real time one has to use the following three prerequisites in the method selection process. Firstly, the method has to retain high sensitivity in order to detect even minor redox potential changes, as intracellular proteins vary in susceptibility to oxidation and will demonstrate a drastic change in oxidation status over a very narrow potential range [8]. In some cases, a change of the redox potential by 30 mV is sufficient to drive protein activation. Secondly, the method of choice should be as close as possible to non-invasive, allowing unbiased detection of downstream events. For example in the glutathione-focused HPLC method, glutathione has been shown to rapidly oxidise upon cell lysis and extraction for HPLC analysis. Thirdly, redox potential measurement should be reversible, to allow for real-time analysis of, often transient, changes in redox events.

A comprehensive list of methods, commonly used to measure redox potential in cells is summarised in Table 3.1.

Assay name	Function summary		Ref.
	Pros	Cons	
Glutathione recycling assay	- Qualitative, but low in resolution - Overall cellular GSH/GSSG concentration	- No compartmentalisation available - Requires cell lysates - Irreversible	[103]
Redoxfluor-1 fluorescent dye	- Hydrocyanine reports concentration of reactive oxygen species	- Irreversible reporter - Measures redox in cytosol and peroxisomes	[104]
High Performance Liquid Chromatography (HPLC)	- Qualitative, but low in resolution of overall cellular GSH/GSSG concentration	- Requires cell lysates	[105]
Glutathione reductase crystals	- Reports on particular potential in the environment around the crystal (yellow in oxidised form, change to orange/red in reduced form)	- Limited range of reporting - A binary output: crystals show only whether the surrounding environment is above or below particular potential.	[106]
Redox responsive Green Fluorescence Proteins (roGFP)	- Ratiometric genetically-encoded sensor, reversibly reports on GSH/GSSG ratio upon Grx-1 activity.	- Reports mainly on GSH/GSSG status of the cellular redox potential - Limited physiological range	[107]

	- Depends on the Grx-1 activity		
Redox responsive SERS nanosensors	- Reversibly reports on particular potential around the sensor - Method under development and subject of measuring redox potential throughout apoptosis later on in this thesis	- Method based on nanosensors, which have to be endocytosed by the cell of interest	[99]

Table 3.1: Summary table of current methods used to investigate intracellular redox potential.

3.1.1 Reduction-oxidation responsive Green Fluorescence Proteins

To study redox potential progression throughout apoptosis at a population level, this study used roGFP2 and roGFP1 since these proteins have been validated as a tool to measure redox potential non-invasively.

The GFP applied in various studies commonly refers to the *Aequorea* GFP, which was first extracted from jellyfish *Aequorea Victoria*. Among all the natural GFP, only the gene of GFP in *Aequorea Victoria* was cloned and expressed. Further studies on the structure of GFP have lead to modifications of the structure and sequence of amino acids, that lead to creation of various clones of roGFP. A comprehensive review by Swarzlander *et al.* summarises most up to date grand prix of GFP selection [10]. Redox responsive Green Fluorescent Protein consists of 238 amino acids and its molecular weight is 26 kDa. It is composed of antiparallel β-strands. Both ends of the roGFP are capped by short helixes antipodes, which restrict accessibility of solvents to the inferior structure of the protein [9, 10].

A

B.

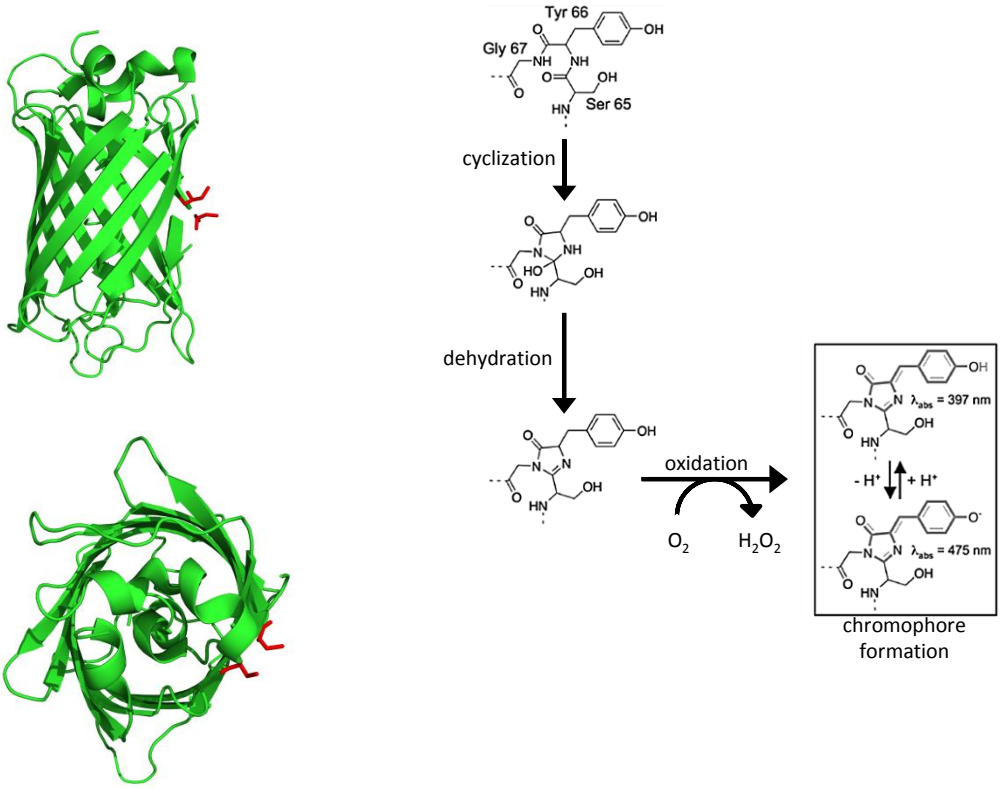

Figure 3.1A. **Top and side view of reduced roGFP2** visualised in PyMOL PDB ID 1JC1 (oxidised form) 1JC0 (reduced form). B. Structure and formation of the chromophore of GFP2 created in ChemDraw. Red indicates Cys147 and Cys204 side chains.

The green light emitting 4-(hydroxybenzylidene) imidazolidin-5-one chromophore is formed by three sequential residues on the interior coaxial helix: Ser65, Tyr66, Gly67 (Figure 3.1). The mutation Ser65Tyr increases the fluorescence and photostability of wild-type GFP (wt GFP). Moreover, this contributes towards the shift of the major excitation peak of GFP to 488nm, making it more compatible with available techniques.

Neither the naked chromophore nor unfolded GFP protein are fluorescent. However, the protein is extremely resistant to protease activity and this property guarantees its stability under harsh conditions. Two mutations, Ser147Cys and Gln204Cys make the protein a valuable tool for studying changes in the redox potential in apoptotic cells.

In publication investigating mitochondrial redox potential with roGFP indicators Hanson *et al.* described roGFP nanosensor creation in an explicit way worth citing: '*Redox-sensitive GFP indicators were successfully created by introduction of disulfides close to a conspicuous bulge in the otherwise regular GFP β-barrel. The bulge is centered on His148, the side chain of which partially fills the bulge and interacts with the chromophore phenol(ate) oxygen'*. [102]

The redox midpoint potential for roGFP1 is -291 mV and for roGFP2 it is -280 mV. In addition, both provide a ratiometric fluorescence readout by comparing the excitation bands of the protonated chromophore (397nm) to the oxidised anionic chromophore (475 nm for roGPF1 and 490 nm for roGFP2). However, roGFP1 can provide false positive results, since prolonged excitation of the chromophore may lead to artificial deprotonation through isomer formation. Therefore, analysis of oxidising conditions would be recorded as reducing, and vice versa.

A number of reporter proteins were generated by using different variants of GFP: wild type (wt) or enhanced GFP (eGFP). A panel of green fluorescent proteins has been developed by the Remington and Tsien labs to improve the temporal resolution of the roGFP response to redox change. The protein has also been targeted to various cellular compartments such as plasma membrane and nucleus [101], endoplasmic reticulum [108, 109], and mitochondria [102] to report on the potential in these cell structures under different conditions.

Structural and analytical properties of two roGFP variants, used in this study of redox potential, are detailed in Table 3.2.

Feature	roGFP1	roGFP2
GFP	wt GFP	eGFP S65T
Alterations	C48S S147C Q204C	C48S S147C Q204C
Excitation wavelengths	400nm, 475nm Main peak 405nm	400nm, 490nm Main peak 488nm
Emission wavelength	510nm	510nm
Relative brightness	Low	High
Specificity	Glutathione via glutaredoxin-1	Glutathione via glutaredoxin-1
Disulfide bond	C147-C204	C147-C204
Midpoint potential	-291 mV	-280mV
Useful reporting range at pH 7.2	-328mV to -272mV	-312mV to -256mV
pH dependence	Less pH dependent	Loss of fluorescence in non-physiological range (above pH 8) due to S65T mutation

Table 3.2 Summarises general similarities and differences between genetically encoded sensors roGFP1 and roGFP2 [107, 110, 111]

The roGFP method mainly tracks changes in glutathione concentration since this is dependent on the Grx-1 enzyme activity. Investigation of the redox potential change using the ratio of reduced to oxidised roGFP protein is convenient as it can be measured by several different methods: confocal and fluorescence microscopy, fluorescence plate reader and flow cytometry, so long as the instruments are equipped with appropriate excitation laser lines: 405 nm and 488 nm lines.

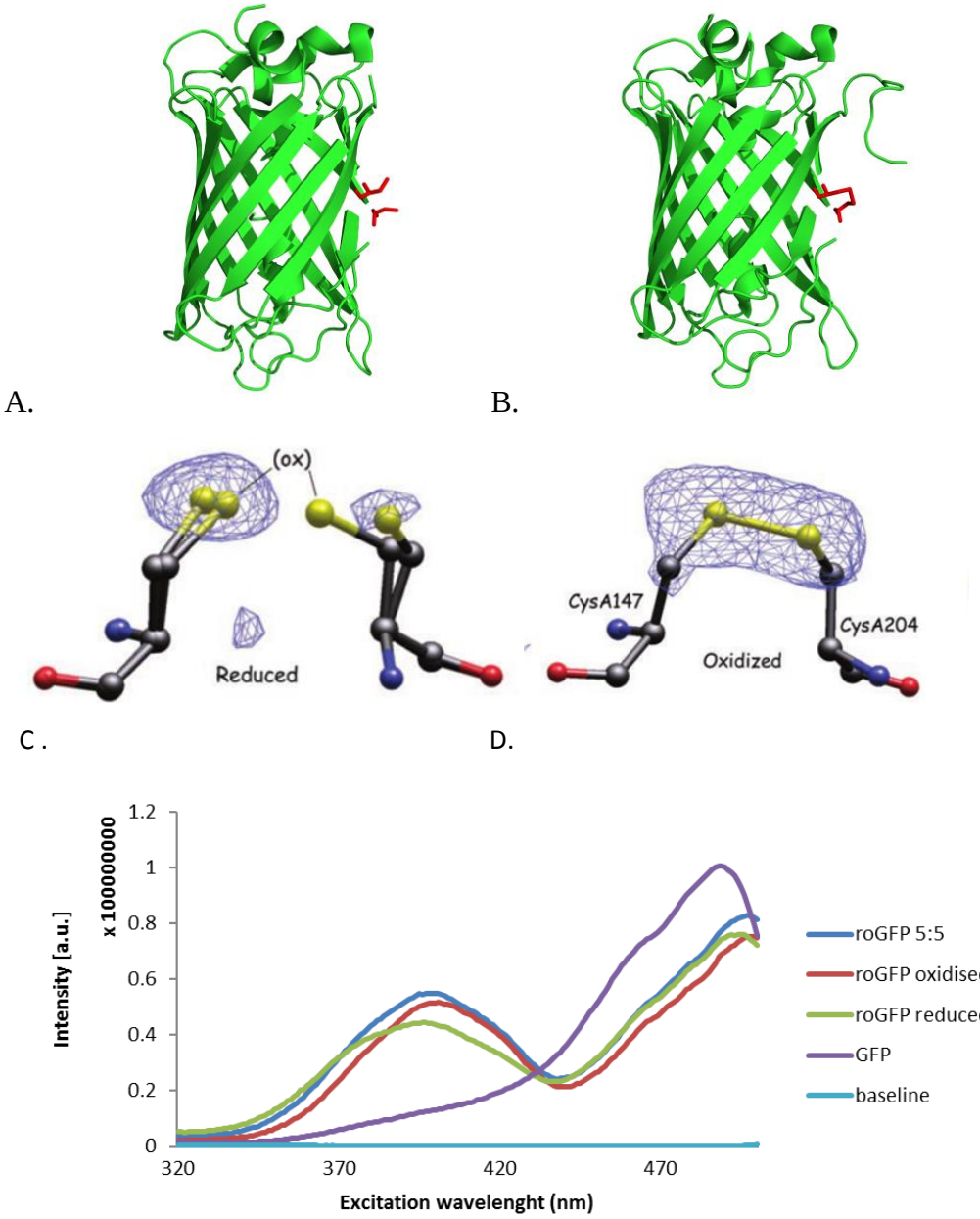

Figure 3.2: A. Reduced roGFP2 B. oxidised roGFP2 visualised by PyMOL software PDB ID 1JC1 (oxidised form) 1JC0 (reduced form) with indicated reduced (C.) and oxidised (D.) states of these cysteine residues as published by [102]Hanson *et al.* E. represents the fluorescence excitation spectra of recombinant roGFP2 and eGFP spectra in reducing and oxidising environments. The spectra were acquired by project students Ankers R, Fan M, Gu S.

3.2 Aim

Work in Chapter 3 aimed to establish grounding high – throughput methodology to measure the redox potential in single cells at a population level. First, stably transfected roGFP1 and roGFP2 HeLa cell lines were developed and the apoptotic capability of cells was monitored. In this chapter flow cytometry was used to validate roGFP1 and roGFP2 expression in HeLa cells and to monitor the changes in redox potential throughout apoptosis of the cells.

3.3 Results

3.3.1 Expression of roGFP in the mammalian HeLa cells

To establish a system to monitor redox changes in real-time, HeLa cells were chosen as an initial cell line with roGFP constructs as this cell line is the most studied cell line in the literature [112]. First, cells were transfected with the roGFP1 and roGFP2 plasmid constructs obtained from Remington Lab (see Materials and Methods section 2.16). HeLa cells were transfected with circular plasmid DNA pEGFP.N1, containing roGFP1 or roGFP2 within the plasmid construct. Yield of transient transfection was 24.3% and 36% after 72 hours for roGFP1 and roGFP2, respectively (Figure 3.3).

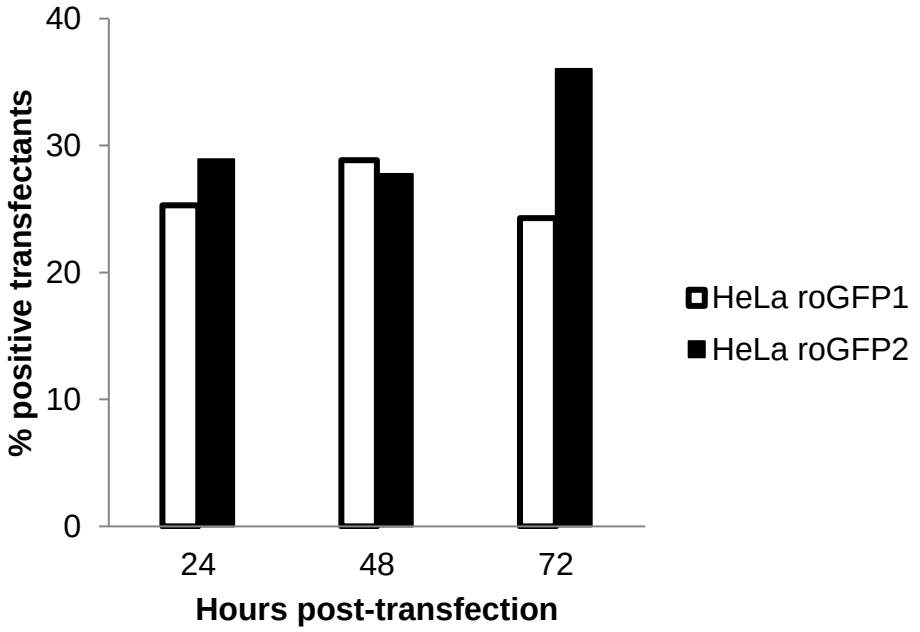

Figure 3.3 Transient transfection of HeLa cells with mammalian expression plasmids containing roGFP1 and roGFP2 – 24, 48, 72 hours post-transfection. Cells were analysed using the fluorescence microscope (bright field and green fluorescence). Pictures of the same field were taken. The percentage of positive transfectants was calculated. Bars represent the average of three fields per condition. In order to enhance and unify the population of roGFP positive cells, fluorescence-activated cell sorting (FACS) was used and cells were collected on the basis of the inherent GFP signal. Following the FACS cells were immediately seeded in 96-well plates at a density of one cell per well to allow growth of single cell colonies in order to remove any genomic variability in the population of cells. A population of cells expressing roGFP1 and roGFP2 has been greatly enriched after FACS (FIGURE 3.4).

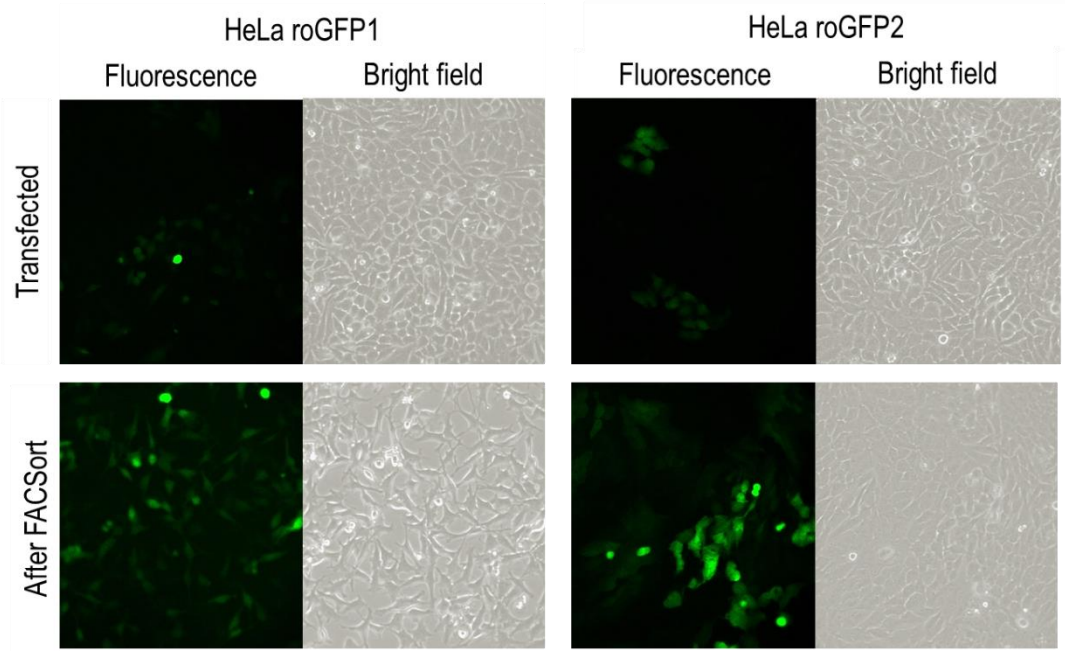

Figure 3.3 continued Selection of roGFP1 and roGFP2 positive cells. Fluorescence Activated Cell Sort (FACS) was performed on the population of cells to isolate green fluorescence positive cells. The graphs show before and after FACS. GFP-positive populations were successfully selected at 488 nm for roGFP2 positive cells and 405 nm for roGFP1 positive cells, as denoted by fluorescence-responsive populations in the right hand side of the "after" dot plots.

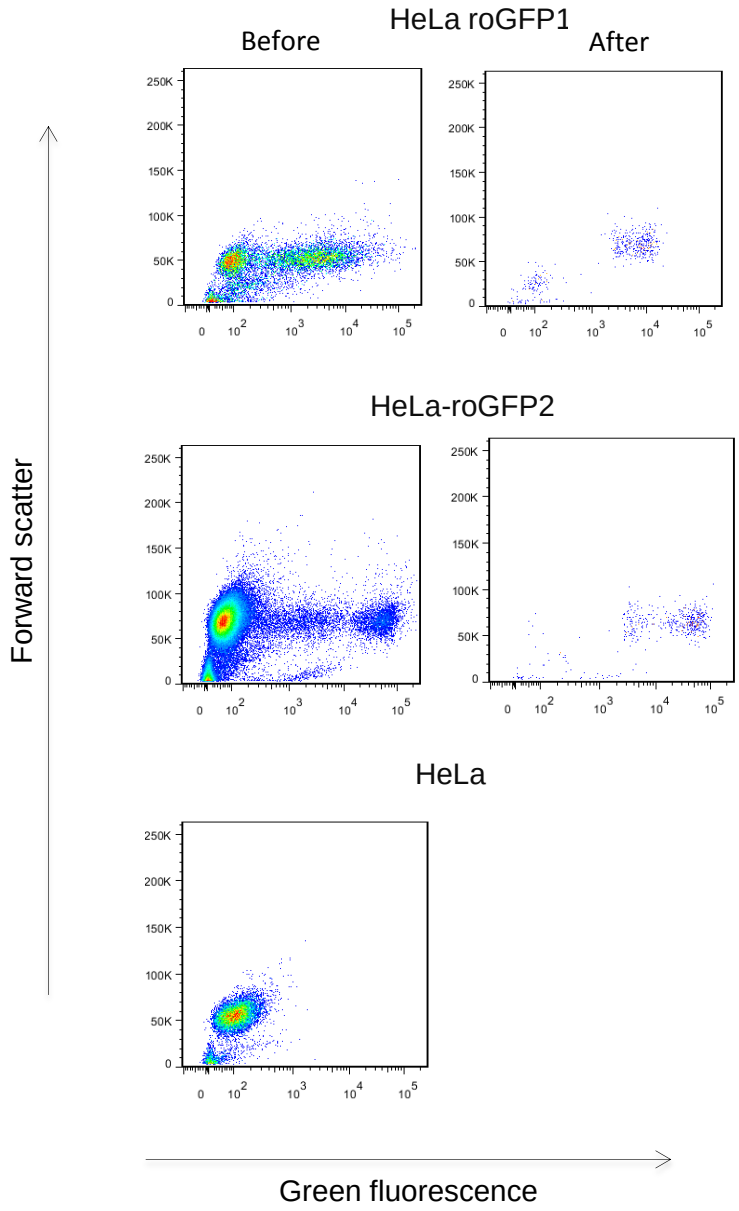

Figure 3.4 Selection of roGFP1 and roGFP2 positive cells. Fluorescence Activated Cell Sort (FACS) was performed on the population of cells to isolate green fluorescence positive cells. The graphs show before and after FACS. GFP-positive populations were successfully selected at 488 nm for roGFP2 positive cells and 405 nm for roGFP1 positive cells, as denoted by fluorescence-responsive populations in the right hand side of the "after" dot plots.

3.3.2 Examination of transfected HeLa cells

In consideration of the fact that the HeLa cells had been exposed to new genetic material, it was crucial to see whether their cell cycle profile, ability to proliferate, and ability to undergo apoptotic cell death had changed.

3.3.3 Proliferation rate

To obtain an accurate estimate of the cell proliferation rate, exponentially growing cells were seeded in 12-well plates at 20,000 cells per well and three wells per cell line were counted every 24 hours for 5 consecutive days until the cells reached full confluency (Figure 3.5).

Cells were trypsinised, stained with trypan blue, and counted using a haemocytometer. Trypan blue dye, which is membrane impermeant and generally excluded from viable cells, was used to assess the viability of the population; however this method was not suitable for distinguishing apoptotic from necrotic cells.

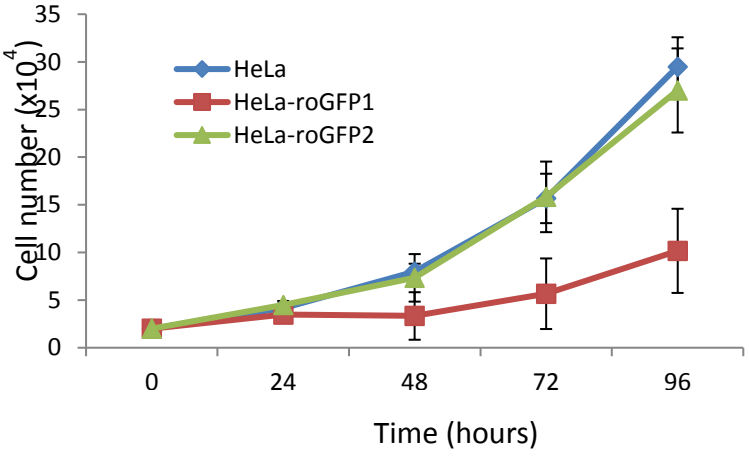

Figure 3.5 Comparison of the proliferation rate of non-transfected and transfected cells; HeLa cells (blue line), HeLa-roGFP1 (red line), HeLa-roGFP2 (green line). Cells were seeded and counted every 24 hours until confluent. Data shows the averages of three repeats per condition from two independent experiments.

No significant differences in growth rates were observed between HeLa and HeLa-roGFP2 cells. However, the HeLa-roGFP1 cell line showed a slower proliferation rate compared to the non-transfected cells (Figure 3.5).

3.3.4 Cell cycle

To confirm and further investigate the cell proliferation rates, the cell cycle of the cells was analysed by monitoring their DNA content.

In a given population of cells there are three major phases of the cell cycle. These include:

- G0/G1 phase where a single cell has one set of chromosomes; 2N
- S phase where a single cell has a variable amount of DNA due to DNA synthesis; >2N<4N
- G2/M phase where a cell has two full sets of chromosomes prior to cell division; 4N.

Flow cytometry is commonly used for analysis of DNA content. The cell cycle profile was acquired using SYTOX Red stain, which binds to nucleic acids including RNA and double stranded DNA with little or no sequence preference and emits a signal proportional to the mass of DNA it is bound to. To determine cell cycle phase, exponentially growing cells were taken from the culture and fixed with 70% ice-cold ethanol. Cells were then treated with RNase A to eliminate nucleic acid material other than DNA.

B.

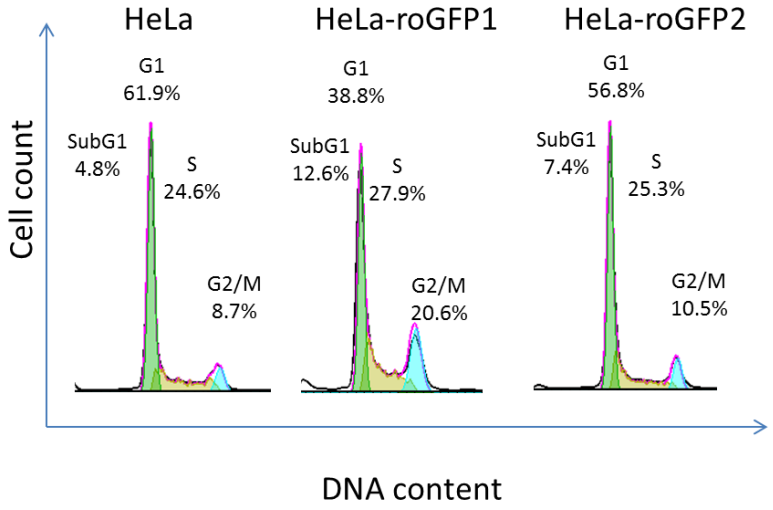

A.

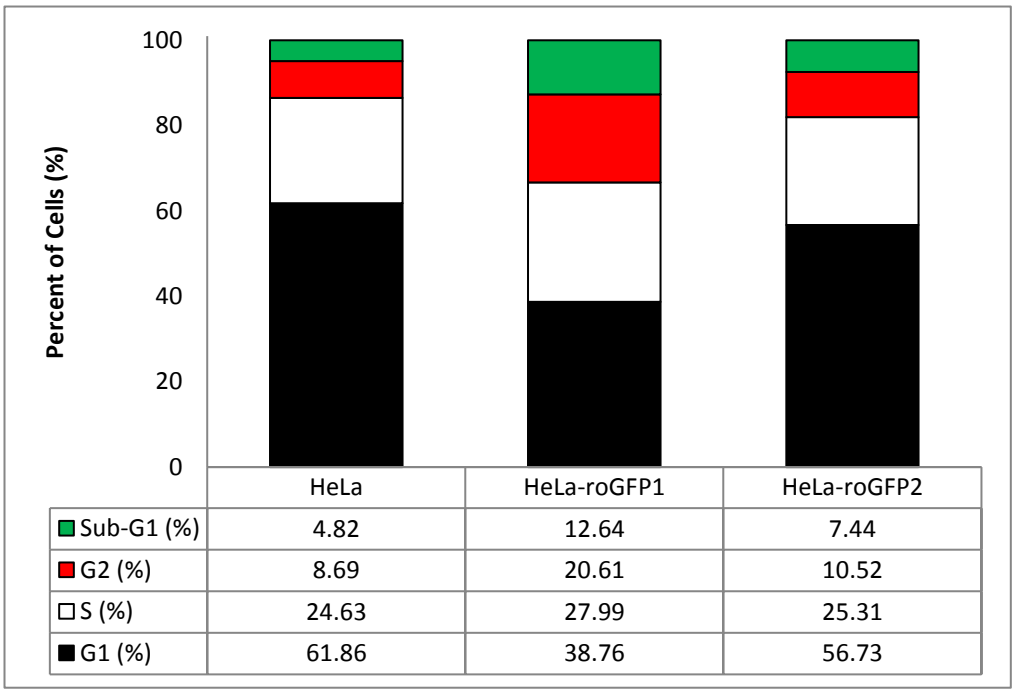

	HeLa	HeLa-roGFP1	HeLa-roGFP2
Sub-G1 (%)	4.82	12.64	7.44
G2 (%)	8.69	20.61	10.52
S (%)	24.63	27.99	25.31
G1 (%)	61.86	38.76	56.73

Figure 3.6 Cell cycle profiles of HeLa cell lines stably transfected with roGFP1 and roGFP2. A shows representative cell cycle profiles for HeLa, HeLa-roGFP1 and HeLa-roGFP2. B. cells shows percent of cells in indicated cell cycle phase.

Flow cytometric analysis of the cell cycle summarised in Figure 3.6 revealed that the HeLa cells had 4.8 % in SubG1 and 61.9 % of cells in G1. HeLa-roGFP1 cells were 12.6 % in SubG1 (apoptotic) phase and only 38.8 % in G1; 27.9 % of cells were in S phase and 20.6 % were in G2/M phase. HeLa-roGFP2 cells had 7.44 % cells in SubG1 and 56.73 % in G1 phase, 25.3 % in S phase and 10.5 % in G2 phase. G2

arrest of the HeLa-roGFP1 cell line suggests that these cells are genetically compromised and attempting DNA repair. Moreover, the cell growth studies shown earlier suggest that the HeLa-roGFP1 cells grew slower and indicated that cells were more prone to cell death.

3.3.5 Apoptosis – nuclear fragmentation

The analysis of the redox potential of apoptotic cells is the focus of this study therefore the rate of progression through the process of programmed cell death in transfected and non-transfected cells was investigated.

Chromatin condensation and DNA fragmentation are hallmarks of the later stages of apoptosis [37, 113]. This can be visualised by 4,6-diamidino-2-pherylinodole (DAPI) dye, which binds to sequences rich with adenine and thymine. These are usually located in the regions of the minor groove of DNA. DAPI is semi- cell permeable and it requires membrane permeabilisation prior to staining.

The intensity of DAPI labelling and the morphology of the chromatin is a major indicator of apoptosis. Pale uniform DAPI staining of an oval-shaped nucleus indicates a viable cell, whereas, bright DAPI staining of irregularly shaped chromatin identifies an apoptotic cell. The presence of staining in the cytoplasm suggests a lack of nuclear condensation indicating necrosis. Figure 3.7 summarises the quantitative data obtained from DAPI staining of cells treated with 1µM staurosporine, an apoptosis inducer.

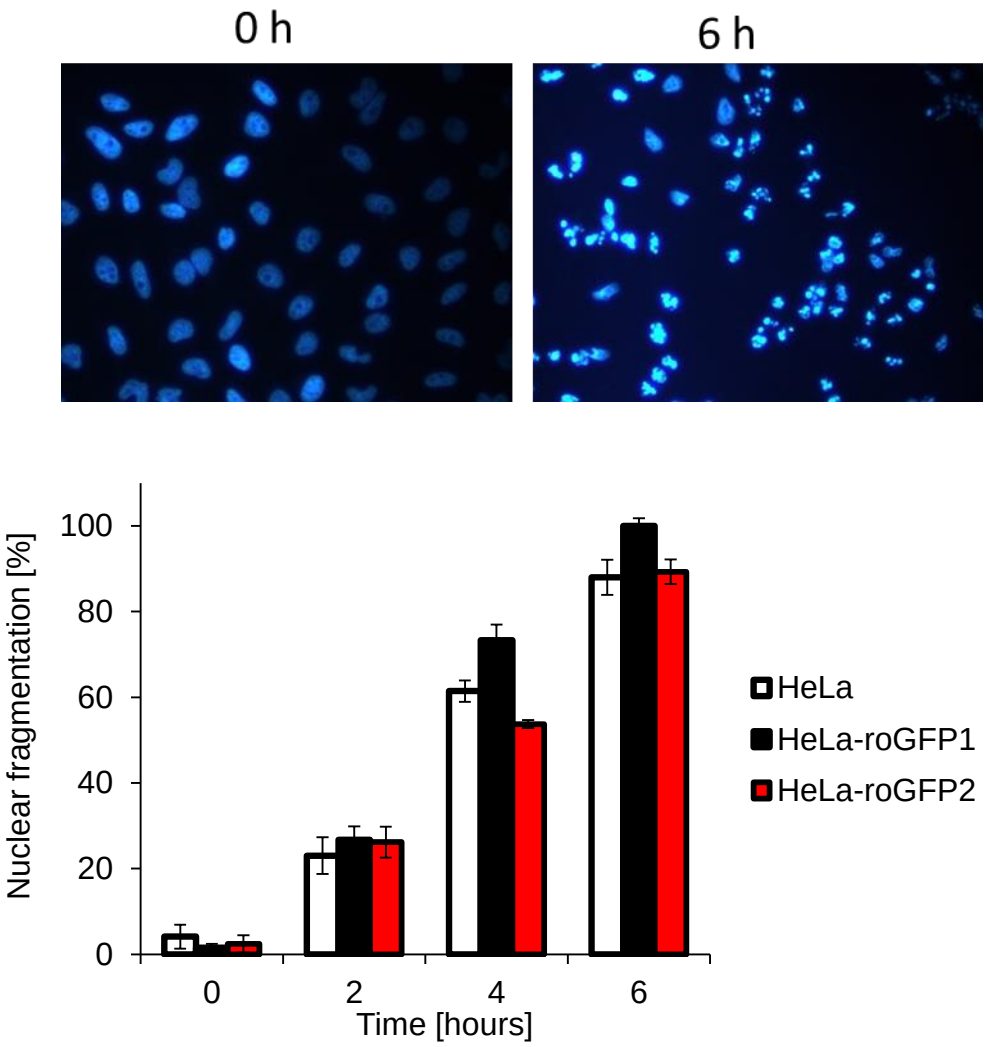

Figure 3.7 Percent of cells displaying nuclear fragmentation, indicating progression through apoptosis, induced by 1uM staurosporine in HeLa, HeLa-roGFP1 and HeLa-roGFP2 cells and measured by DAPI staining. Data represents three independent experiments where more than 300 cells were counted per condition. Error bars indicate SEM.

Stimulation with 1µM staurosporine and analysis of nuclear fragmentation showed no significant differences in apoptotic progression of non-transfected HeLa and HeLa-roGFP2 cells. However, these results confirmed that HeLa-roGFP1 cells showed higher levels of spontaneous apoptosis progression.

3.3.6 Titration of roGFP2

In order to establish whether the redox potential, measured by the ratiometric property of roGFP2, can be quantified by the flow cytometry method, a standard potential curve was determined. This was done by titration of purified roGFP2 protein in various redox buffers at different potentials (Figure 3.8). Purified roGFP2 protein was expressed in *E.coli* and purified by Menglu (Lily) Wang, University of Edinburgh.

Since the flow cytometry apparatus used in this project is able to reliably detect objects equal to or greater than 1µm in diameter, the roGFP2 purified protein was conjugated to beads with a mean diameter of 2.8 µm. This bead size provides sufficient area for protein attachment, but at the same time, they provide a smaller magnetic field, which can negatively influence separation of beads in liquid phase.

The conjugation beads employed in this study were supramagnetic with N-hydroxysuccinimide (NHS) functional groups. Availability of the NHS functional group allows for covalent immobilisation of roGFP2 protein on the beads by forming stable amide linkages via reaction with primary amines. The coupling reaction was performed in degassed sodium phosphate buffer at pH 7.2. The full scheme of conjugation, as well as roGFP profile of lysine and arginine residues is shown in Figure 3.8.

A.

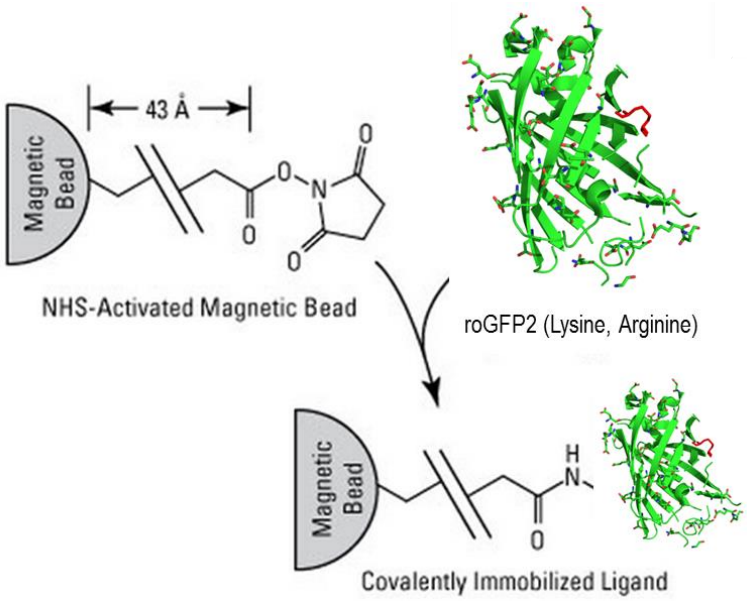

B.

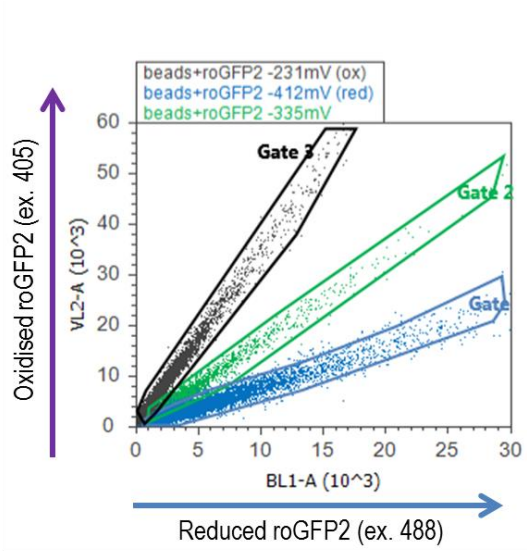

Figure 3.8 A. Conjugation of NHS-activated magnetic beads to roGFP2. 10µg of roGFP2 protein was incubated with 1mg of magnetic beads to ensure uniform conjugation. Protein and beads were incubated for 2.5 hours under the nitrogen conditions, following the analysis via flow cytometry B. Flow cytometry analysis of the complex formed the reduced roGFP2 was collected at excitation 488 nm (Blue Laser Line and emission at 503/30 nm BL1-A) and oxidised version was measured with 405 nm excitation (Violet Laser Line and emission at 503/30nm VL2-A).

The hypothetical profiles of the reduced and oxidised forms of roGFP2 extracted in pyMOL showed no potential interference between the beads and cysteines 147 and 204, change in hydrogen bond conformation of which defines change in the redox potential status. 10µg of roGFP2 protein was incubated with 1mg of magnetic beads to ensure uniform conjugation.

To determine the standard curve of roGFP2, protein-conjugated beads were incubated in sodium phosphate buffer pH 7.2 solutions containing three soluble redox couples at varying ratios to obtain a specific redox potential of a solution. A full flow chart of the experiment is shown below:

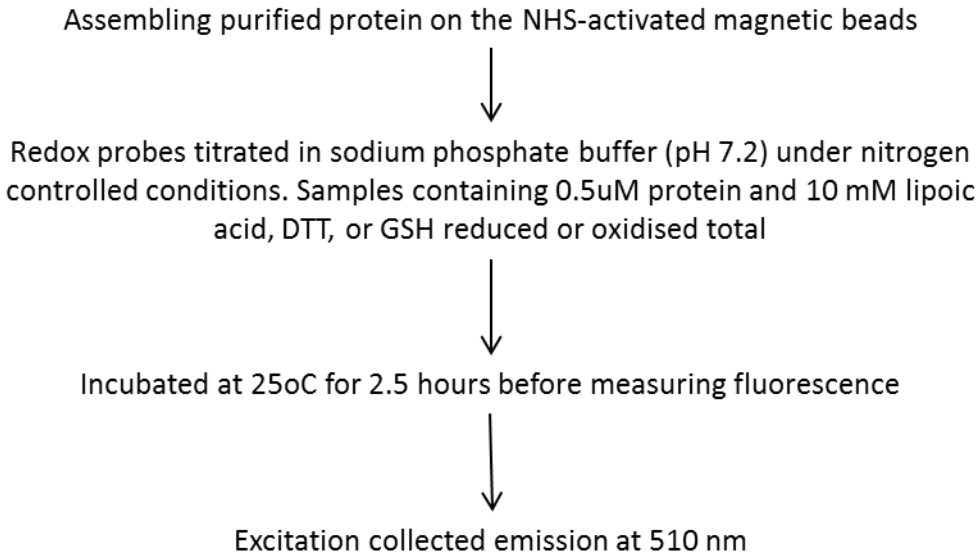

The redox potential of a solution can be calculated if all the variables of the Nernst equation are known (as shown in Chapter 1). Equilibration of the roGFP2 protein in such solution will cause free cysteine residues to come to a thermodynamic equilibrium with the solutions' redox potential and so the redox potential of the roGFP2 could be determined. A series of solutions of different potentials allows for the more accurate calculation of the E^0 of a protein of interest.

Table 3.3 shows redox pairs and midpoint potential of the biological redox pair in mV at pH 7.0 as a reference.

	E^{θ} [mV] at pH 7.0	Reference
DL-dithiothreitol/trans-4,5-dihydroxy-1,2-dithiane (DTT),	-330	[114]
DL-6,8-thioctic acid/DL-α-lipoic acid (LA)	-288	[115]
glutathione/glutathione disulfide (2GSH/GSSG)	-240	[8, 116]

Table 3.3 shows biological redox couples with their standard midpoint potential E^{θ} values [mV].

Varying ratios of the redox couples represented a continuum between fully-reduced (no thiol bonds present) and fully-oxidised (ubiquitous thiol bonding) variants of the redox couple. Each redox couple was incubated for 2.5 hours at 25^{o}C under nitrogen conditions, eliminating the possibility of sample contamination with oxygen.

During the flow cytometry analysis of the conjugated beads, roGFP2 in oxidised conformation was defined by intensity of the fluorescent signal after excitation at 405nm (50mW), whereas the signal from the reporter protein with reduced roGFP2 was collected after excitation at 488 nm (150 mW). Emission filters were 510/30 nm for both excitation wavelengths. The raw data ratio was plotted as a ratio of oxidised (on y axis) and reduced (on x axis) as seen in Figure 3.8 and the raw data was extracted to excel sheet to further analyse and derive a standard curve for roGFP2 by flow cytometric method.

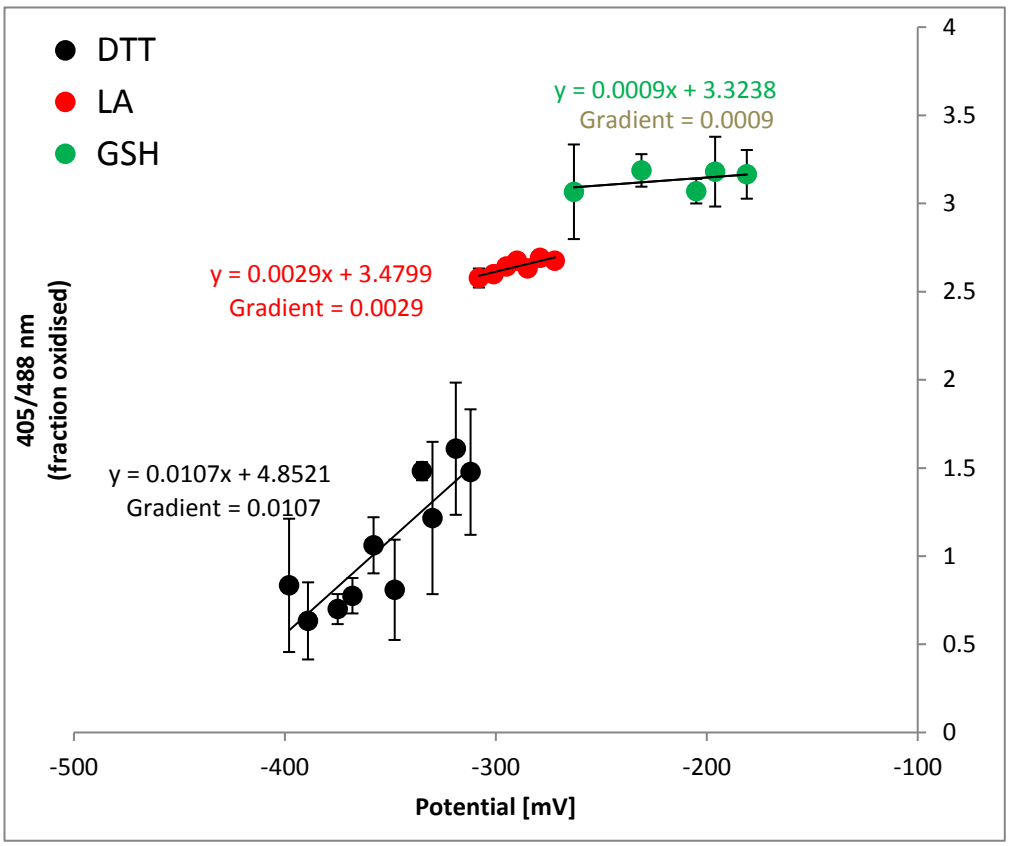

Figure 3.9 Redox potential standard curve for roGFP2 by flow cytometry Dot plot graph depicting oxidised (405 laser line, emission at 510nm) to reduced (488 laser line emission at 510nm) ratio of roGFP2 protein conjugated to N-hydroxycuccinimide (NHS) magnetic beads and incubated with DTT, LA or GSH redox couples. Individual couples were mixed at different ratios and incubated with protein for 2.5 hours. The ratio between detected signals from the interaction with reduced and oxidised couples formed a single data point on the plot at a given redox potential . Error bars showing standard deviation of three independent experiments.

By mixing contrary variants of the redox couples, and thereby producing environments with varying redox potential, a controlled environment for recording the response values of roGFP2 was provided. This approach allowed the generation of a standard curve of response for a very broad redox potential range, between -181 mV and -398 mV (Figure 3.9).

Recurring trends for all 3 redox couples were observed, where an increase in the reducing agent concentration was detected as an increase in signal from reduced roGFP2 (at 405 nm) over oxidised (at 488 nm) and is reflected in the gradual increase in the ratio values.

During analysis of the data point trends, a linear pattern was clearly observed (Figure 3.9) in all redox couples. By performing linear trend-line fitting, coordinates of two points were obtained, allowing the calculation of a gradient value for each data set. Saying that a change in the potential from DTT results in a sharp change in the fluorescence ratio, thus the roGFP2 is good at measuring this. DTT demonstrated the steepest increase of the data point trend, with the positive gradient of 0.0107. For LA and GSH the same is true, however, the fluorescence ratio changes less. roGFP2 incubated with LA and GSH also demonstrate an increase close to linear, but demonstrate a different trajectory. However, at a closer look, roGFP2 in LA and GSH also demonstrate a positive gradient of 0.0029 and 0.0009, respectively.

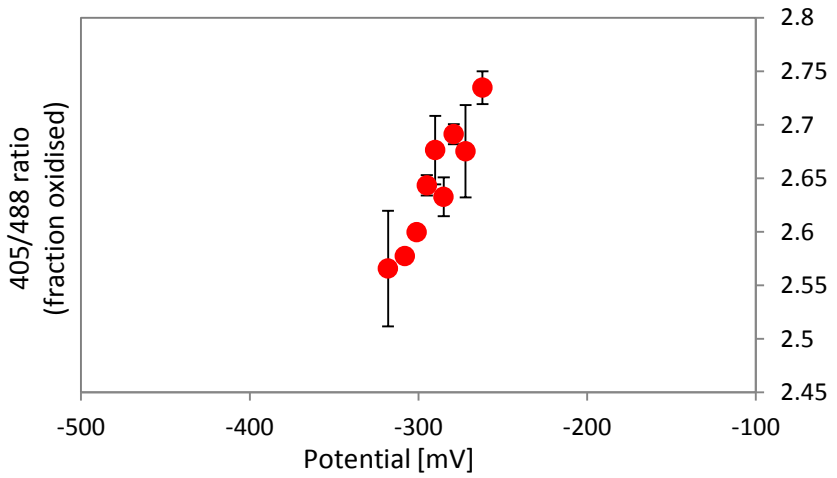

Figure 3.10 zoom in from Figure 3.9. Redox potential standard curve for roGFP2 conjugated to NHS-activated magnetic beads and incubated in lipoic acid. Followed by measurement of the fraction of reduced to oxidised substrate by flow cytometry. Error bars showing standard deviation of three independent experiments.

3.3.7 Validation of roGFP-expressing cell lines for measuring dynamic changes in the redox potential

Titration of recombinant, purified roGFP2 protein in various redox buffers allowed the midpoint potential of roGFP2 to be determined, which was then applied to the calculations of the redox potential measured in cells. Flow cytometric analysis of the redox potential changes during staurosporine-induced apoptosis of HeLa cells transfected with roGFP1 or roGFP2 showed the cells were becoming more oxidised

during cell death (Figure 3.11). Due to large variations in the standard deviation values, it was difficult to determine statistical significance of this data set. However, an increasing trend, based on averaged values, was observed. After 6 hours of exposure to 1μM staurosporine, both roGFP1 and roGFP2 HeLa cell lines demonstrated a marked increase in the proportion of oxidised cells in the samples, increasing from 31% and 27.4% to 60.6% and 50%, respectively. This observation suggests that both of the roGFP variants are sensitive to apoptosis-driven oxidation and hence they are reflecting the expected cell death dynamics. Therefore, roGFPs represent a suitable method for measuring redox potential changes in the population of HeLa cells by flow cytometry.

Changes in the oxidised species of apoptotic HeLa cells are represented in Figure 3.12, showing that roGFP1 has a stronger response to the redox potential changes characteristic of early onset of apoptosis. After 2 hour of exposure to 1μM staurosporine roGFP1 HeLa cells demonstrated a rapid increase in oxidation-linked apoptosis, when compared to the performance of roGFP2 HeLa cells. Such discrepancy can be explained by two theories: the roGFP1 construct may have a toxic effect on the cells carrying the roGFP1 construct, or it is more responsive to the redox change than cells expressing roGFP2. Furthermore, analysis of the redox potential in the untreated sample showed that cells carrying roGFP1 are more oxidised (oxidation in more than 27.4% of cells) even at the resting potential (Figure 3.11). However, those cells showed faster oxidation throughout the apoptosis process and this would be consistent with their measurement range as indicated by the midpoint potential (Table 3.2).

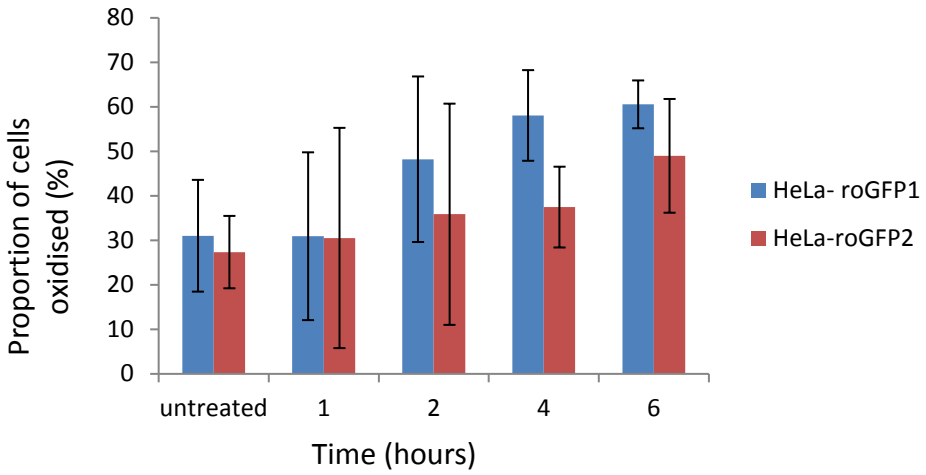

Figure 3.11: Detection of the oxidation status of HeLa cells by roGFP1 and roGFP2 fluorescent proteins in control samples and in cells with staurosporine – induced apoptosis. HeLa cells with roGFP constructs were exposed to 1μM staurosporine for up to 6 hours. Error bars show the standard error of the mean of three independent experiments.

3.3.8 Detection of the oxidation status in transfected HeLa cells (percent oxidised)

Investigation of the percentage of oxidised species by flow cytometry of HeLa-roGFP1 and HeLa-roGFP2 cells revealed the percent of oxidised species was 45% in HeLa-roGFP1 after 0.5 hour post-staurosporine treatment as opposed to HeLa-roGFP2 cells which were 15% oxidised at this time point Figure 3.12. This suggests that the HeLa-roGFP1 cells were more prone to cell damage than the HeLa-roGFP2 cells. However, this result also suggests that the oxidation of the species is higher in genetically modified cells that have a higher proportion of cells in SubG1 phase. A positive growth-over-time trend in cell oxidation was observed for both roGFP variants. Thus indicating a strong correlation between cell oxidation and cell growth.

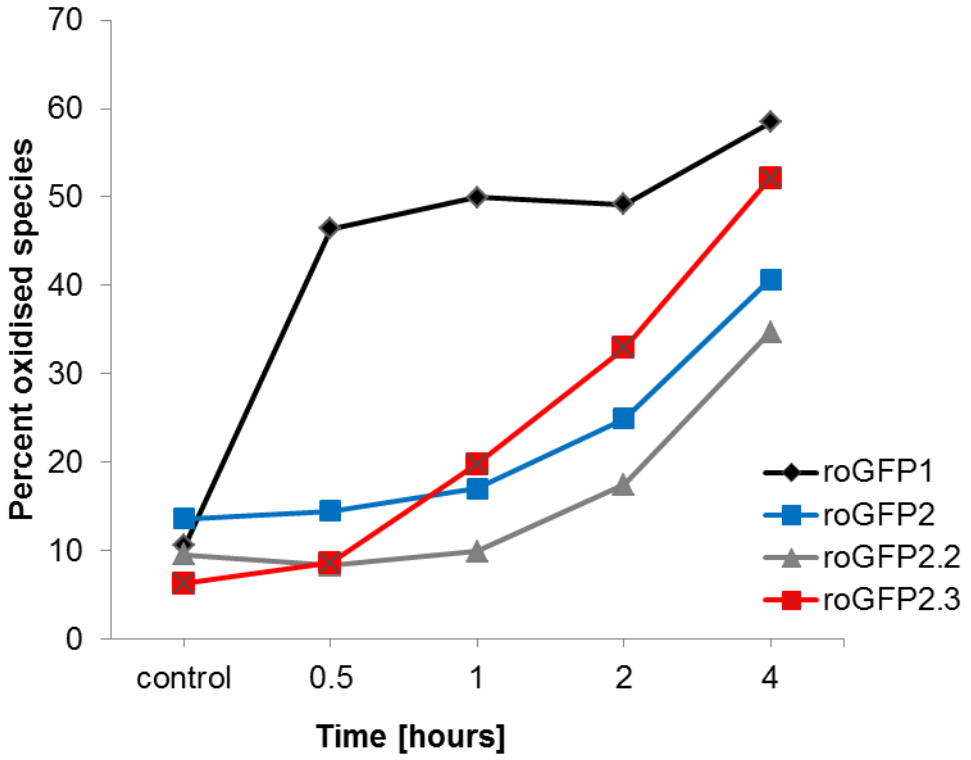

Figure 3.12 Flow cytometric analysis of the proportion of oxidised species during staurosporine-induced apoptosis in clones of HeLa cells carrying redox-responsive green fluorescent proteins. This figure shows various clones of roGFP1 and roGFP2 populations of cells, each derived from single cell colonies.

Due to the difference in the characteristics of the cell cycle and induced apoptosis in cells expressing roGFP1, the decision was made that this cell line would not be used any further in this study as it was not appropriate for use in the studies of redox potential.

3.3.9 Development of alternative cell lines for roGFP vector expression

Expression of the pEGFP plasmid, containing roGFP1 or roGFP2, by viral transduction or using a lipid-based method was used to transfect human (BL2) and mouse (lambda-myc) Burkitt's lymphoma cell lines. In contrast to HeLa cells, both of these cell lines grow in an anchorage-independent manner. Both the viral and

lipid-based transfection approaches resulted in a successful inoculation but insufficient plasmid integration since expression of the constructs was poor in both cell types tested.

Although different techniques and improvements were made by optimising the protocols, expression of the protein was not successful. Less than 5% transfection efficiency in all cases was observed and out of those cells none survived for more than 24 hours. In addition, the fluorescence of these proteins remained too dim to be useful in further investigation. Both cell lines exhibited high autofluorescence upon cell death.

3.4 Discussion and Conclusions

The first aim of this thesis was achieved by performing ground work to investigate the redox potential of cells via flow cytometry at a population level.

Work described in this chapter shows that flow cytometry is a valid method to use to investigate the redox potential in individual cells at cells' population level:

- It has been shown here that the roGFP2 ratio can be detected by flow cytometry and successfully used as a method to investigate the redox potential in a cell population
- roGFP1-transfected cells showed increased susceptibility to apoptosis when compared to non-transfected and roGFP2 transfected HeLa cells.

Numerous studies report the importance of GSH as a main determinant of cell fate [17][16]. The depletion of GSH has been reported to be a major cause of cells to commit to programmed cell death [117-119]. The majority of glutathione resides are in the cytosol; however, the exchange of reduced glutathione between cytoplasm and the intracellular organelles is crucial for maintenance of the cells' homeostasis. However, roGFP2 only reflects the status of the redox potential of glutathione and glutathione disulfide redox couple. Furthermore, this depends on the activity of glutathione reductase 1 enzyme (Grx-1) and its enzymatic capability.

The difference in the cell cycle distribution of HeLa-roGFP1 cells compared to HeLa cells suggests that the HeLa-roGFP1 cells were genetically altered, but it also suggests that the cells were attempting self-repair (Figure 3.6). Normally cells rely on three major checkpoints as they progress through the cell cycle. At the transition between G1 and S phase cells are examined for normal growth patterns: potential space limitations and contact inhibitions, growth factor release and DNA damage. Following DNA synthesis during S phase, the G2 checkpoint gives the cell a chance to identify DNA damage or mismatches that may have been introduced during replication. If such a fault is found, the cell arrests its progression through the cell cycle at the G2 checkpoint until these errors have been corrected. In the case of HeLa-roGFP1 cells, transition past the G2 phase into M-phase does occur at a much slower rate, as chromosomal alterations are beyond repair. There is an increase in apoptotic cells, suggesting that many may die. This is clearly reflected in the cell

cycle analysis (Figure 3.6) when roGFP1-transfected cells are compared to control HeLa cells.

However, cells could have been taken at different growth phases from the culture; therefore it was important to check whether the cell's apoptotic ability was affected. The cells transfected with roGFP1 did show a faster apoptosis rate, suggesting that the cells were more sensitive to stimuli, becoming functionally too distant from the control HeLa cell line and might not be suitable for the analysis of the redox potential in HeLa cells.

Furthermore, when roGFP1-transfected cells were compared to both non-transfected HeLa and HeLa-roGFP2 cell lines an increased susceptibility to apoptosis is observed, leading us to hypothesise that the roGFP1 construct may have a toxic effect on cells carrying the construct.

Analysis of the redox potential showed that cells carrying roGFP1 are more oxidised even at the resting potential (Figure 3.3 and Figure 3.5 (middle column)). However, cells with roGFP1 showed faster oxidation during apoptosis, and this is consistent with their measurement range, as indicated by the midpoint potential. This observation was, however, not observed or reported previously.

At the same time, results from the analysis of the redox potential showed that roGFP1 cells did indeed go faster into the more oxidative status as opposed to the roGFP2 cells. This may be explained in two ways:

1) The rise in redox potential preceded the apoptosis in those cells and was an indicator of more rapid induction and processing of apoptosis in those cells, showing that the cells were more susceptible to staurosporine-induced apoptosis.
2) Cells were fragile at the beginning, and more fragile cells tend to shift towards cell death to save the population from genetic mutation.

This might have been followed or preceded by a rise in oxidised roGFP1 form in the cell. Further investigations would be desirable, however because the cells were genetically compromised the decision was made not to take this cell line further and to focus on roGFP2-transfected cells exclusively.

Data from purified protein showed that positive gradients, observed in all 3 redox couples, allowed validation of the sensitivity and response range for the roGFP2 protein. Comparison of the gradients shows that the rate of change for the DTT couple was 3.7 and 11.8 times higher than in LA and GSH, respectively. Furthermore, the rate of change of LA was 3.2 times higher than in GSH. In comparison to DTT and LA, GSH has the smallest gradient with minimal changes in the ratio between GSH (reduced) and GSSG (oxidised) variants of the couple. On the basis of this observation it can be concluded that the difference between titration occurs because of various half-cell potentials of the redox couples.

The reason that the purified protein was not or barely affected by different redox potentials in a GSH/GSSG couple might be caused by the absence of direct interference between roGFP2 and GSH. Such observation might be explained by the reactivity between roGFP2 and Grx-1, an enzyme which is responsible for the reduction and oxidation status of the glutathione itself and is directly linked to reducing or oxidising the roGFP2 protein in the cell. The roGFP2 protein does react to the reduction by Grx1 (glutaredoxin-1) and is equilibrated to the same redox state as GSH/GSSG by this enzyme. roGFP2 has a similar halfway potential to the glutathione therefore it is not affected as much as with the DTT or LA [9, 10].

When the ratio of excitation 405/488 at emission 530 nm was plotted against the potential, the mid-point potential correlated with the potential previously reported by Meyer and Dick at the value of -280 mV.

Even though the glutathione redox couple is the major buffering system in the cell, there are other thiol/disulfide redox couples. These include thioredoxin 1 and 2, NADP+/NADPH, NAD+/NADH. These couples are not in mutual equilibrium and are distributed differently between the cellular organelles, as discussed in Chapter 1. It is also important to note that GSH is only synthesised in the cytoplasm. Therefore, in the example of mitochondria, the mitochondrial GSH pool is dependent on GSH transport from the cytoplasm. It is crucial to acknowledge limitation of the GSH/GSSG system in tracking the redox potential, in order to gain a clear mechanistic and quantitative understanding of the overall redox potential state of the cell. Analysis of the data, presented in this chapter, led to an interesting and

important question: are the changes in the redox potential preceding the apoptosis process and driving the cells to the point of no return? And when are cells fully committed to apoptosis?

Chapter 4

Redox potential in cell populations undergoing staurosporine-induced apoptosis

4.1 Introduction

The previous chapter evaluated the method of analysis of redox potential in HeLa cells expressing roGFP2 protein. Here that method was used to investigate redox potential of cells undergoing apoptosis. Changes in the mitochondrial membrane potential, a central mechanism of the intrinsic apoptosis pathway, were studied in relation to those occurring in the cytoplasmic redox potential.

4.1.1 Loss of mitochondrial function and generation of ROS during apoptosis

Activation of the intrinsic pathway is associated with mitochondrial outer membrane permeabilisation (MOMP), leading to release of pro-apoptotic factors such as cytochrome c and is regulated by the Bcl-2 family of proteins (Figure 4.1).

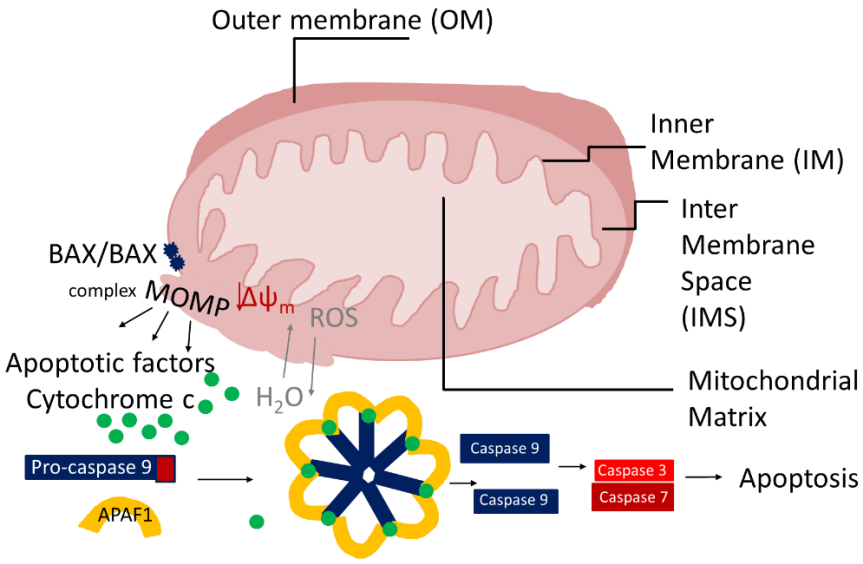

Figure 4.1 Diagram depicting loss of function of mitochondria during apoptosis. Pro-apoptotic Bcl-2 family proteins dimerise and form pores in the OM of mitochondria causing the content of IMS to leak to the cytosol. These proteins are involved in formation of apoptosome that serves the activation of caspase-9, which then directly activates executioner caspases 3 and 7 to complete apoptosis.

The interaction between Bcl-2 family members is selective and this provides an important mechanistic basis for triggering pro-apoptotic or pro-survival signalling pathways. Bcl-2 has been reported to act as an antioxidant [65], thus inhibiting apoptosis.

4.1.2 Caspase-mediated loss of mitochondrial function

Caspases are another critical group of proteins orchestrating apoptosis. This group of enzymes is characteristic of apoptosis and involved in activation (caspases -2, -4, -8, -9), and execution (caspases -3, -6, -7) of cell death. They also mediate inflammation response (caspases -1, -5). Interestingly, activator caspases are specifically recruited to different sites of cell death – caspase-8 is recruited by death-receptor signalling; caspase-2 facilitates genotoxic stress-mediated death; caspase-4 is involved in mediating ER-stress-mediated death; caspase-9 is activated by an apoptosome (downstream of cytochrome c). Most importantly the major executioner caspase is caspase-3 [76]. Circu *et al.* also reported that staurosporine activates caspase-3 independently to some degree of caspase-8 and -9 and this is also associated with temporal GSH efflux from the cell.[76]

4.1.3 Apoptosis in relation to redox potential change

Apoptosis is said to occur when the redox potential reaches its oxidative range i.e. when the balance between free radicals and scavengers (antioxidants) is disturbed. The depletion of glutathione by active transport away from cellular structures has been reported to contribute to oxidative stress [42, 120]. Oxidative stress can then trigger the apoptotic process. For example, it has been postulated that the redox status of the cysteine residues of the proteins involved in the apoptotic process is critical for their function[41] [37]. Consequently, drainage of GSH out of the cell leaves only the oxidised form of glutathione disulfide, which will result in an increased oxidation of certain pro-apoptotic proteins such as caspases [76].

4.1.1.1 Loss of mitochondrial membrane potential in relation to change in redox potential

It has been reported that depletion of glutathione can trigger a decrease in Bcl-2 expression [121]. In a highly oxidative environment, the transcription factor p53

enhances the expression of pro-apoptotic proteins, especially BH3-domain-only Bcl-family members, and therefore promotes the intrinsic apoptotic pathway. BAX is expressed in response to stress by a p53-dependent mechanism. It undergoes conformational change and penetrates through the mitochondrial membrane (Figure 4.1). As a consequence, cytochrome c is released from mitochondria into the cytoplasm and together with pro-caspase-9 and APAF-1 (which activates pro-caspase-9) forms a complex called the apoptosome. This in turn recruits pro-caspases through direct Caspase Recruitment Domains (CARD). As a result, the caspase cascade is initiated, culminating in cleavage and hence activation of executioner caspases and the demolition of key cellular structures.

4.1.4 Aims and Objectives

This chapter aimed to identify optimal conditions to study apoptosis in HeLa and HeLa-roGFP2 cells in relation to the redox potential. The outcome of this chapter will establish, at the cell population level, the association between changes in redox potential and apoptosis progression in these cells. It also aimed to provide the ground work for the investigation of a more detailed, low throughput, single-cell based assay using SERS nanosensors.

The first objective was to define biomarkers of apoptosis and to establish a valid time course to monitor the process. The second goal was to characterise the intracellular redox potential change throughout apoptosis and relate it to the identified markers.

4.2 Results

In order to detect possible changes in the intracellular redox potential during apoptosis, the redox potential was measured whilst monitoring specific apoptotic biomarkers.

4.1.5 Establishing controlled conditions for apoptosis

Timing is crucial when measuring specific biomarkers of apoptosis. For that reason, the first step was to establish in detail the apoptosis kinetics within a population of cells using the available biomarkers. The protein kinase inhibitor, staurosporine and ultraviolet radiation (UVB) were used to trigger apoptosis of HeLa cells. These two methods were chosen as they trigger apoptosis in two independent ways. UV induces DNA damage and it is related to extrinsic apoptotic pathway, while staurosporine mainly through mitochondrial pathway [122].

4.1.6 Staurosporine

Staurosporine (STS), shown in Figure 4.2, is a natural product commonly used as an inducer of apoptosis in cells [76]. It is a non-oxidant compound and non-specific inhibitor of protein kinases.

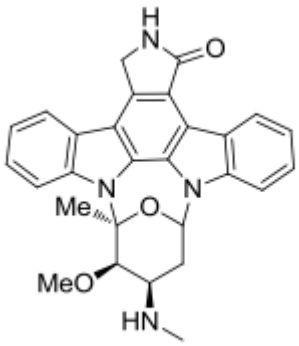

Figure 4.2 Staurosporine structure.

Staurosporine-induced apoptosis of HeLa cells was assessed by examining the nuclear morphology over a 6 hour culture period. Figure 4.3A shows an increase in nuclear fragmentation over this time course. The dose of staurosporine employed (1µM) was chosen on the basis of previous data obtained in the Gregory Lab.

A.

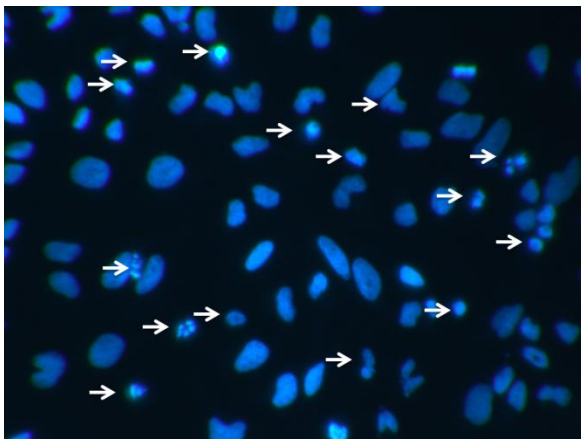

B.

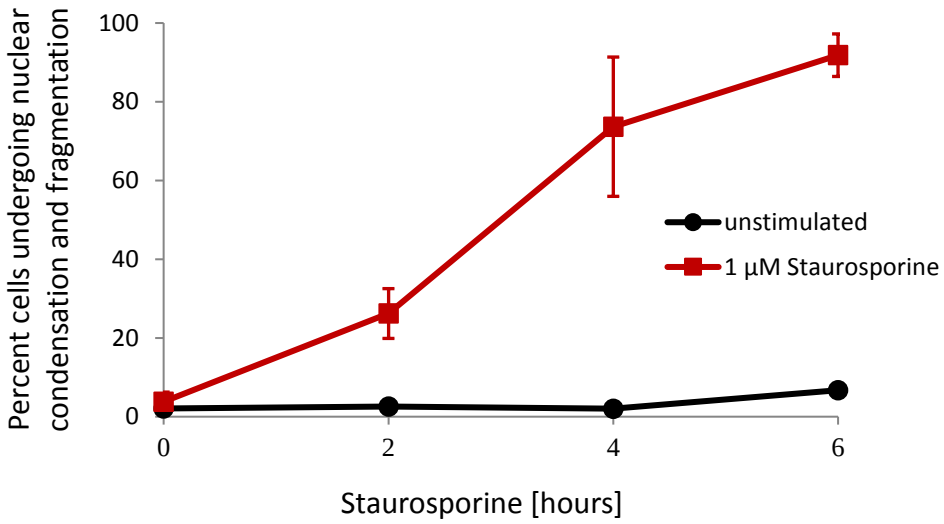

Figure 4.3 Apoptosis-associated nuclear fragmentation induced in HeLa cells by staurosporine. Quantitative analysis of apoptosis as assessed by nuclear fragmentation of DAPI-stained HeLa cells. Exponentially growing sub-confluent HeLa cells were cultured with staurosporine (1µM) and after various intervals they were fixed and stained with DAPI to reveal the nuclear morphology as indicated in panel A with arrows. Results are means ± standard deviations from three independent experiments, with 500 cells assessed per experiment.

4.1.7 UVB-induced apoptosis

4.2.1.1 UVB

UV radiation can generate free radicals and ROS, causing oxidative stress and cell death. UVB radiation was investigated as an alternative trigger of apoptosis in HeLa cells. The cells were exposed to various doses of UVB irradiation and then cultured for up to six hours. The cells were fixed 0, 2, 4, and 6 hours after UVB irradiation and the induction of nuclear fragmentation was determined (Figure 4.4).

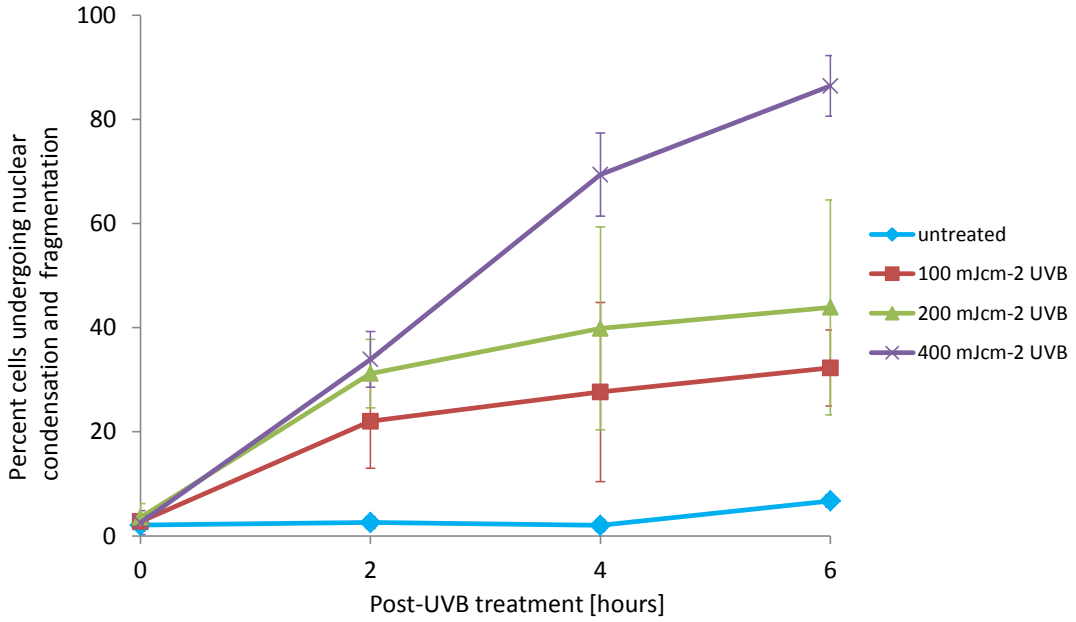

Figure 4.4 Apoptosis-associated nuclear fragmentation induced in HeLa cells by various doses of UVB irradiation.
Exponentially growing subconfluent HeLa cells were subjected to the UVB doses shown in the legend and then re-cultured. Quantitative analysis of apoptosis was assessed after cells were cultured for up to 6 hours cells following UVB-exposure. Cells were fixed and stained with DAPI to reveal their nuclear morphology. Results are means ± standard deviation for three independent experiments , with 500 cells assessed per experiment.

The condensation and fragmentation of the nuclei was dependent upon the dose of UVB irradiation. Initially the no more than 7% of the cells showed the characteristic apoptosis-associated nuclear morphology (as shown in Figure 4.3B indicated by white arrows; shrinkage, nuclear fragmentation); however, the percentage of cells affected increased with time post-exposure and this was dependent on the dose of

UVB (Figure 4.4), with higher doses inducing more cells to undergo morphological changes.

This method of induction of apoptosis was not taken further in the study due to the risk of photo bleaching of the roGFP2 protein [123, 124]. As roGFP2 is based on the enhanced GFP (eGFP) protein, it has been shown that this might not affect the 405/488 ratio but to avoid the complications of low signal/high background noise alternative methods of apoptosis stimulation were used when continuing this study [124].

As HeLa cells are deficient in death receptors such as Fas-receptor or TNF-a Related Apoptosis Inducing Ligand (TRAIL)-receptor, these cells need to be first sensitised with a drug prior to the addition of Fas-ligand or TRAIL [125]. This sensitisation would make it difficult to establish whether the redox potential changed in response to the extrinsic inducer of apoptosis or the sensitisation with the drug, which would not be a true representation of redox potential change.

Having established the time window and method to induce apoptosis in HeLa cells, the activation of caspase-3 and caspase-7 during apoptosis in conjunction with monitoring changes in the redox potential was established.

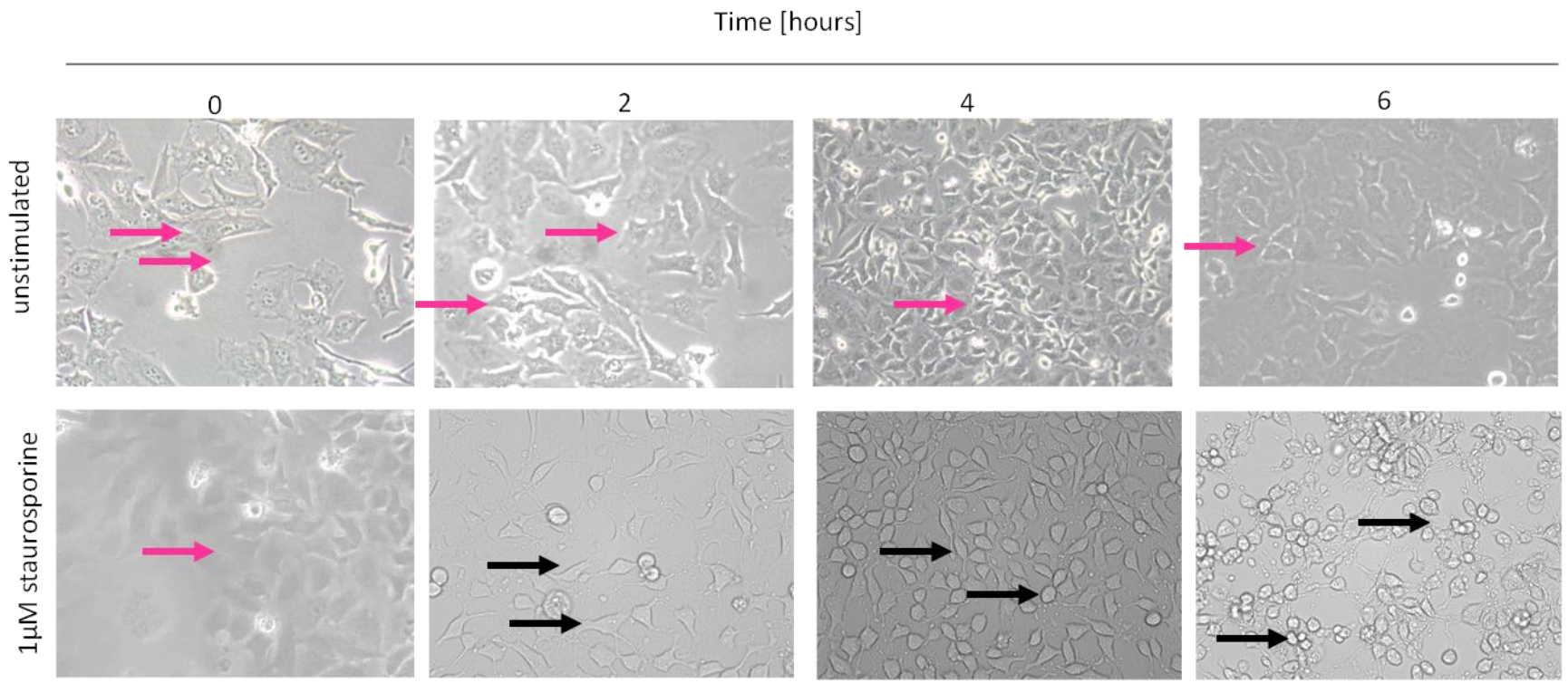

Figure 4.5 Morphological changes in HeLa cells undergoing staurosporine-induced apoptosis
Morphology of HeLa cells cultured alone (top row) or with staurosporine (1µM, bottom row) for periods up to 6 hours recorded using an inverted phase-contrast microscope. In the unstimulated cells no difference in cell shape was observed. The pink arrows show example of HeLa cells, which are not undergoing any morphological change. Cells are spread, attached to the bottom of the culture flask. Cells treated with staurosporine showed progressive shrinkage and development of apoptotic bodies throughout the course of apoptotic progression as indicated by black arrows. Representative images from three independent experiments.

4.1.8 Activation of effector caspases: caspase-3 and caspase-7 in real time

Caspase-3 is the major effector caspase, synthesised as an inactive zymogen. The caspase-3 zymogen is cleaved at the aspartate residues by caspase-9 or caspase-8 resulting in the removal of the pro-peptide sequence and separation of the two subunits, p17 and p12. The removal of the pro-domain promotes the protein's structural rearrangement and increases its enzymatic activity. The two subunits dimerise to form an active caspase-3 enzyme [126, 127].

Caspase-3 recognises the tetra-peptide motif Asp-x-x-Asp and cleaves C-terminal to the 4^{th} residue. In this study, real time activation of caspase-3 was investigated in order to confirm the induction of mitochondria-mediated apoptosis. Activation of effector caspase-3 is an important marker of a cell's commitment to programmed cell death.

To monitor real time caspase-3 activity, and relate these results to the redox potential in further experiments, Caspase-3 CellEvent™ Caspase-3/-7 Green Detection Reagent was used, which consists of a four amino acid peptide Asp-Glu-Val-Asp (DEVD) conjugated to a nucleic acid binding dye. Upon progression of apoptosis the DEVD sequence is cleaved from the dye, this allows the dye to migrate to the nucleus and bind to DNA, leading to activation of fluorescence at an absorption/emission maxima of ~502/530 nm. The fluorescent signal increases relative to the activity of caspases- 3 and -7 as the DEVD sequence is a preferential sequence for these two caspases.

Treatment of HeLa cells with staurosporine resulted in increased caspase-3/-7 activity from basal levels of 9.8%±1.8% to 41.5% and 93.9% after 2 hours and 3 hours, respectively. The increase in enzyme activity was first observed at 2 hours after staurosporine treatment (Figure 4.6).

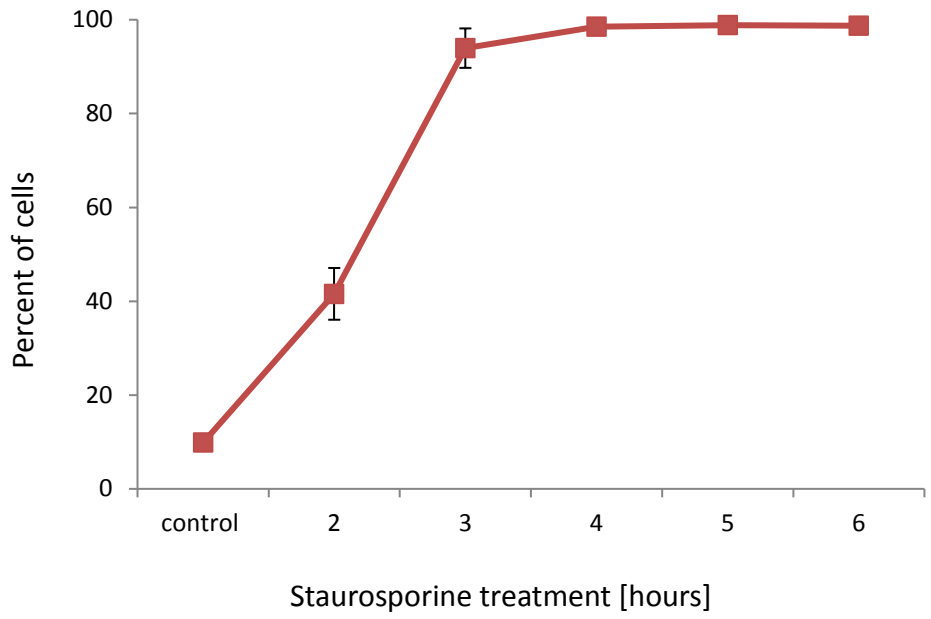

Figure 4.6 Caspase-3/7 activity in HeLa cells treated with staurosporine
Exponentially growing sub-confluent HeLa cells were cultured with staurosporine (1µM) for the indicated time periods and harvested. Cells were stained with CellEvent Caspase 3/7 Green reagent and fluorescence was detected by flow cytometry. Results are means ± standard deviations for three independent experiments.

Because the excitation and emission spectra of roGFP2 and the caspase-3/7 detection reagent overlap, western blotting analysis was employed to compare the activity of caspase 3 between HeLa and HeLa-roGFP2 cell lines (Figure 4.7). The caspase-3 antibody used in western blotting detects endogenous levels of the inactive caspase-3, as well as p17 kDa subunit and 19 kDa form of cleaved caspase-3 as well as inactive. Western blotting for caspase-3 protein showed that HeLa and HeLa-roGFP2 cells had similar responses. Densitometry analysis confirmed that the cell death process was not grossly affected by transfection of HeLa cells with roGFP2.

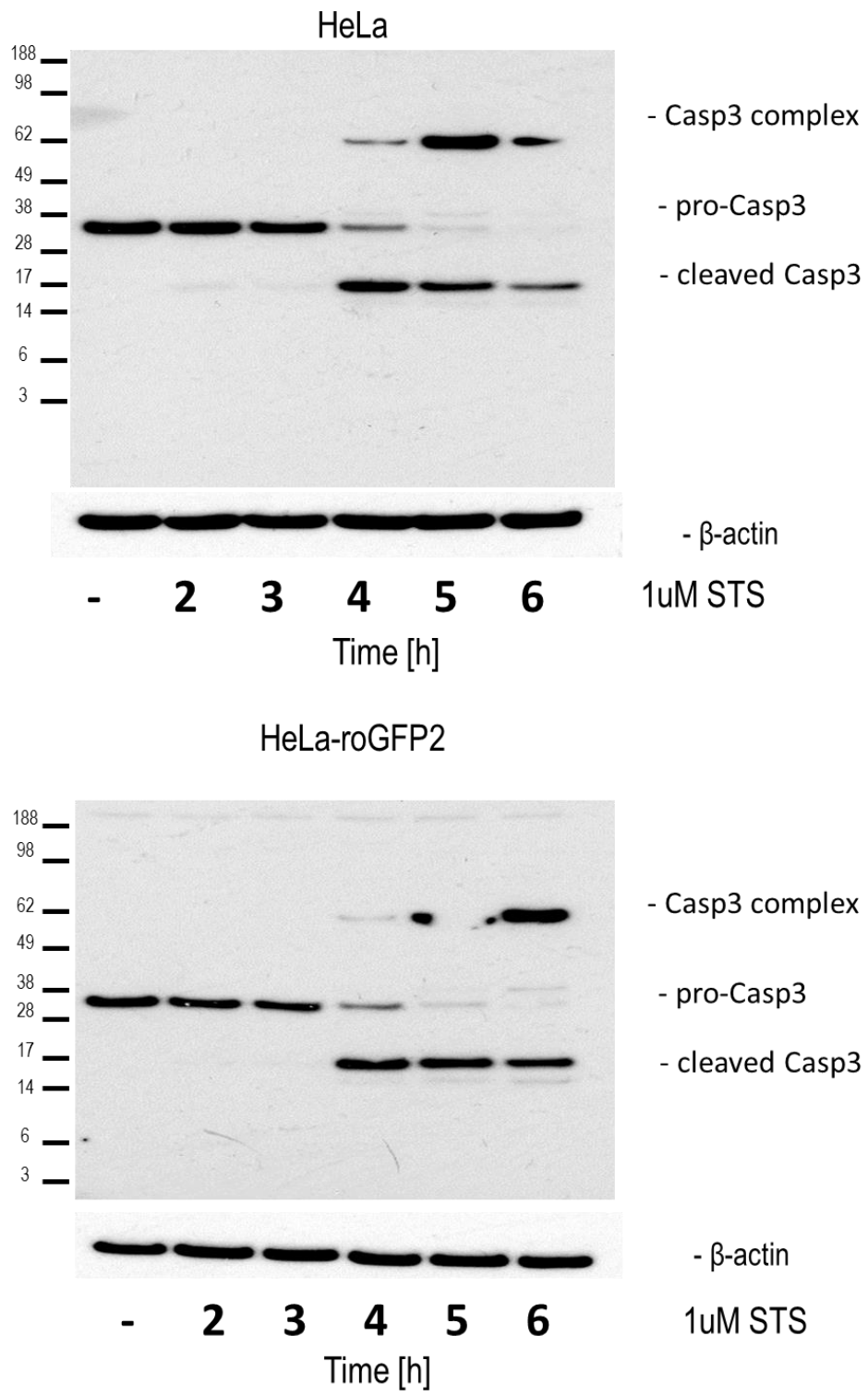

Figure 4.7 Caspase-3 activity in HeLa and HeLa-roGFP2 cells

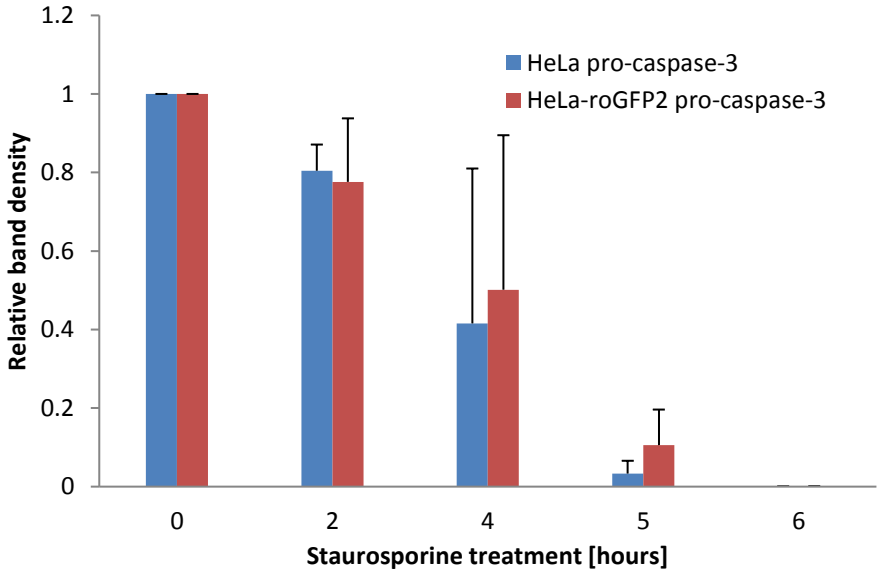

Figure 4.7 continued. Caspase-3 activity in HeLa and HeLa-roGFP2 cells

Western blot analysis for the detection of pro-caspase-3 and its cleaved fragments in whole cell HeLa extracts after exposure to staurosporine (1µM) for the indicated time periods. Densitometry analysis of pro-caspase-3 was performed using ImageJ software; all data points were normalised to 0 time point. Beta-actin was used as a loading control. Results are representative of 2 independent experiments.

4.1.9 Assessment of cell membrane integrity and phospholipid symmetry

One of the hallmarks of apoptosis is phosphatidyl serine (PS) exposure, which precedes plasma membrane rupture. In healthy, quiescent cells PS is non-randomly distributed to the inner leaflet of the plasma membrane by an amino-phospholipid translocase. However, upon induction of apoptosis this enzyme loses its activity and as a consequence, asymmetrical phospholipid distribution becomes altered and PS is exposed on the cell surface [128].

This exposure allows Annexin V (AxV), one of a family of calcium-dependent phospholipid-binding proteins, to bind to the exposed PS in a calcium-dependent manner (Figure 4.8), and, as a result, induce phagocytosis. Phagocytosis of apoptotic cells is driven by many points of recognition between phagocytes and the apoptotic cells as there are multiple PS-binding proteins. This PS exposure is assumed to be a limiting factor for any inflammatory response [129, 130].

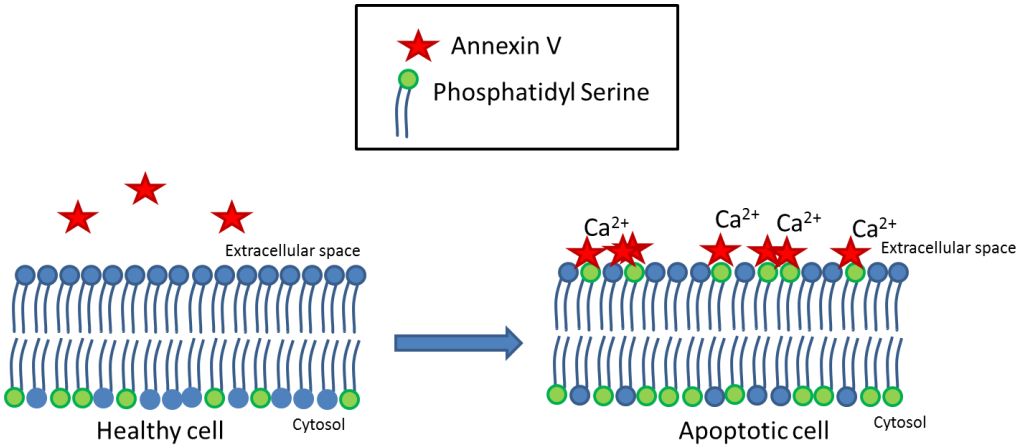

Figure 4.8 Scheme of phosphatidyl serine exposure and Ca^{2+}- dependent Annexin V binding.

Annexin V can be conjugated to one of the fluorescent tags, such as FITC or PerCP Cy 5.5, making it a useful tool for assessment of apoptosis. It is often used in combination with DNA-binding dyes tagged with different orthogonal fluorescent conjugates, to assess the stage of apoptosis in a population of cells.

Thus AxV-binding was used here to assess a further hallmark of apoptosis. It was used in conjunction with the DNA-binding dye, propidium iodide (PI), which can only enter

cells in which the plasma membrane is porous, thereby allowing discrimination of non-apoptotic (AxV-/PI-), early apoptotic (AxV+/PI-), late stage apoptotic/necrotic (AxV+/PI+) and necrotic (AxV-/PI+) subpopulations.

Results indicate that cells treated with 1µM staurosporine (38%±9.5%) were in early apoptosis (AxV+/PI-) after 2 hours of apoptosis induction (Figure 4.9). 43% of cells were in early apoptotic stage at 4 hours staurosporine treatment and this increased throughout the time course of apoptosis. There was no apparent evidence of necrosis in any of the time points, as there were no cells in AxV-/PI+ quadrant. This indicates that AxV/PI are a suitable measure of apoptosis in HeLa cells.

A.

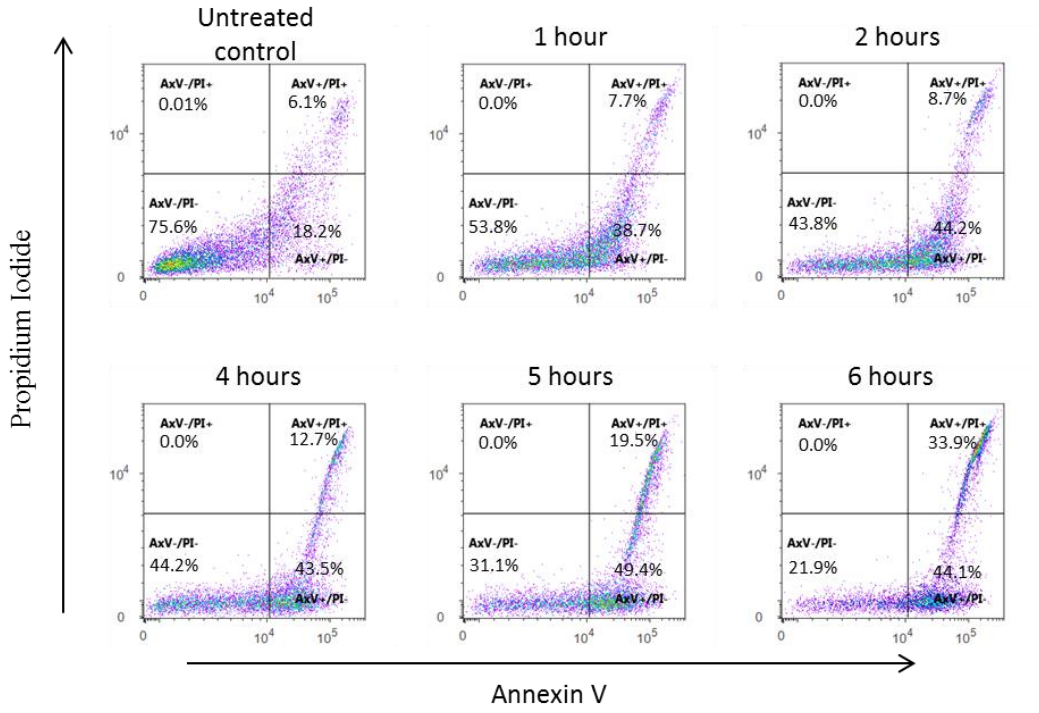

B.

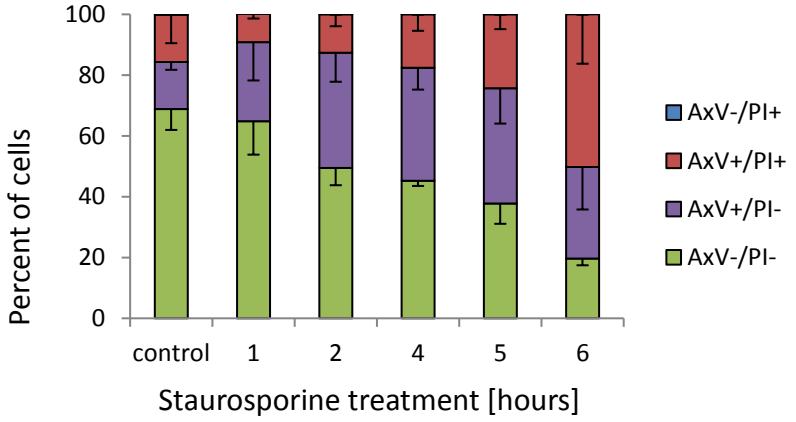

Figure 4.9 Analysis of staurosporine-induced apoptosis in HeLa cells by flow cytometry of annexin V and propidium iodide binding. Upper panel (A) shows representative dual parameter fluorescence dot plots of cell binding of FITC-labelled annexin V and propidium iodide over 6 hours culture with staurosporine (1 μM). Lower panel (B): Summary of results (dot plot quadrant percentages, mean and SD) from three experiments. The population of necrotic cells (AxV-/PI+) varied between 0% and 0.01% thus it is not seen at the summary diagram.

As HeLa cells are adherent cells they may expose phosphatidyl serine upon trypsinisation thus become false positive for AxV binding. It was therefore important to eliminate false positive populations of cells. Caspase-3/-7 and PI co-staining was used to investigate whether the cells were apoptotic and/or necrotic. PI only staining indicates that cells are necrotic, which were not observed in this study throughout the time-course of staurosporine treatment. Healthy cells with intact membrane undergoing apoptosis first become Caspase-3/-7 positive, followed by PI binding to the DNA once the cell membrane has disintegrated. This can be observed in Figure 4.10 where after 2 hours 15.6% of the population is Caspase3/7 positive and PI negative (C+/PI-), following the trend of 57.1% after 2 hours through to 79.3% of cells in this quadrant after 6 hours of incubation with staurosporine.

A.

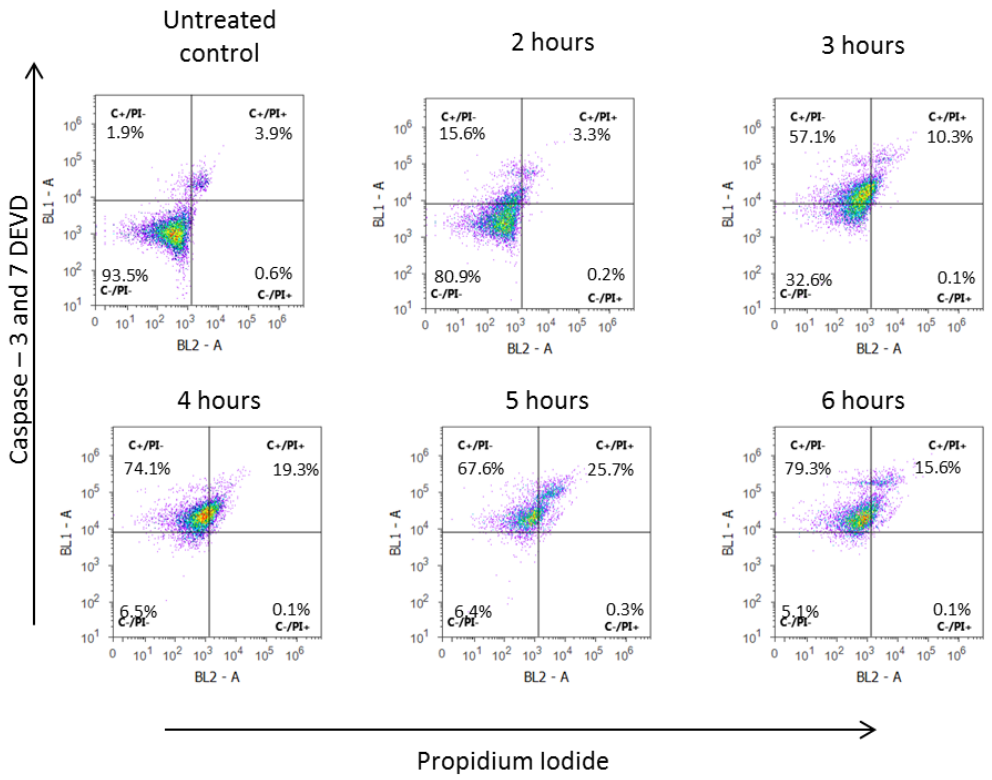

Figure 4.10 Caspase-3/7 activity (C) and propidium iodide (PI) co-staining of HeLa cells undergoing staurosporine-induced apoptosis.

B.

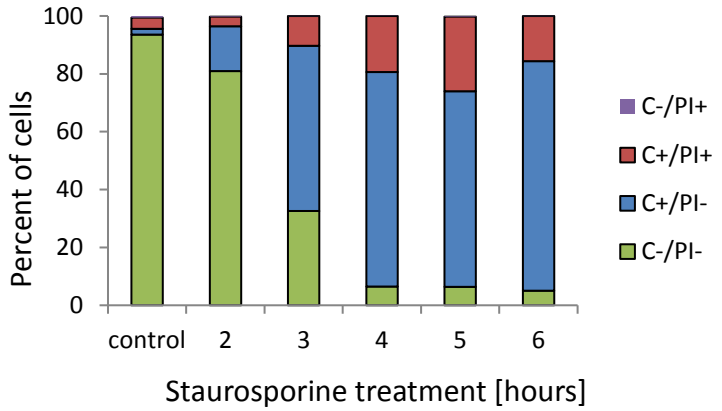

Figure 4.10 continued Caspase-3/7 activity (C) and propidium iodide (PI) co-staining of HeLa cells undergoing staurosporine-induced apoptosis.
HeLa cell binding of CellEvent caspase 3/7 green reagent and PI over 6 hours culture with staurosporine (1 μM). Upper panel (A) shows dual parameter fluorescent dot plots data and a summary of the quadrant data is given in (B). Blue rectangles: C(+), PI(-); red: C(+), PI(+); green: C(-), PI(-); violet: C(-), PI(+).

Results shown in Figure 4.10 indicate that the cells were undergoing apoptosis: 93.5% of cells were caspase 3/7 and PI negative at time zero, which then shifted towards activation of caspases. 74.1% of cells were caspase-3/7 positive after four hours of exposure to staurosporine. This is in line with annexin V/PI staining, and also shows that the majority of the population is in the later stages of apoptosis after four hours.

From the onset of staurosporine exposure, the population of double positive (C+/PI+) cells, demonstrated a linear and rapid increase, with c.3 % observed at 2 hours and reaching 26 % by 5 hours, whereas at 6 hours the same subpopulation was reduced from 26 % to 16 % of cells. The observed trend might be due to cells processing through the steps of staining and preparation to flow cytometric analysis. As dead cells are easily disrupted with centrifugation steps, this may affect the overall percentage of cells at five and six hours of treatment. This indicates that cells at 6 hour time point are very fragile and dead rather than apoptotic.

4.1.10 Detection of mitochondrial membrane potential ($\Delta\Psi_m$)

An upstream event in apoptosis, by many considered as a point of no return [131], is mitochondrial membrane permeabilisation and the precedes executioner, caspase-

dependent phase of apoptosis. Once the cell undergoes a significant amount of mitochondrial depolarisation it is committed to apoptosis by activating a cascade of proteolytic enzymes.

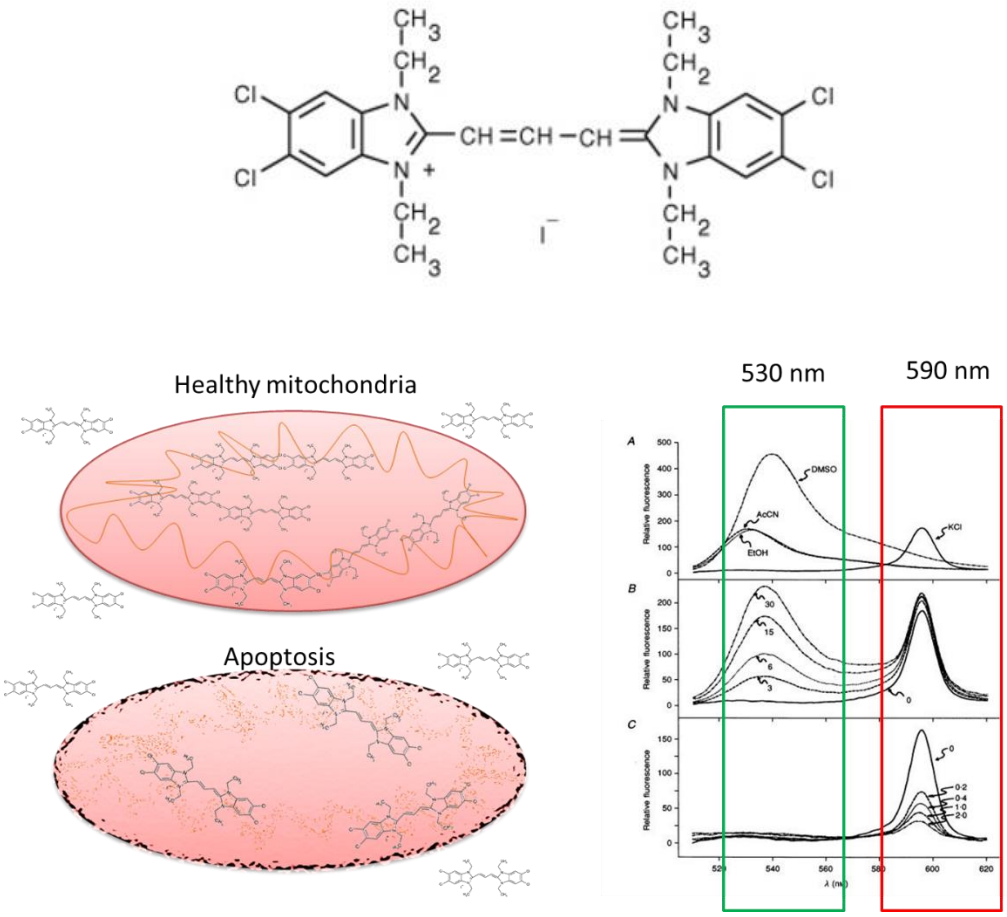

Figure 4.11 1H-Benzimidazolium, 5,6-dichloro-2-[3-(5,6-dichloro-1,3-diethyl-1,3-dihydro-2H-benzimidazol-2-ylidene)-1-propenyl]-1,3-diethyl-, iodide (JC-1).
Spectra of the JC-1 compound adapted from Di Lisa *et al.* [132]

In viable cells, the cationic lipophilic j-aggregate forming dye, JC-1 (Figure 4.11), accumulates in mitochondria upon polarisation and in the cytoplasm. In mitochondria it emits orange-red light and in the cytoplasm it forms monomers, which emit green fluorescence. Upon mitochondrial depolarisation of the mitochondrial membrane during apoptosis, JC-1 leaves the mitochondria and in the cytoplasm the dye forms monomers which emit green fluorescence [133]. In healthy cells, positive fluorescence in both channels is observed. Upon progression through apoptosis, loss of membrane potential

results in loss of red fluorescence and appearance of green fluorescence. The results were expressed as percentage of total events (Figure 4.12).

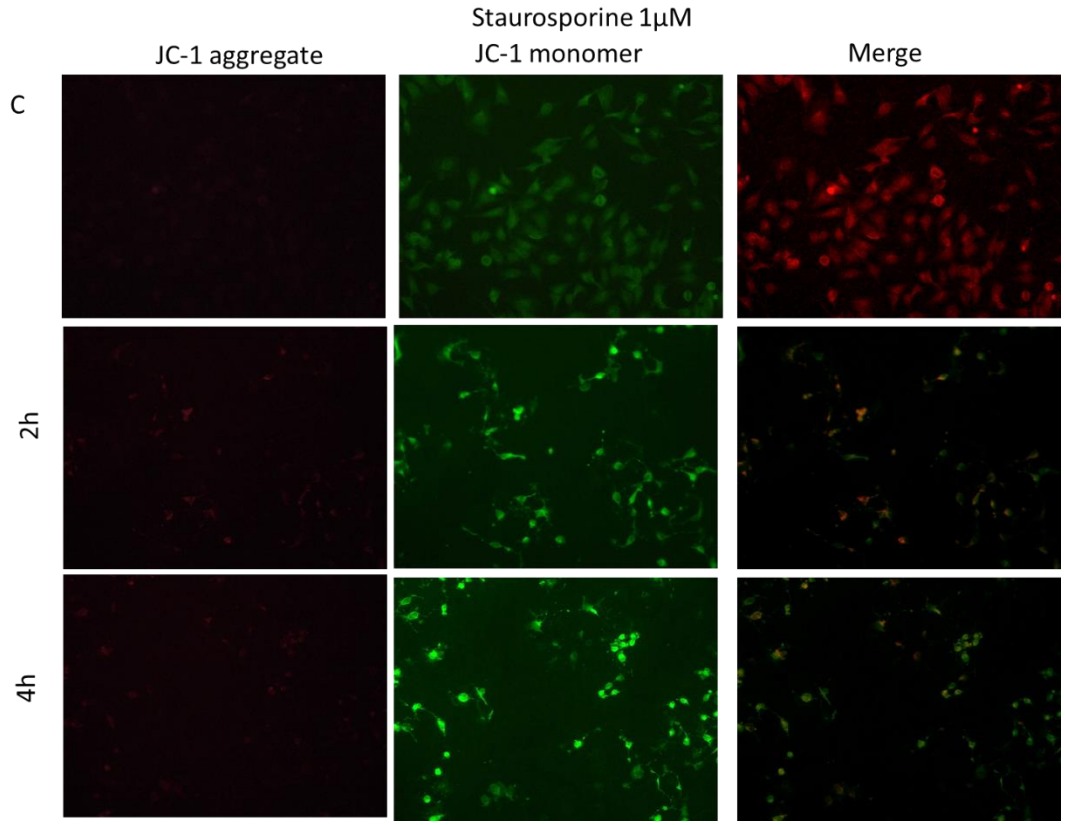

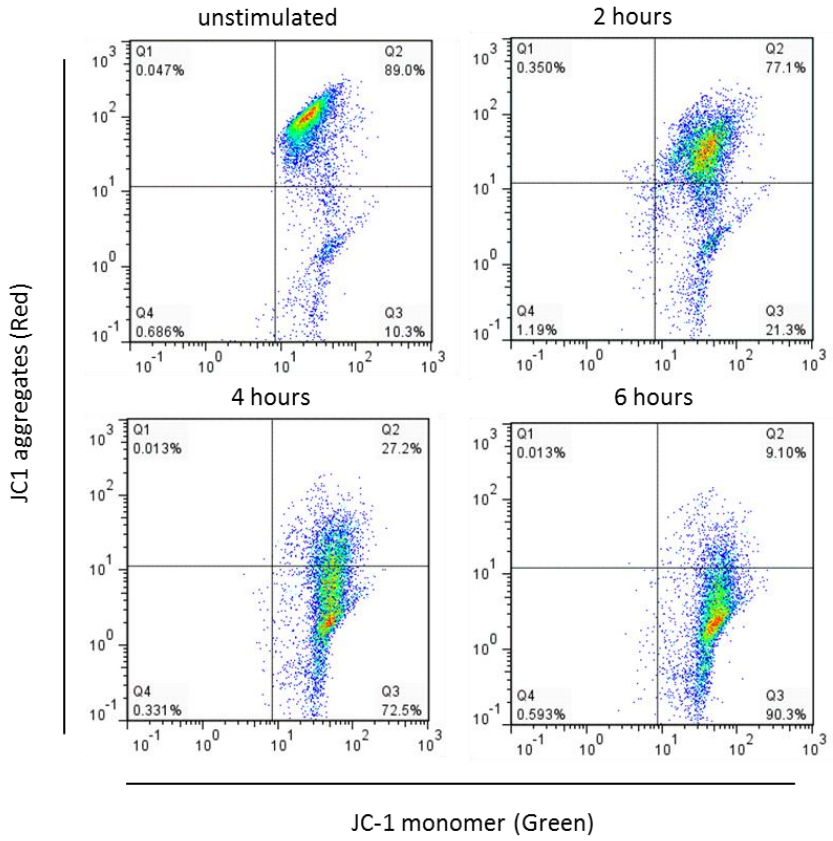

Figure 4.12 Changes in mitochondrial membrane potential of HeLa cells following culture with staurosporine.

Cells were cultured with staurosporine (1 μM) for 6 hours and samples were taken at various intervals for flow cytometric analysis. Flow cytometry was performed on stained cells. Briefly, cells were treated with 1 μM staurosporine for indicated times and then working solutions of JC-1 were added. Approximately 10,000 events were analysed for mitochondrial depolarisation at excitation of 488 nm and emissions at 590 nm (J-aggregates) or 535 nm (monomers). Data was analysed using FlowJo software.

As can be seen from Figure 4.12, a continuous reduction in the red/green fluorescence intensity ratio which is associated with mitochondrial membrane potential occurred over 6 hours in cells treated with staurosporine. Before staurosporine treatment 89 % of the cells were double positive, with 10 % of cells with depolarised mitochondria Two hours post staurosporine treatment, approx. 10 % of the cells lost their membrane potential, and more and more cells lost their potential over time, until, after 6 hours of staurosporine treatment, 90.3 % of the cells had depolarised mitochondria.

Despite its value, several disadvantages have been reported such as, that JC-1 is better suited for end-point measurements, given the time it takes to equilibrate between non-

aggregated and aggregated forms. In addition, this process is not usually dynamically reversible, and thus not allowing for future time-resolved measurements. Another drawback of using JC-1 is its false-positive/spurious binding outside mitochondria; this might cause a false positive change that is responsive to plasma membrane changes [134, 135].

For further investigation of the mitochondrial membrane potential, several fluorescent dyes were considered, however only tetramethylrhodamine methyl (TMRM) and ethyl esters (TMRE) were suitable for this study as they both are reversibly measures mitochondrial membrane polarisation. Although both TMRE and TMRM are rhodamine-based, TMRM is slower than TMRE to reach equilibrium across an electrochemical gradient, requiring a few seconds to a minute longer, however TMRE has been reported to be a more potent inhibitor of mitochondrial respiration than TMRM [124]. Therefore TMRM was chosen to be used in this study.

Both TMRM and roGFP2 are excited by the 488 nm laser line. The laser line has three emission filters: 510 nm (green), 570 nm (yellow/orange), and 670 nm (red/far red). Compensation of the two channels, where one dye does not leak to the other channel, was performed before each experiment. The emission wavelength of the TMRM dye was measured with a 573 nm emission filter, this did not interfere with the emission wavelength of the roGFP2 protein (535nm) in the green channel of the flow cytometry multiplexing experiments.

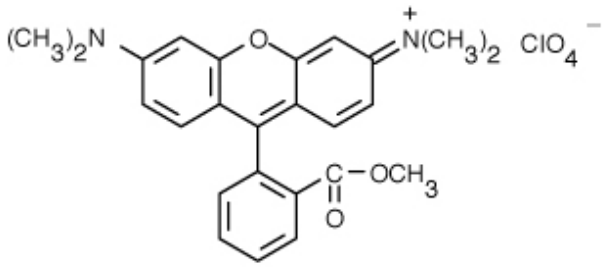

Figure 4.13 Tetramethylrodamine, Methyl Ester, Perchlorate (TMRM)

This cationic lipophilic dye enters the cell in a form of a methyl ester that is hydrolysed and converted to tetramethylrhodamine, which can accumulate in the negatively charged mitochondrial matrix upon mitochondrial polarisation or depolarisation. To

enable a comparison between experiments the cell culture conditions (buffers, temperature and sample preparation) used to measure the mitochondrial depolarisation with TMRM were the same as had been used when apoptosis was monitored with Annexin V.

Experimental control number	Percent of TMRM positive cells
1	30.6
2	59.3
3	83.0
4	46.5
5	89.5
6	81.1
7	79.9
Mean	67.1
SD	20.5

Table 4.1 Fluctuation of mitochondrial membrane potential in unstimulated HeLa-roGFP2 cells. TMRM positive control conditions (untreated with staurosporine). Individual data points taken from seven independent experiments.

Cells show variability in the levels of mitochondrial membrane polarisation between different stages of apoptosis therefore it was important to make sure that they were harvested from the log phase of growth (Table 4.1). The experimental data showed that when cells were harvested at different confluency, the initial mitochondrial membrane potential differed between the control samples. This was also observed in previous studies of Morgan *et al*. who studied the redox potential and the dependability of redox potential value in relation to the density of cells [123].

When undertaking experiments that measure such a delicate parameter as the redox potential, one has to remember that the variability in redox potential between samples may occur due to experimental procedures. It has been shown previously that passage number, seeding density of cells, growth medium composition, mycoplasma infection, trypsinisation, and transfection of cells all influence the redox processes and the redox potential, thus one has to remember to keep experimental variability between experiments as low as possible [123].

The use of the TMRM reagent allows for time-resolved imaging, where pre-stained cells can be treated and the decrease in intensity is measured over time. When measuring redox potential and mitochondrial depolarisation, culture medium without phenol red was used, because of the auto-fluorescence of the dye [123][114]. In addition, it can also be the source of UV-induced cytotoxic species [124] that influence the cells' ability to undergo apoptosis. TMRM is a sensitive reagent that detects mitochondrial depolarisation quicker than JC-1 does. Hence, much shorter time points were needed to establish the period for the loss of mitochondrial depolarisation. Also, these studies will allow for establishment the sequence and correlation of redox potential change versus mitochondrial depolarisation.

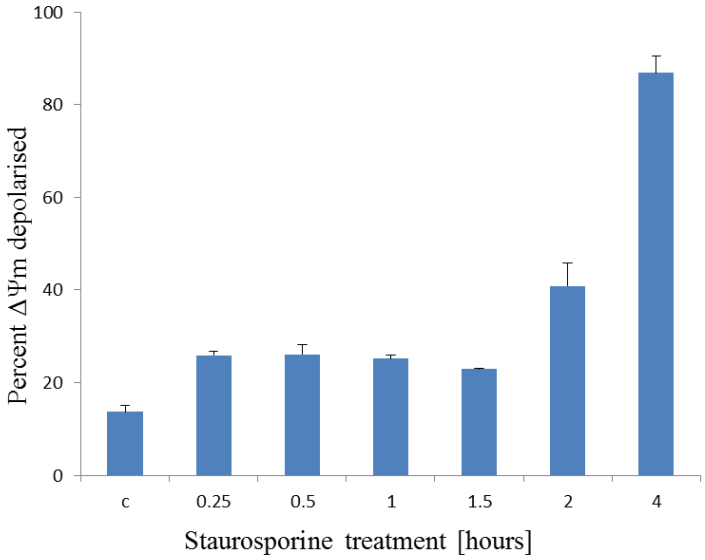

Figure 4.14 Changes in mitochondrial membrane potential measured with TMRM in HeLa-roGFP2 cells undergoing staurosporine-induced cell death time course measured in hours. First sample being control (c). Error bars indicate SEM of three independent experiments.

Mitochondrial depolarisation was detectable 15 minutes after exposure to staurosporine, when the proportion of cells with depolarised mitochondria had increased by 90% compared with untreated controls (Figure 4.14). Up until the two hour time point the variance of the means shows that the fluctuation is not statistically significant ($F(3,8)=3.306$, $p = 0.078$). The 2 hour time point marked a rapid increase in the

measured values (6.4-fold increase). By 4 hours mitochondria were depolarised in 86.8% ±3.7% of the cells. Previously reported fluctuations of mitochondrial swelling and contraction, are reported by Scarlett et al. [136].

4.1.11 Establishing the sequence of apoptotic events in HeLa cells

4.1.12 Annexin V binding to PS precedes caspase 3/7 activation

In order to establish the sequence of apoptotic events, each dye was compared with each other in the same cells. The sensitivity of the various assays needs to be taken into consideration when measuring the dynamics of the process and establishing the sequence of events.

This study shows that PS exposure precedes caspase 3/7 activation since 84% ± 3.37% of cells were active caspase 3/7 negative and annexin V negative in the untreated control, which is characteristic of healthy cells (Figure 4.15). Two hours after staurosporine treatment the population of cells had a similar distribution of cells in all quadrants: 32% of cells were caspase 3 positive and annexin V positive, while c.30% of cells were caspase 3 negative and annexin V positive. Furthermore, 11% of cells still remained caspase 3 positive and annexin V negative and 26.4% of cells were caspase 3 negative and annexin V negative.

Combining various fluorescently tagged apoptotic markers allows for precision in determining the sequence of apoptotic events. However, one has to be careful to not over-interpret the results given that the sensitivity of various assays may differ.

A.

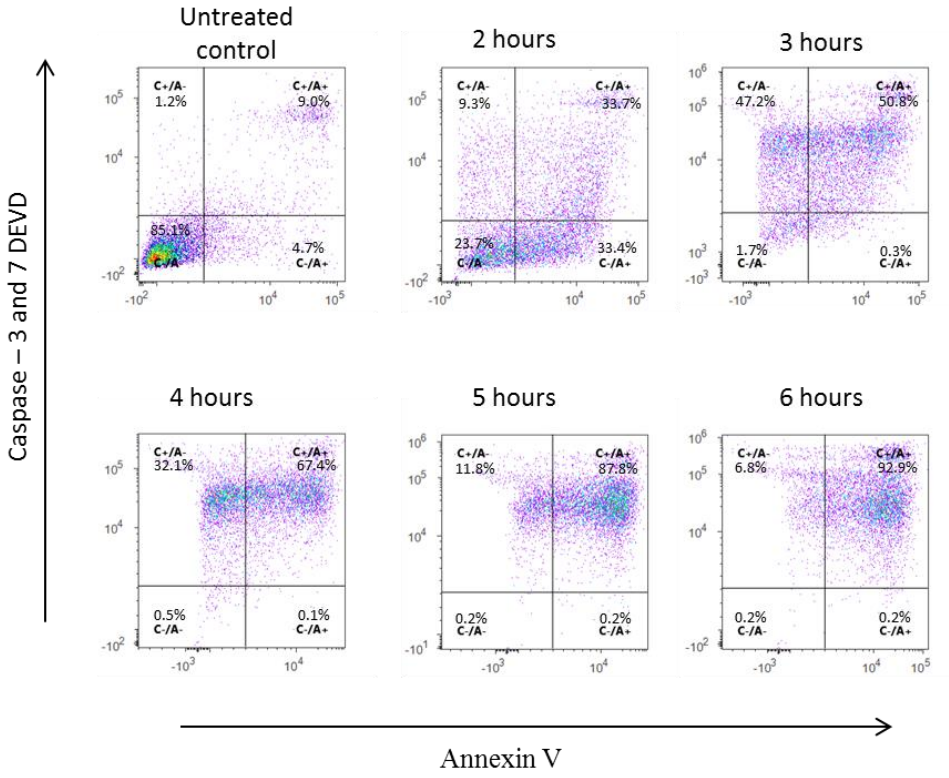

B.

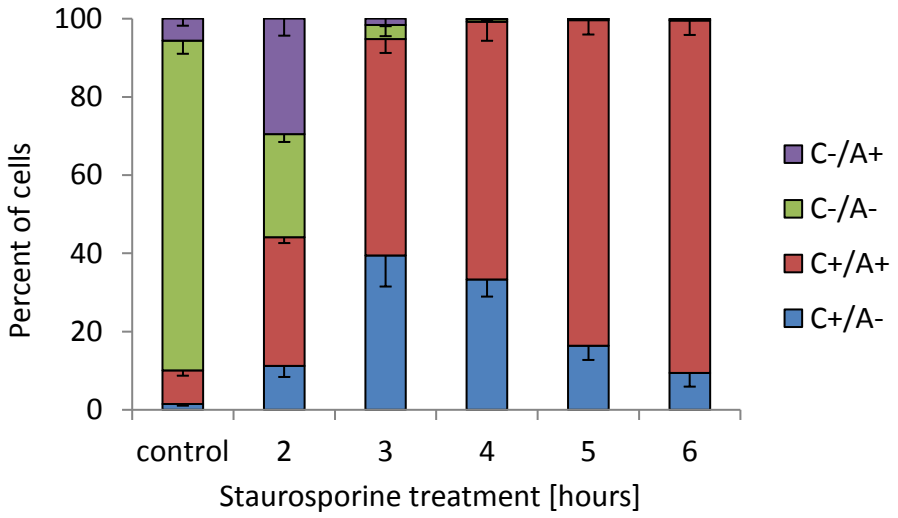

Figure 4.15 Activity of caspases 3 and 7 measured against annexin V binding in HeLa cells.

Cells were co-stained with Annexin V and Caspase- 3/-7 DEVD live cell stain following staurosporine treatment. Upper panel (A): representative dot plots of AxV/caspase3/7 staining. Lower panel (B): mean percent of cells averaged from three independent experiments. Bar chart summarises the tendency of cells' population. Caspase (C) and Annexin V (A).

4.1.13 Caspase 3 and 7 activity is preceded by mitochondrial depolarisation

Comparison of two datasets: showing annexin V and caspase 3 activities, suggests that annexin V staining precedes caspase 3 activation at the 2 hour time point. At subsequent time points a clear trajectory was observed, where the already dominant C+/A+ segment of cells was further populated by AxV+ cells. At the terminal time point of 6 hours, the overall majority of cells (90.1%) were found in the C+/A+ quadrant, with 9.4% C+/A- and the residual 0.5% were shared between the other two quadrants.

A.

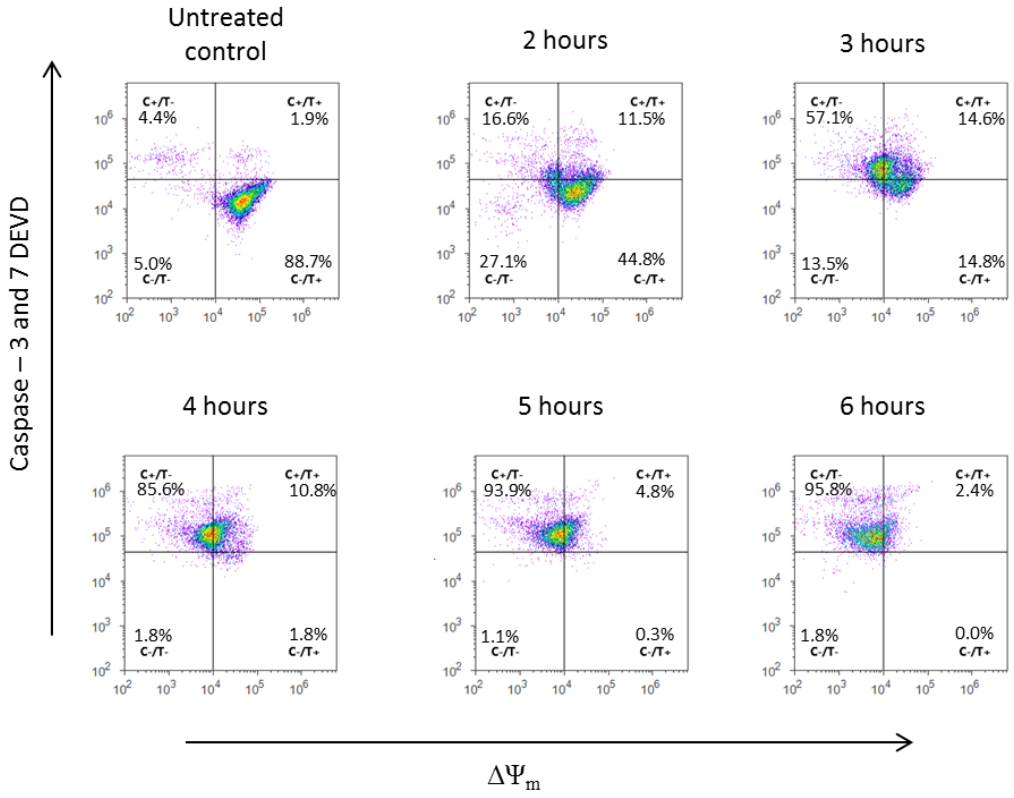

Figure 4.16 Caspase-3/7 activity (C) and mitochondrial depolarisation (T) co-staining of HeLa cells undergoing staurosporine induced cell death.

B.

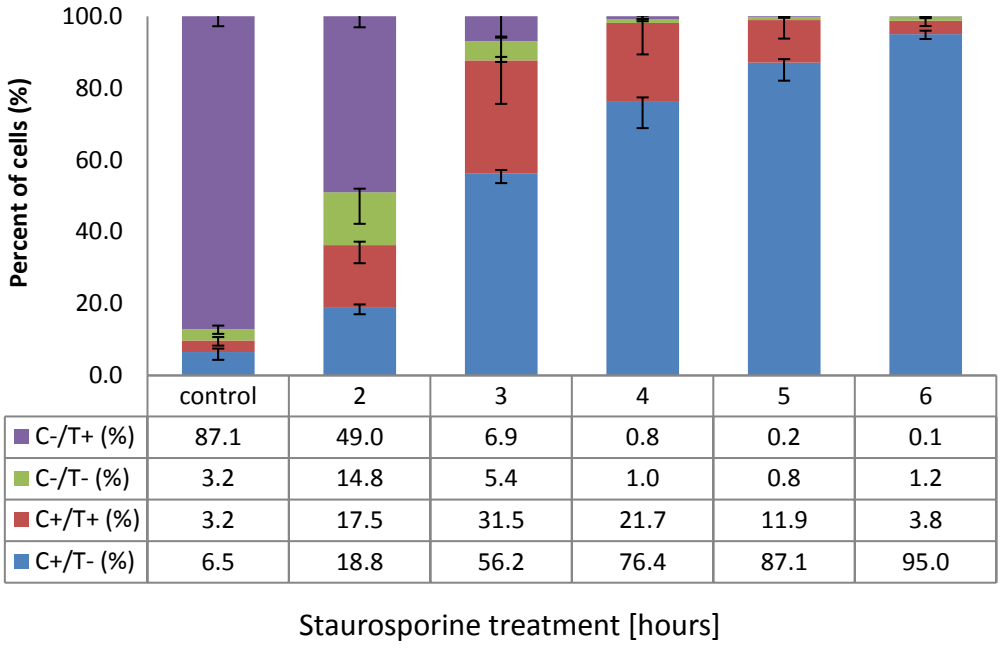

	control	2	3	4	5	6
C-/T+ (%)	87.1	49.0	6.9	0.8	0.2	0.1
C-/T- (%)	3.2	14.8	5.4	1.0	0.8	1.2
C+/T+ (%)	3.2	17.5	31.5	21.7	11.9	3.8
C+/T- (%)	6.5	18.8	56.2	76.4	87.1	95.0

Staurosporine treatment [hours]

FIGURE 4.16 continued Caspase-3/7 activity (C) and mitochondrial depolarisation (T) co-staining of HeLa cells undergoing staurosporine induced cell death.
Analysis of the effect of 1µM staurosporine on progression through cell death by flow cytometry using cells co-stained with caspase-3 (C) and TMRM (T). The upper panel (A) shows representative data and the lower panel (B) summarises the experiment in a bar chart. Blue rectangles: caspase positive (C+), TMRM negative (T-); red rectangles: C(+), T(+); green rectangles: C(-), T(-); violet rectangles: C(-), T(+).

Figure 4.16 shows clearly that cells with depolarised mitochondria and active caspase -3 were observed by 3 hour post-staurosporine exposure. However, the data suggests that the mitochondrial depolarisation precedes caspase -3/ -7 activity which is in line with the literature which reports that the activity of caspase -3/ -7 (effector caspases) is preceded by the loss in mitochondrial membrane potential [137].

4.1.14 Mitochondrial depolarisation precedes Annexin V binding to PS

Characteristic morphological and biochemical changes distinguish apoptosis from necrosis. In viable cells PS is located in the innerspace of the cell membrane, however upon loss of the membrane symmetry, the PS is exposed to extracellular space allowing Annexin V binding. High mitochondrial membrane potential is characteristic to healthy cells and it diminishes while cells undergo apoptotic changes. In order to confirm the sequence of events the phosphatidyl serine exposure and mitochondrial depolarisation were measured [138]. To date it is not clear what exact mechanism causes phosphatidyl serine residues to be exposed at the surface of apoptotic cell, however studies from C. elegans suggest that this is the direct consequence of caspase cleavage. Since caspase activity os direct consequence of mitochondrial depolarisation it is suggested that the Annexin V will follow the mitochondrial depolarisation [138].

A healthy HeLa population is characterised by the dominance of cells with a strong TMRM signal, pinpointing active and polarised mitochondria, and absence of PS from the cell surface. Dominance of such cells is seen in untreated and STS-exposed samples, treated for 1 hour (Figure 4.17, lower panel). Following 1 hour exposure to STS, Annexin V negative and TMRM positive cells (AxV-/T+) depleted from 64.6% down to 56.1%. During the following 5 hours the percentage of AxV-/T+ phenotype decreased progressively such that by 6 hours only 0.3% of the cells were AxV-/T+ indicating that mitochondrial depolarisation precedes the PS exposure in the first two hours of apoptosis triggered by staurosporine, following the trend and after six hours 74% of cells showed mitochondrial depolarisation and PS exposure.

After 2 hours, the rate of loss of the TMRM signal increased, indicating depolarisation of the mitochondria. After 6 hours 98.9% of cells demonstrated an absence of TMRM. At 4 hours, TMRM-negative cells in the majority were also AxV-negative (74%). It can be concluded that mitochondrial depolarisation, as a key step in apoptosis, is taking place first, followed by exposure of PS for AxV binding.

A.

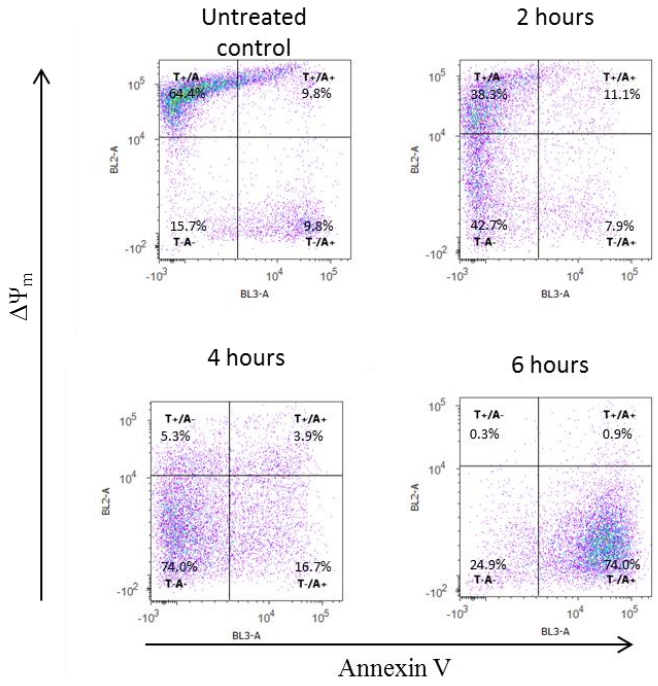

B.

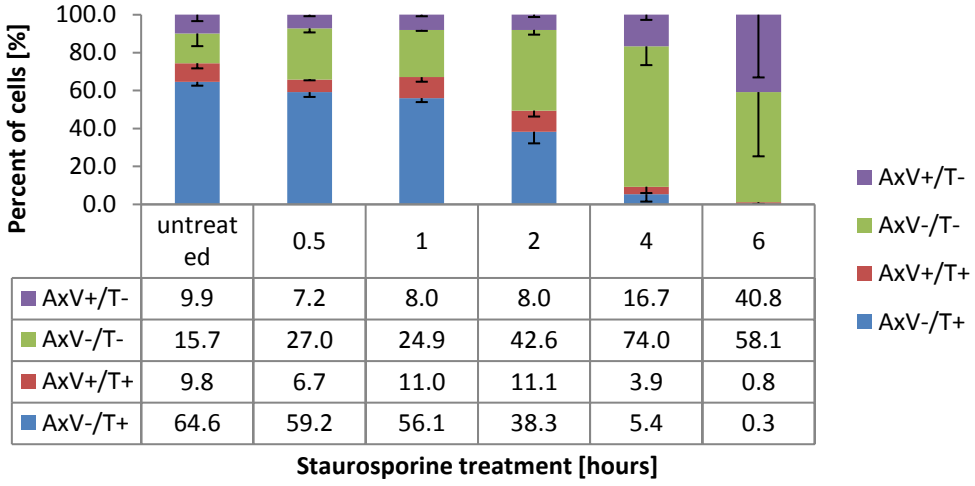

	untreated	0.5	1	2	4	6
AxV+/T-	9.9	7.2	8.0	8.0	16.7	40.8
AxV-/T-	15.7	27.0	24.9	42.6	74.0	58.1
AxV+/T+	9.8	6.7	11.0	11.1	3.9	0.8
AxV-/T+	64.6	59.2	56.1	38.3	5.4	0.3

Figure 4.17 Annexin V and mitochondrial depolarisation co-staining of HeLa cells undergoing staurosporine induced cell death.
Analysis of the effect of staurosporine on progression through cell death by flow cytometry assay using cells co-stained with caspase-3 and annexin V.

4.1.15 Redox potential change is preceded by Annexin V binding

It is still a matter of debate whether the redox potential is a cause or a consequence of apoptotic events. The work in this chapter investigated the redox status of the intracellular environment by monitoring the oxidation state of roGFP2 which has been stably transfected into the HeLa cells. In order to establish whether the shift of redox potential towards a more oxidative range, in cells undergoing apoptosis, is linked to other functional changes in the cell the comparison of redox potential with AxV, mitochondrial depolarisation, and caspase-3 activity was used.

A multiplexing experiment by flow cytometry recording simultaneously multi-parameters, including reduced and oxidised ratio of roGFP2 combined with other apoptotic hallmarks, for individual cells allowed for discrimination and determination of the sequence of events across the cell population. The data shown in Figure 4.18 confirmed the sequence of apoptotic events in HeLa and HeLa-roGFP2 cells.

A.

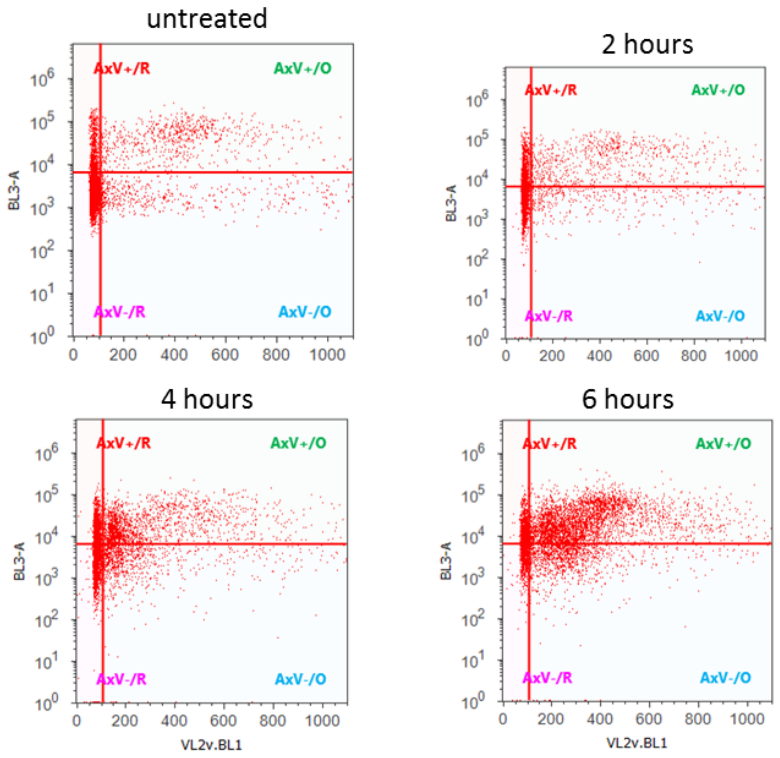

B.

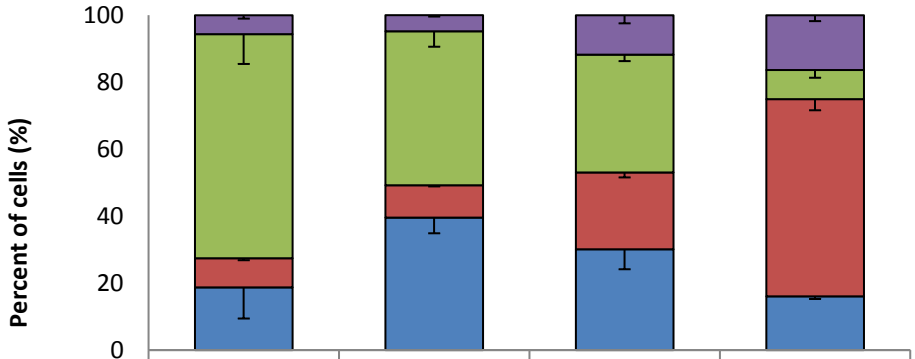

	untreated	2 h	4 h	6 h
AxV-/O (%)	5.7	4.8	11.7	16.4
AxV-/R (%)	66.9	46.0	35.2	8.7
AxV+/O (%)	8.7	9.7	23.0	58.9
AxV+/R (%)	18.7	39.5	30.1	16.0

Figure 4.18 Measurements of redox potential (R – reduced; O – oxidised) along with annexin V (AxV) binding in HeLa-roGFP2 cells treated with staurosporine for the indicated amount of time (hours). Dot plots (A) are a depiction of one experiment, whilst bar charts (B) are a depiction of three independent experiments and error bars indicate SEM.

Multi-parametric and simultaneous analysis of redox potential and AxV binding in HeLa-roGFP2 cells was performed at four time points (Figure 4.18). In the absence of staurosporine treatment, the cell population was dominated (66.9%) by cells not expressing phosphatidylserine (PS), indicating an AxV negative status, and being in a reduced state. The parametrically-opposite cell population, being AxV positive and in an oxidised state (A+/O), was represented by 8.7% of cells.

Two hours exposure to staurosporine markedly reduced the total pool of AxV-negative cells (from 72.6 % to 50.8%). However, the joint redox potential remained unaffected (85.6% in untreated samples and 85.5% after 2 hour exposure).

During the next four hours of exposure to staurosporine, a shift in cell distribution was observed. At 6 hours a 6.8-fold increase in AxV-positive and in oxidised state cells was noted, making this subset of cells the prevailing group (58.9%). Furthermore, after 6 hours the total number of cells demonstrating an oxidative status was 65.3%, a 4.5-fold increase in comparison to untreated samples.

4.1.16 Redox potential change is preceded by loss of mitochondrial membrane potential

To observe the progression of mitochondrial depolarisation as one of the central apoptotic events, in combination with changes in redox potential, a multiplexing study was performed (Figure 4.19). The untreated samples were dominated by cells with polarised mitochondria (TMRM-positive (T+)) and in a reduced state (73.7%), which is characteristic of a healthy cell. Whereas the contrary parameters (TMRM-negative (T-) and in oxidised state) were observed in 10.5% of cells in the same samples.

A.

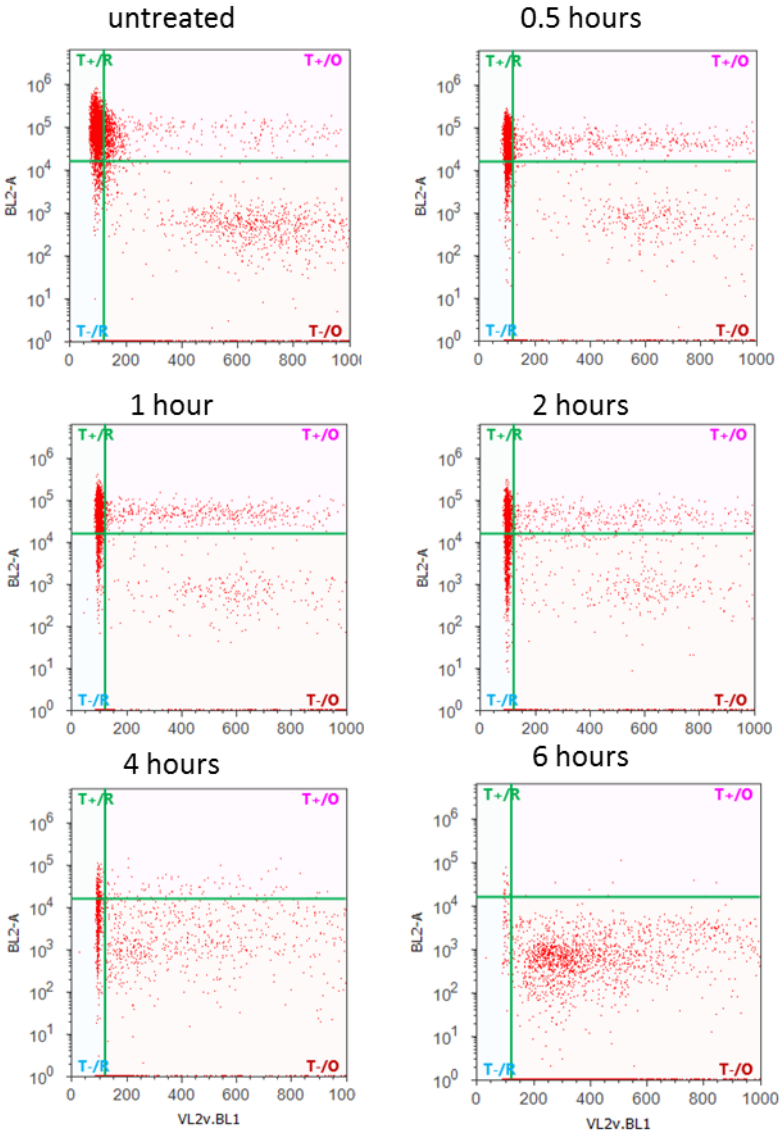

Figure 4.19 Redox potential (oxidised and reduced states) against mitochondrial depolarisation in HeLa–roGFP2 cells.

B.

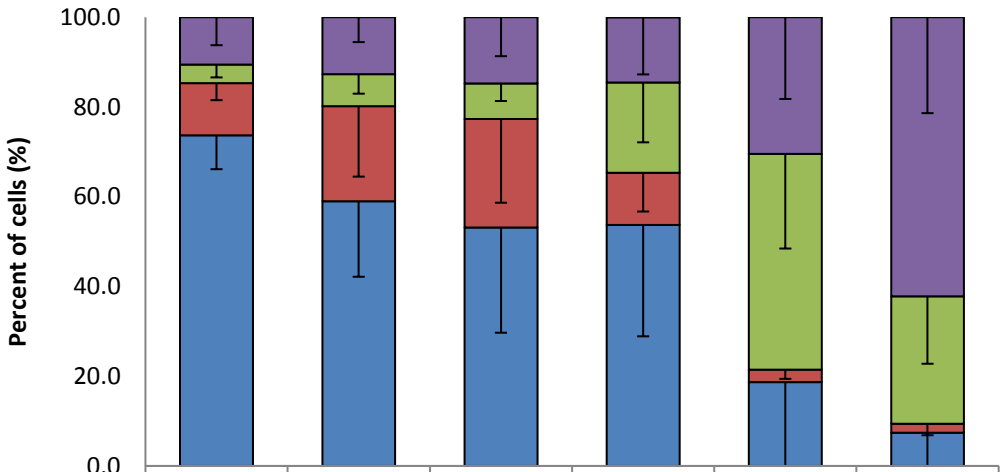

	untreated	0.5 h	1 h	2 h	4 h	6 h
T-/O (%)	10.5	12.7	14.8	14.5	30.4	62.2
T-/R (%)	4.2	7.2	7.9	20.2	48.1	28.4
T+/O (%)	11.6	21.1	24.2	11.6	2.8	2.0
T+/R (%)	73.7	59.0	53.1	53.7	18.7	7.4

FIGURE 4.19 continued. Redox potential (oxidised and reduced states) against mitochondrial depolarisation in HeLa–roGFP2 cells. Upper panel (A), an example of mitochondrial depolarisation and redox change in HeLa roGFP2. Lower panel (B), chart summary for three independent experiments. In untreated sample 73.7 % of cell population are in the TMRM positive and reduced range of redox potential quadrant. Upon induction of apoptosis by staurosporine there is a visual shift in trend of cells being still TMRM positive, but more oxidising range of redox potential, this trend prevailed until around 2 hour time point. After this time point cells with depolarised mitochondria and reductive redox potential range subsitised 48.1 % of the population while depolarised and oxidised range was 30.4 %. This trend prevailed through to the last time point where 28.4 % of the population was T-/R and 62.2 % were T-/O .

During the first 2 hours after exposure to 1µM staurosporine three analyses were performed (at 0.5, 1 and 2 hours). During this time a healthy cell phenotype (T+/R) was still dominant, but gradually reducing from 59% to 53% of the population. Concurrently, acceleration in mitochondrial depolarisation was also observed, where the population of T- cells in a reduced state underwent a 4.8-fold increase (from 4.2% in untreated samples to 20.2% at 2 hour point).

The most prominent shift from a healthy cell phenotype to the majority of cells with depolarised mitochondria (T-) occurred during the following 4 hours of exposure to 1 µM staurosporine. By the 4 hour time point, 78.5% of the cell population had

depolarised mitochondria, and by the 6 hour time point an oxidised sub-population with depolarised mitochondria were representing the majority of cells at 62.2%.

Summative analysis of T- (irrespective of redox status) and oxidised cells (irrespective of mitochondria's status) showed that T- cells were starting to dominate (≥ 50%) the cell pool at the 4 hour time point, and oxidised cells (O) became dominant at the 6 hour time point. This observation identifies mitochondrial depolarisation as an earlier event than oxidation in the apoptosis cascade. The same observation was confirmed by analysis of individual, not multiplex, channels for T+/- and O/R (data not shown).

This observation indicates that the change in redox potential triggers the initial depolarisation of the mitochondria, however after the prolonged mitochondrial damage; the content from the mitochondria leaking to the cytoplasm might have changed the overall redox potential indicated by the change in the shift. The redox potential in the cells was being progressively oxidised.

4.1.17 Redox potential in HeLa-roGFP2 is independent of mitochondrial membrane depolarisation

In order to test the hypothesis that the redox potential is influenced by the loss of mitochondrial membrane potential, Bongkrekic acid (Figure 4.20) was used to inhibit mitochondrial permeability transition pore opening.

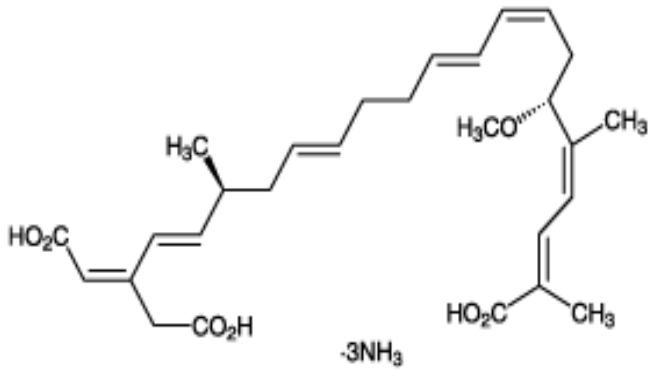

Figure 4.20 Bongkrekic acid scheme

Bongkrekic acid (BKA) is a specific ligand of adenine nucleotide translocase (a component of the mitochondrial permeability transition pore complex) and fixes its conformation in the m-state [128]. It prevents mitochondrial depolarization, swelling,

rupture of the mitochondrial outer membrane, and release of apoptogenic proteins such as cytochrome c. It has been used in various studies using staurosporine induced apoptosis in Jurkat cells or by hypochlorous acid in hepatoma HepG2 cells [139][129].

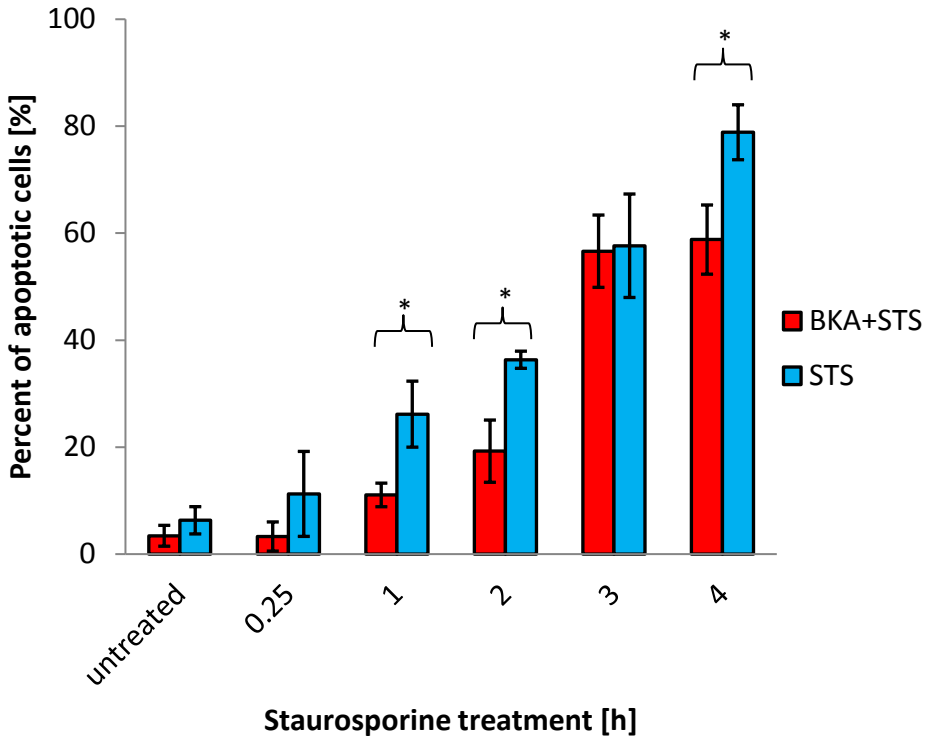

Figure 4.21 Nuclear fragmentation in cells pretreated with BKA or 1 µM staurosporine only in HeLa-roGFP2 cells. Where indicated, the cells were pretreated for 1 hour with bongkrekic acid (BKA, 100 µM), washed and then stimulated with staurosporine (1 µM).

During the first 2 hours of exposure to STS both BKA-pretreated and BKA-free HeLa cells transfected with roGFP2samples demonstrated a linear increase in apoptotic cell number, from 3.4% to 19.2% and from 6.3% to 36.3% at 0 and 2 hours, respctively . However the rates of increase were not the same due to the effect of BKA. Smaples not pre-treated with BKA demonstrated 3.4, 2.4 and 1.8-fold higher difference in the number of apoptotic cells at 15 minutes, 1 and 2 hours respectively.

In the following 2 to 4 hours apoptosis progressed promptly, with 58.8% of the BKA-pretreated cell population undergoing nuclear enevelope fragmentation at the 4 hour

timepoint, which represented a 3.1-fold increase in comparison to the 2 hour timepoint. At the same time, non-pretreated staurosporine only samples exhibited continued linear gowth trajectory in apoptotic cell numbers, representing 78.9% of cell population at 4 hours.

Rapid acceleration of nuclear envelope fragmentation after 2 hours of exposure to STS indicated a reduction in the apoptosis-protective properties of BKA (after 1 hour of pre-treatment). In addition, it is widely known that mitochondrial depolarisation happens before nuclear fragmentation in the apoptotic cascade. Therefore, this study showed that apoptosis is delayed after pre-treatment with BKA, this was due to a delay in mitochondrial depolarisation (Figure 4.21).

This data showed that nuclear fragmentation was delayed in the first two hours in cells pretreated with Bongkrekic acid: 19.2%±5.8% of cells were apoptotic, while 36.34%±1.6% cells were apoptotic in staurosporine only treated cells. This corresponds to 78.8%±5.13% of cells with a fragmented nucleus at 4 hours post-staurosporine treatment and 58.5%±9.6% of cells with Bongkrekic acid pretreatment.

4.1.18 Mitochondrial depolarisation in HeLa and HeLa-roGFP2

To gain a more accurate understanding of the timing of the apoptotic process in HeLa cells after roGFP2 transfection, apoptosis was triggered by STS and changes in the mitochondrial polarisation were assessed. In addition, it was important to see if the miotochondrial polarisation status, one of the key markers of apoptosis, was affected by the transfection. Therefore, HeLa and HeLa-roGFP2 were investigated.

Mitochondiral polarisation was assesed by tracking TMRM fluorescent signal loss after exposure to 1 µM STS for up to 3 hours (Figure 4.22). As in the above experiment, half of the samples were pre-treated with BKA for 1 hour.

After 15 minutes and 1 hour of exposure to STS, the variance of the means between parental HeLa and HeLa-roGFP2, with and without BKA pre-treatment, was equal across the four treatments, according to one-way ANOVA (15 minutes: $F(3,8)=2.52$, $p=0.132$; 1 hour: $F(3,8)=2.51$, $p=0.132$). However, at the 2 hour time point BKA pre-treatment had a significant effect on the mitochondrial depolarisation rate, both in

parental and roGFP2-transfected HeLa cells ($F(3,8)=10.01$, $p=0.004$), when compared to non-pretreated samples (HeLa: $p=0.025$; HeLa-roGFP2: $p=0.016$). Further comparison between HeLa and HeLa-roGFP2, at respective conditions, did not find significant differ at the 2 hour time point ($p=0.253$).

The observed results, taken together, confirmed the effect of BKA on mitochondrial depolarisation both in HeLa and HeLa-roGFP2. In addition, the close to identical response of parental and roGFP2-transfected cells to STS, as analysed through loss of TMRM, suggests that mitochondrial activity was not affected by roGFP2 transfection.

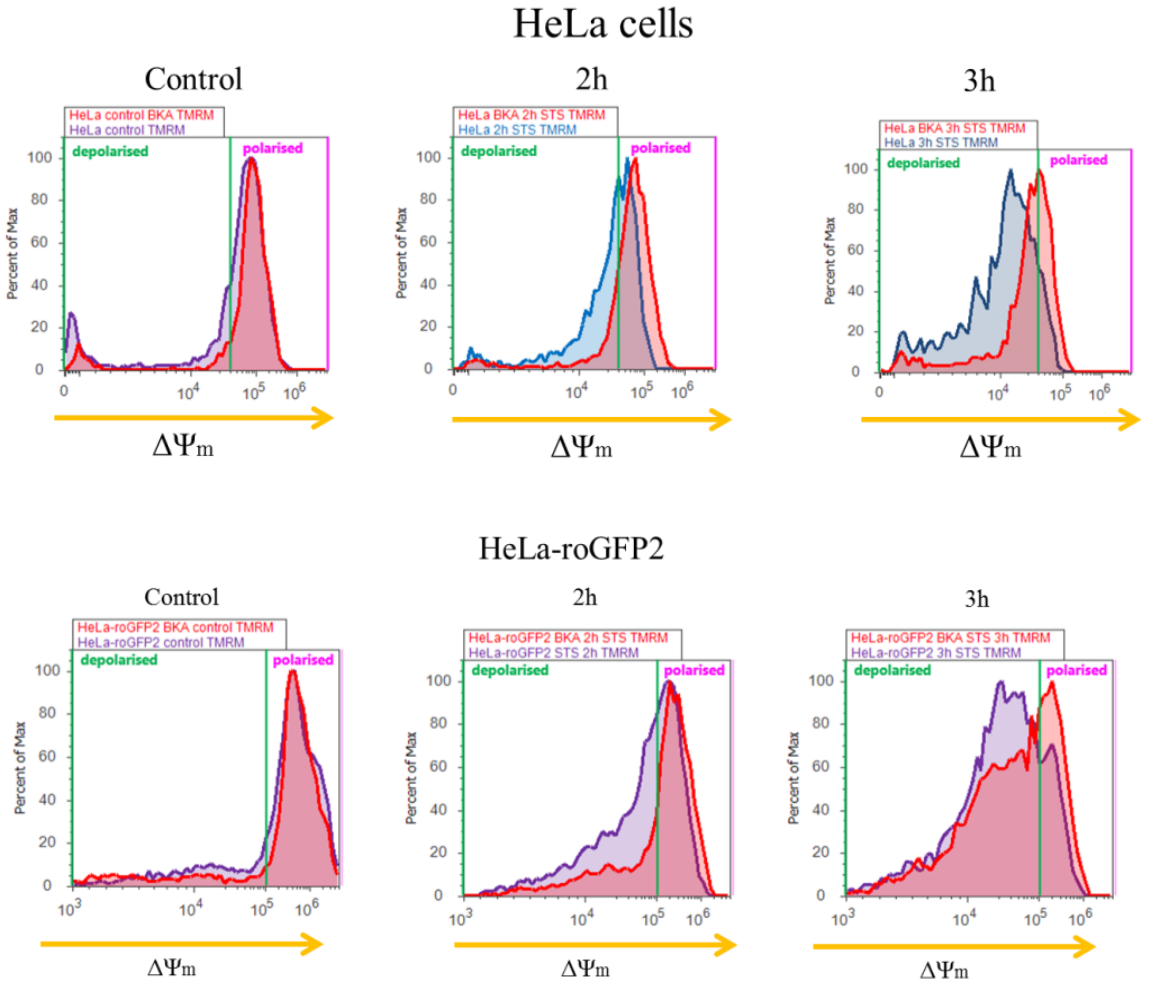

Figure 4.22 Tracking of mitochondrial depolarisation in HeLa and HeLa-roGFP2 cells, during exposure to STS.

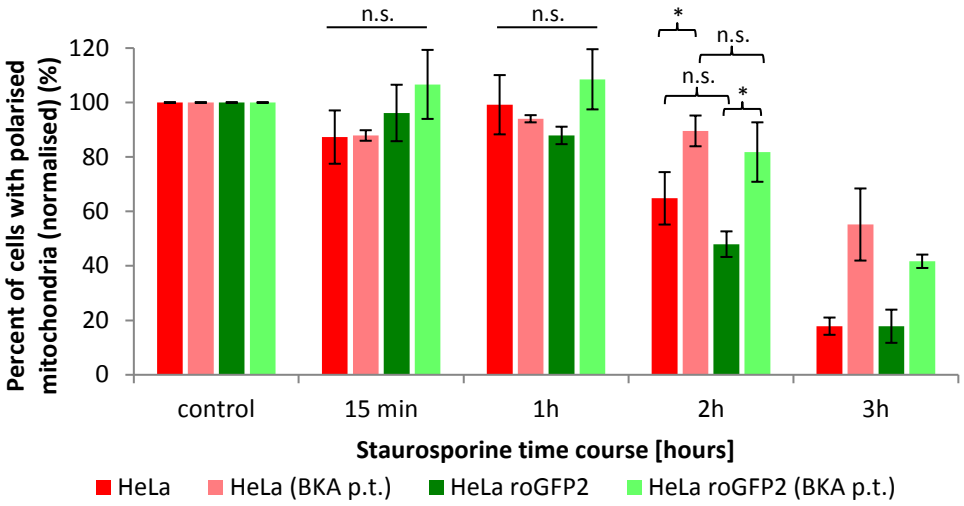

Figure 4.22 continued Tracking of mitochondrial depolarisation in HeLa and HeLa-roGFP2 cells, during exposure to STS. Half of the cell samples were pre-treated with 100µM BKA for 1 hour prior to STS treatment. During 1 hour of STS exposure, variance of the means in four conditions remained equal (n.s.) ($F(3,8)=2.51$, $p=0.132$). The effect of BKA in the attenuation of mitochondrial depolarisation was clearly observed after 2 hours of STS exposure (HeLa: $p=0.025$; HeLa-roGFP2: $p=0.016$). No difference in mitochondrial activity was observed between HeLa and HeLa-roGFP2, in both BKA-pretreated and non-treated samples ($p=0.684$ and $p=0.253$, respectively). One-way ANOVA and equal variance t-test, (*) $p<0.05$; n.s. – no significant difference.

4.1.19 Redox potential change throughout apoptosis

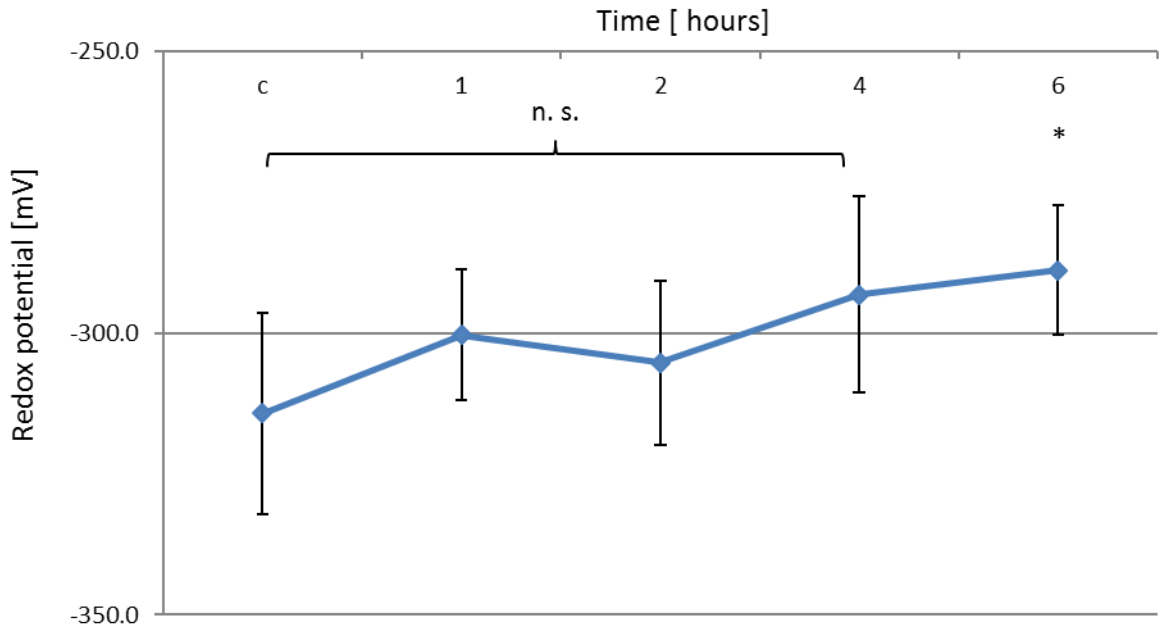

staurosporine treatment [hours]	Redox potential Mean [mV]	Standard Deviation [mV]
control	-314.3	17.8
1	-300.4	11.5
2	-305.3	14.6
4	-293.2	17.4
6	-288.9	11.5

Figure 4.23 Redox potential change measured with roGFP2 stably expressed in HeLa population of cells undergoing apoptotic cell death.

No difference in the redox potential was observed between the control sample and staurosporine-treated samples up to four hours of exposure. The redox potential was significantly different only after six hours of exposure to staurosporine (Figure 4.23).

.

4.1.20 Redox potential change in apoptosis and mitochondrial depolarisation

To assess a possible link between mitochondrial depolarisation and redox potential changes during apoptosis, one set of samples was pre-treated with BKA to delay mitochondrial depolarisation. During 3 hour exposure to STS and tracking changes in redox potential through roGFP2, a linear change trajectory towards oxidative state was observed, in both non-treated and BKA pre-treated samples (Figure 4.24).

Work in this thesis also provides validation of use of roGFP2 as a measure of redox potential at the population level. This has been done to achieve a standard curve for roGFP2, measured by flow cytometry. The data showed that the mid-point potential of roGFP2 is -285 mV, which is in accordance with literature reports for roGFP2 [107, 140].

The redox potential in apoptosis change spans 25.4 mV (from -314.3 mV to – 288.9 mV), as shown in (Figure 4.23, Chapter 4). It has been shown here that at one hour of the exposure of PS the redox potential is -306.37±15.4 mV. The redox potential change is not significant during the first four hours of treatment with staurosporine.

However, one-way ANOVA analysis has indicated that cells which were not pre-treated with BKA do not experience change in redox potential, after exposure to STS ($F(3,8) = 1.832$, $p = 0.219$). Whereas, BKA-pretreated cells did show significant difference between the means ($F(3,8) = 5.316$, $p = 0.026$) - means of 15 minute and 3 hour time points were found to be significantly different ($p = 0.026$). This observation suggests that the trend is fluctuating, although this may be because of the effect of mitochondria swelling reported previously.

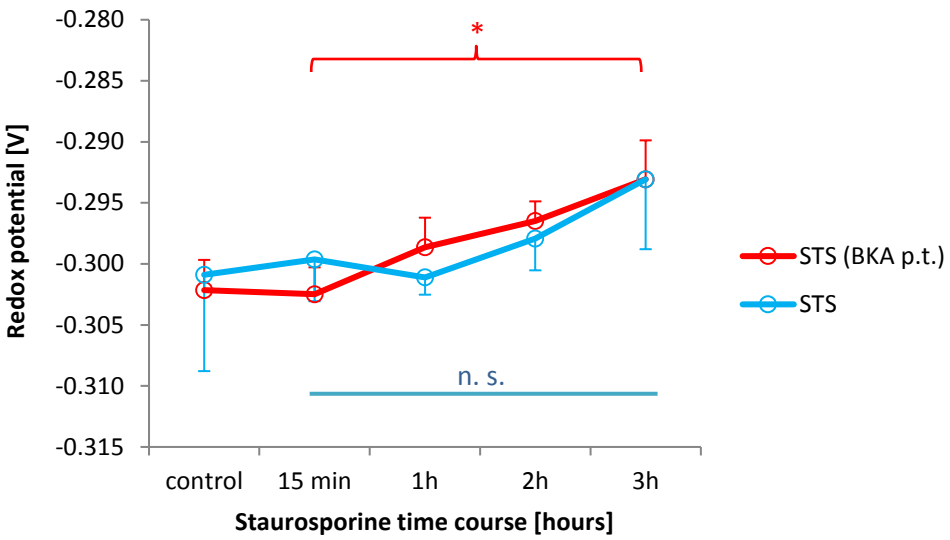

Figure 4.24 Time course analysis of redox potential change in HeLa-roGFP2 cells during exposure to 1 µM STS. Half of the cell samples were pre-treated with 100 µM BKA for 1.5 hours prior exposure to staurosporine. Three independent experiments. Error bars representing SEM, *p<0.02.

One-way ANOVA analysis has indicated that means of BKA pre-treated cells at four hour time points, when treated with STS, were not equal ($F(3,8) = 5.316$, $p = 0.026$). Equal variance t-test was used, as individual samples were used for every time point. Means of 15 minute and 3 hour time points were found to be significantly different ($p = 0.026$; (*)). One-way ANOVA test found non-pretreated cells to have equal means (non-significant difference, n.s.), when exposed to STS ($F(3,8) = 1.832$, $p = 0.219$).

These results suggest that the redox potential measured by roGFP2 at the population level does not change significantly throughout apoptosis. However, treatment with BKA has been shown to change the redox potential significantly. Mitochondrial depolarisation does not contribute to changes in the redox potential and this is indicating that the cellular redox is more oxidative independently of mitochondrial transition pore opening at the population level.

4.3 Conclusions

The results of this section can be summarised as follows:

- Cells undergoing staurosporine-induced cell death displayed typical apoptotic morphology;
- The order of apoptotic events was determined to be as follows: phosphatidyl serine exposure, mitochondrial depolarisation, followed by caspase 3/7 activity.

The mechanism of staurosporine-induced apoptosis in cells is a subject of debate [141, 142], as both involvement of caspase-dependent and caspase-independent pathways have been described [110][102]. Nicolier et al. reported that staurosporine initially induces death of HeLa cells via cytochrome c release from the mitochondria, followed by activation of caspase-9 and caspase-3. Nevertheless, a delayed caspase-independent pathway may also be present [110].

In addition, it has been shown previously that staurosporine induces cell death through formation of reactive oxygen species. A study by Circu et al[76] showed that the cell death induced by staurosporine was in fact preceded by GSH efflux and activation of caspase-3. These changes were independent of the cellular redox status of total GSH and total GSSG measured by HPLC.

An increase in activity of active caspase-3 after 4 hours of exposure to staurosporine was observed. At the same time there was a caspase-3 complex forming, which appeared to be a high-molecular-weight complex (around 64 kDa) of caspase-3. The data from western blotting suggests that the subunits formed a quadruple procaspase-3 complex. Caspase-3 complex formation of much higher molecular weight was previously reported in rat brain tissue [16], and caused by starvation [17]. One of the explanations for complex formation at the later stages of apoptosis might be due to cysteine oxidation driving the formation of complexes. As the redox potential becomes more oxidative over the time course of apoptosis, the oxidation of active site cysteine residues might influence the formation of such 64 kDa complex (miss folding of the complex). This results in decreased activity of caspase-3 as previously reported by Aucheviole *et al[99]*.

The western blotting investigation of active caspase-3 revealed that there was no difference in the apoptosis progression between the HeLa and HeLa-roGFP2 cells, suggesting that the caspase activity measured by the CellEvent™ Caspase-3/7 Green Detection Reagent has the same dynamics as the caspase-3 activity in HeLa-roGFP2 cells.

The high percent of AxV-positive cells in the untreated population makes the data difficult to interpret and suggests a flaw in the method employed. Indeed, the detachment of cells with trypsin can result in false positive population of cells, where phosphatidyl serine flips to the outer layer of membrane upon stimulation with trypsin. This study employed use of a milder EDTA only detachment reagent called Versene from Thermofisher. However, the amount of AxV positive cells was still high for the population of HeLa cells. Phosphatidyl serine may be exposed on the outer membrane when trypsinised and the cells might be false-positive for AxV binding even though they are not apoptotic.

HeLa-roGFP2 cells do not show a difference in staurosporine-induced apoptotic progression when compared to non-transfected cells. HeLa-roGFP2 cells show a tendency towards oxidative redox potential change throughout apoptosis.

BKA is reported to have a biphasic effect on MPTP; in the first minutes after application it stabilized the mitochondrial membrane, followed by a pronounced opening of PTP. BKA is also reported to inhibit MPTP pore opening in response to pro-oxidants and protonophores, but failed to interfere with MPTP induction by Ca^{2+} and chemical thiol crosslinking [143].

BKA is also reported to prevent events linked to apoptosis such as: depletion of reduced glutathione, generation of reactive oxygen species, translocation of NFκB, exposure of phosphatidylserine residues on the outer plasma membrane, cytoplasmic vacuolization, chromatin condensation, and oligonucleosomal DNA fragmentation [143].

Data from Figure 4.18 and Figure 4.19 shows that rise in redox potential is associated with a later onset of apoptotic events and it occurs after mitochondrial depolarisation. It thus might be influenced by the loss of mitochondrial membrane potential.

This data shows that redox potential in HeLa-roGFP2 cells rises independently of mitochondrial depolarisation. BKA pre-treatment of cells showed no significant difference in rise in redox potential between cells undergoing staurosporine-induced apoptosis. Even if mitochondrial depolarisation was inhibited, redox potential in cells pre-treated with BKA progressed at the same rate as in staurosporine only treatment. This suggests that there is no effect of mitochondrial depolarisation, on redox change through apoptosis.

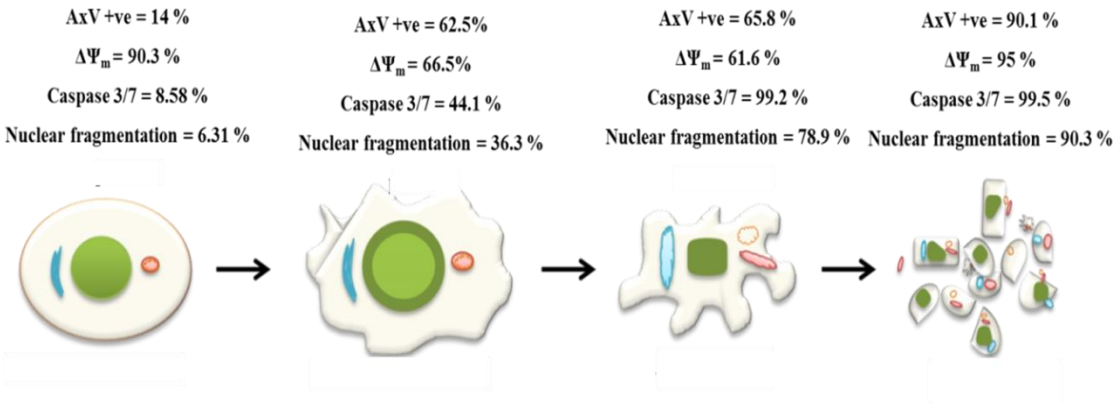

Figure 4.25 Summary view of key apoptotic events in HeLa cells. Events are ordered from left to right as they occur in the cell. Displayed are summary data from Chapter 4. The data shows percent of cells at each stage of apoptosis with exposed phospohatidylserine (AxV +ve), polarised mitochondria ($\Delta\Psi_m$), activity of caspases 3 and 7 (caspase 3/7), fragmented nucleus (nuclear fragmentation). Redox potential was measured by roGFP2.

However, roGFP2 is reported to not be responsive to any pH change within the physiological range, and previously reported studies show that pH becomes more alkaline when cells undergo apoptosis. Still, there is no evidence that this acidification is due to mitochondrial depolarisation.

Flow cytometry analysis was used to investigate the collective behaviour of individual cells (Figure 4.25). Each cell was labeled with an apoptotic marker and this was examined via flow cytometry, which gave an insight into the dynamics of the apoptotic processes at the population level. However, there was some variability between experiments as well as between the control samples. This indicates that the study of variability between single cells is required to further understand whether this subtle

effect was caused by the variability between conditions of the experiment or the representation of variability between the cells in a given population (Figure 4.25).

Flow cytometry data gives more information regarding single cell behaviour than the fluorescence plate readouts. This is due to the type of data acquired from each technique. The plate reader gives data in batch of the population of the cells in the well; however it is an average of the readout that is the final result, not giving the information on the single cells. Thus, this might not be representative of the variability between the cells in the population as presented by various studies.

Thus, in the following chapter each cell was treated as a single experiment, and the variability between experiments was determined. This may have a potential for use in monitoring of single cells' resistance to undergoing apoptosis and in consequence detection of a single cell that evades apoptosis. As suggested by Meyer *et al.* the redox potential might differ dependent on the location in the cytoplasm.

Chapter 5

Investigation of redox potential change in apoptosis at the single cell level

5.1 Introduction

The findings presented in Chapter 4 suggested that changes in the redox potential are associated with apoptosis since the redox potential shifts towards a more oxidative range when cells are undergoing programmed cell death. Results of the high throughput studies at a population level suggested that the rise in redox potential occurs independently of mitochondrial depolarisation; however, it is not clear whether it is a cause or a consequence of the apoptotic process.

It has been previously reported that the cytoplasm undergoes substantial acidification upon induction of apoptosis in various cell lines such as human T lymphocyte Jurkat cells [134] and Human promyelocytic leukemia HL-60 cells (pH 7.8 to pH 6.2) [144]. Acidification of the cytoplasm has been reported to occur concurrently with phosphatidyl serine exposure [145]. At the same time, anti-apoptotic Bcl-2 has been shown to be upstream of the acidification, thus protecting cells from apoptosis. Acidification can also be prevented by z-VAD-fmk, a non-specific protease inhibitor, suggesting that acidification is a consequence of protease switches [145]. These studies used flow cytometry, where a trend in a population was measured, but not exact values of pH. For the purpose of measuring redox potential, it is important to measure the pH quantitatively since an increase in 1 pH unit results in a change of redox potential of 59.1 mV at 298 K according to the Nernst equation. Common methods used to quantify the pH in cells use a fluorescent dye followed by incubation with nigericin and potassium ions at various external pH's between 6.5 and 8.8. [146]

The flow cytometry method developed in Chapter 4 is of advantage to investigate the single cells at a high throughput thus showing the overall trend of the population, but single cell resolution together with assay sensitivity might be lost and it is difficult to

establish whether the oxidative change is a trigger of mitochondrial depolarisation or *vice versa*. While roGFP2 reports on relative GSH/GSSG ratios, it is dependent on the activity of Grx-1 enzyme, which may delay the response to redox change in the environment couples such as NAD(P)H/NAD(P)$^+$ and does not take into account changes in pH. roGFP2 therefore may not give a truly quantitative representation of the general intracellular redox potential.

5.1.1 Aims

Work in Chapter 5 aims to quantitatively measure the redox potential and pH in real time by surface enhanced Raman spectroscopy (SERS). To investigate the relationship between the redox potential and apoptosis at the single cell level a novel method established by the Campbell lab employing redox-responsive nanosensors was used [98]. This relies on quinone-based reporter molecules to quantitatively measure the redox potential in real time by SERS. The method offers a potentially more reliable alternative to fluorescence-based techniques, especially for the early events of apoptosis, due to a more rapid response time, the ability to measure an overall potential (i.e. not biased to a particular redox couple) and the ability to multiplex with pH.

5.1.2 Raman spectroscopy

Recent years have seen several new techniques for the investigation of cellular processes at a single cell level [147-149]. One such technique, Raman Spectroscopy, utilises marker-free optical technology enabling the observation of a range of cellular processes including discernment of cell death pathways [150].

Raman spectroscopy gives information about the structural properties of molecules based on their vibrational and rotational transitions. Each molecule has its own vibrational signatures, determined by atoms and individual bonds in the molecule and each molecule thus has a characteristic Raman spectrum. Raman spectroscopy measures the shift in frequency of photons as a result of inelastic scattering. [151]

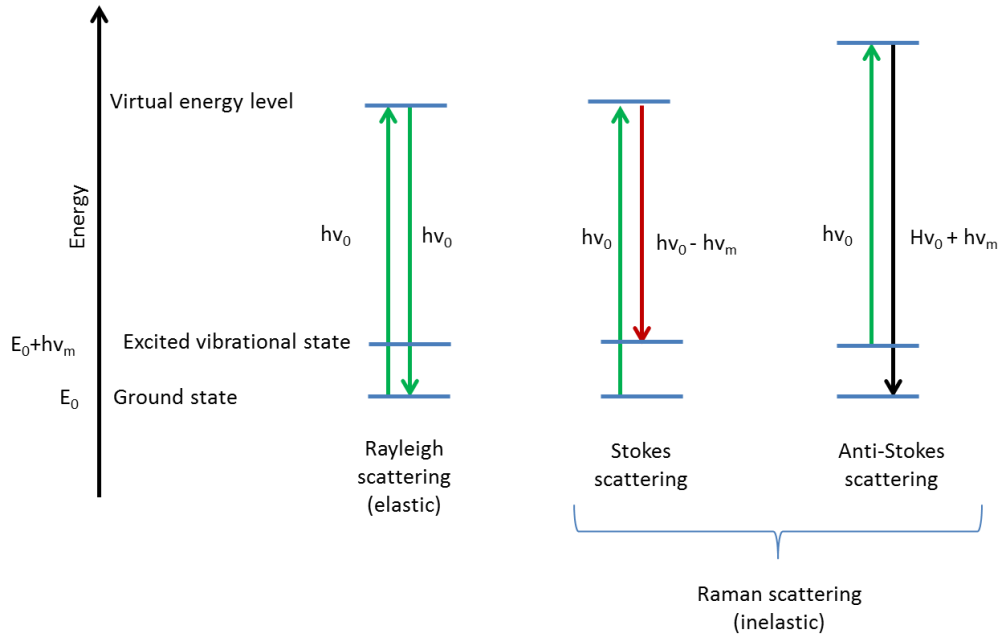

Figure 5.1 Jablonski diagram depicting Rayleigh and Raman scattering of the incident photon: the molecule can relax back down to the ground state and emit a photon of equal energy (Rayleigh scattering); the molecule can relax to a "real" vibrational state and emit a photon with less energy than the incident photon (Stokes scattering); the molecule is already in an excited vibrational state and is excited to a higher virtual state and then relaxes back to the ground state emitting more energy than that of the incident photon (anti-Stokes scattering).

When incident light interacts with a molecule it induces a dipole moment and the light is scattered. A Jablonski diagram (Figure 5.1) describes the quantum energy transitions for both Rayleigh and Raman scattering of incident photons. Rayleigh (elastic) scattering dominates the effect and does not result in a change in frequency of the scattered light.

Raman (inelastic) scattering occurs in only 1 in 10^8 of the incidence photons [152] and shifts the frequency of incident light by increasing (anti-Stokes) or reducing (Stokes) the frequency of the photon. The Raman effect provides a means of directly measuring the vibrational frequency of a molecular bond because the incident photon changes energy by the same amount as required to excite the vibrational transition. The Raman spectra are plotted as intensity versus frequency diagrams depicting energy levels of vibrations of different functional groups.

Raman spectrometry is attractive for analysing vibrational transitions in molecules of interest within intracellular environments: it does not suffer from interference from water in the way that infrared spectrometry (IR) does; and by tuning the laser excitation wavelength background fluorescence can be minimised.

Even though it is often possible to qualitatively and quantitatively assess a molecule of interest with Raman spectrometry, this process becomes substantially more difficult in biological samples (i.e. non-fractionated cells) due to the number of molecules (deconvolution options are limited) and low signal intensity (high noise/signal ratio). To overcome this hurdle, conjugation of the target molecule to silver or gold nanoparticles causes amplification by as much as a factor of 10^{14} [153]. This method of signal enhancement is known as surface enhanced Raman spectroscopy (SERS).

5.1.2.1 Surface Enhanced Raman Spectroscopy

While Raman spectroscopy has been successfully applied to biological systems to investigate the difference between healthy and diseased cells [152] spontaneous Raman spectra usually suffer from low intensity. Recently, SERS which uses the property of surface plasmon resonance to amplify the signal of a molecule that is in close proximity to their surface, has been successfully applied to biological systems [154, 155]. The amplification of the signal has been reported to be as high as 10^{12} if the molecule is adsorbed on a nanoparticle's noble metal surface and the particle is spherical or rod-shaped. [154] After the initial discovery of SERS in 1973, an extensive number of studies have shown applicability of this method for human tissue analysis [154, 155].

5.1.2.2 SERS nanoparticles

The nanoparticles used in this study had a 120 nm diameter silica core and were coated with an outer layer of gold giving approximately 150 nm total diameter (Figure 5.2).

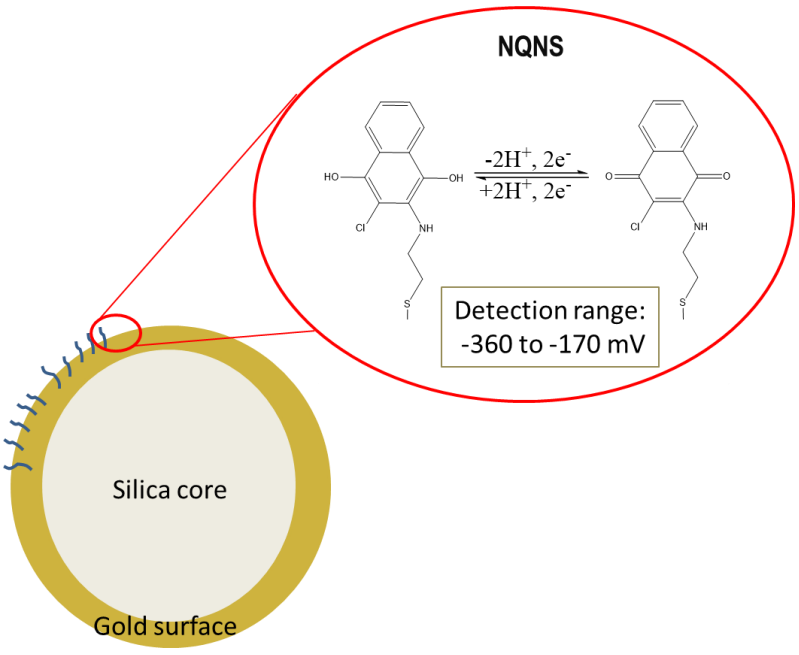

Figure 5.2 The structure of nanosensor (in this case NQ-NS).

These gold nanoshells (NS) have been identified as an attractive material for application in biological systems [156] as they are biocompatible and have tunable plasmon resonance between 780 nm and 820 nm (near infrared, NIR). NIR compatibility is

desirable for biological SERS measurements because there is less intrinsic fluorescence from cells and tissues in this region of the spectrum. These gold nanosensors do not aggregate and are easily absorbed by entocytosis by the cell; therefore, they are suitable to conduct cytoplasmic measurements of redox potential. However, the size of the nanosensor might be problematic when measuring redox potential in other compartments (such as nucleus, mitochondria), as these sensors are larger than the pores they could potentially enter through. The ongoing work in the Campbell's lab investigates different types of the nanosperes and nanorods to enable further studies, however the current issue is the tendency of nanorods to aggregate within the cells' cytoplasm close to targeted compartment (data not shown).

5.1.2.3 Redox responsive molecules

Two redox molecules designed by Campbell's lab have been used in this study:

1) 1,8-diaza-4,5-dithian-1,8-di(2-chloro-[1,4]-naphthoquinone-3-yl)octane (NQ).
2) N-[2-(disulfanyl)ethyl]-9,10-dioxo-9,10-dihydroanthracene-2-carboxamide (bis-(2-Anthraquinone carboxamide) (AQ).

These molecules can be reversibly reduced and oxidised in response to changes in the redox environment (FIGURE 5.2 and FIGURE 5.3). [99, 157, 158][97, 149, 150]

It has been reported previously that Density Functional Theory (DFT) calculations corresponded with observed spectroelectrochemical data and pinpoints signals that change in response to variable redox potentials. Therefore the redox potential reported by the molecule is highly dependent on the environment surrounding the molecule.

Reduced and oxidised states of AQ and NQ molecules used in this study differ in optical properties and these changes can be depicted in SERS spectra (Figure 5.3 and Figure 5.4 lower panels). For the AQ reporter, the ratio of signals at 1666 cm^{-1} (C=O stretching in oxidised) and 1606cm^{-1} (constant C=C stretching in both reduced and oxidised forms) measured at a range of potentials was used to construct a calibration curve (Figure 5.3). AQ-NS covers a working range of redox potentials spanning from -450 mV to -250 mV.

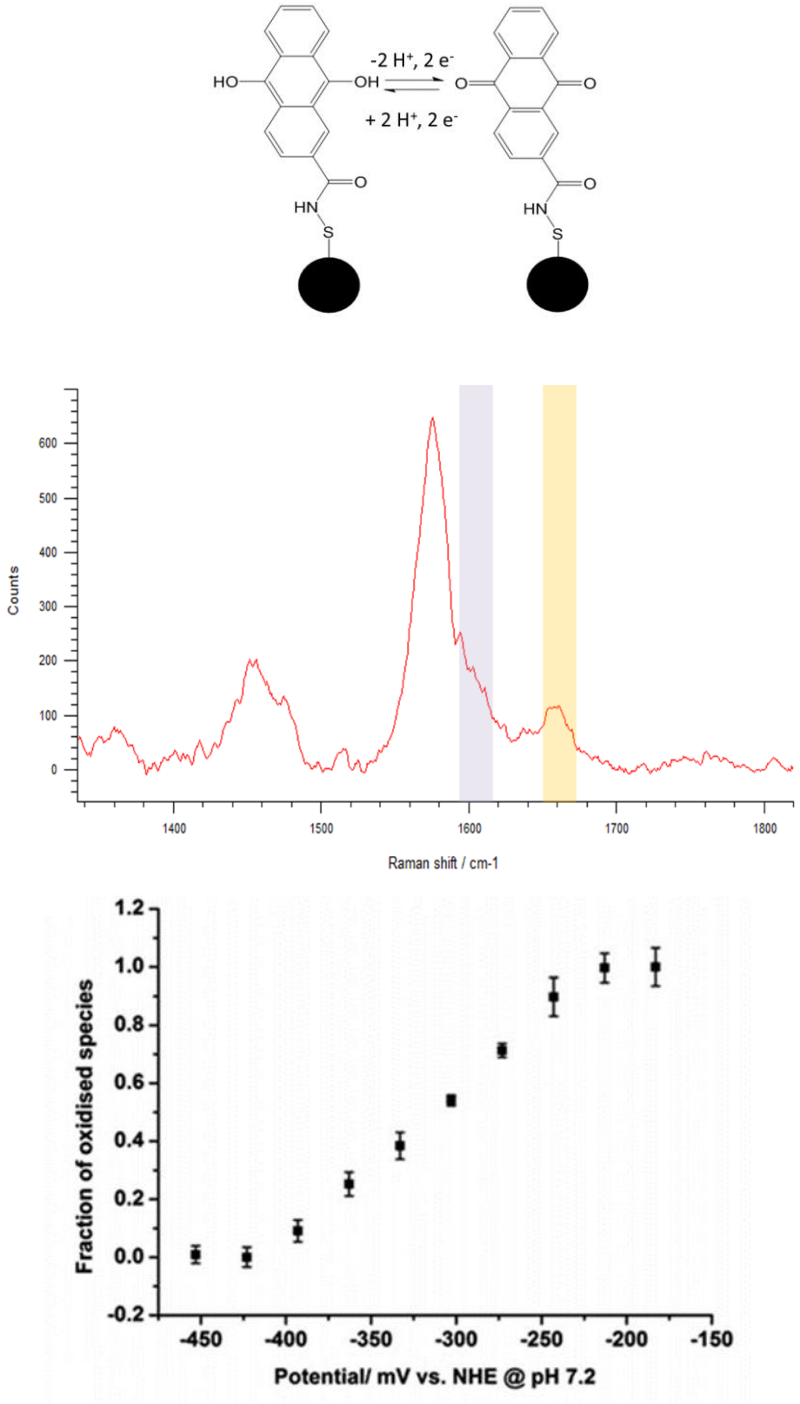

Figure 5.3 Structure of reporter molecule (AQ) in reduced and oxidised form assembled on gold surface of a nanosphere. A. Calibration curve adapted from Jiang et al. [138]. B. Example of a Raman spectrum of AQ-NS in cells. Acquisition time 30 seconds and 785 nm laser at 10% power. For AQ molecule the redox potential is calculated from ratio of signals at 1666 cm^{-1} (C=O stretching in oxidised) and 1606cm^{-1} (constant C=C stretching in both reduced and oxidised forms).

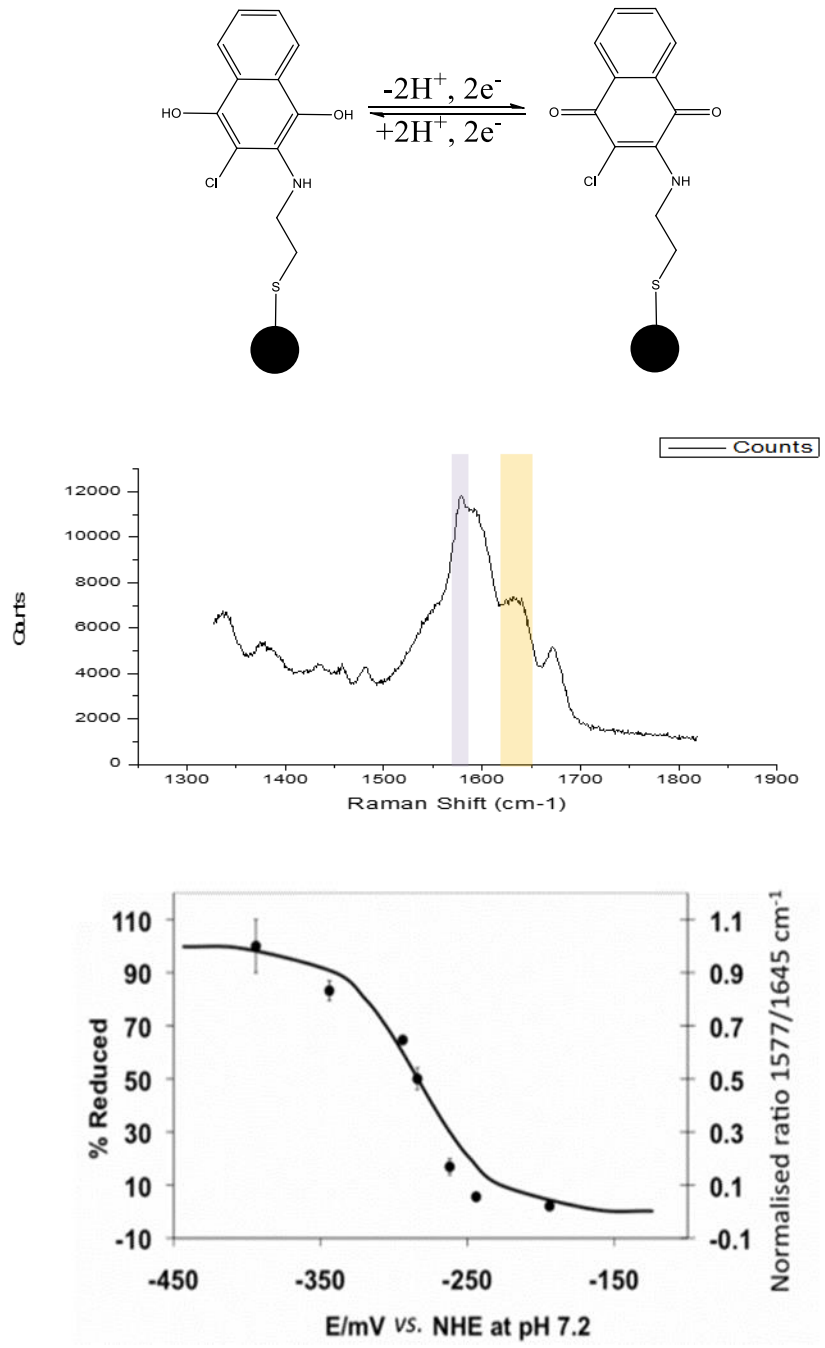

Figure 5.4 Reporter molecule (NQ) in reduced and oxidised form on left and right, respectively; assembled on the gold nanoparticle (black dot). A. Calibration curve for NQ adapted from . B. Example of a Raman spectrum of NQ-NS in cells. For the NQ molecule the intensity of signals of 1633 cm-1 (C=O stretching seen only in an oxidised environment) and 1579 cm-1 (symmetric ring breathing in both oxidised and reduced conditions) measured at a range of potentials was used to construct a calibration curve.

Peak 1577 cm^{-1} shows symmetric ring breathing (reduced version of NQ), while peak at 1633cm^{-1} corresponds to C=O stretching (reference peak for reduced and oxidised NQ). The ratio of two peaks is then applied in the Nernst equation and the redox potential is calculated. The measuring range of redox potential of NQ-NS spans from -394 mV to -194 mV.

Both redox reporter molecules used in this study have been previously tested and confirmed to be responsive to all thiol based buffers, therefore they were suitable for quantification of the overall intracellular redox potential [99, 157]. Those molecules were successfully mounted onto the gold nanoshells by sulfur-gold bonds. The advantageous characteristic of reporter molecules is that the characteristic Raman shift frequencies for distinguishing oxidised from reduced forms of reporter molecule differ from the typical vibrational modes of DNA, proteins, and lipids [155].

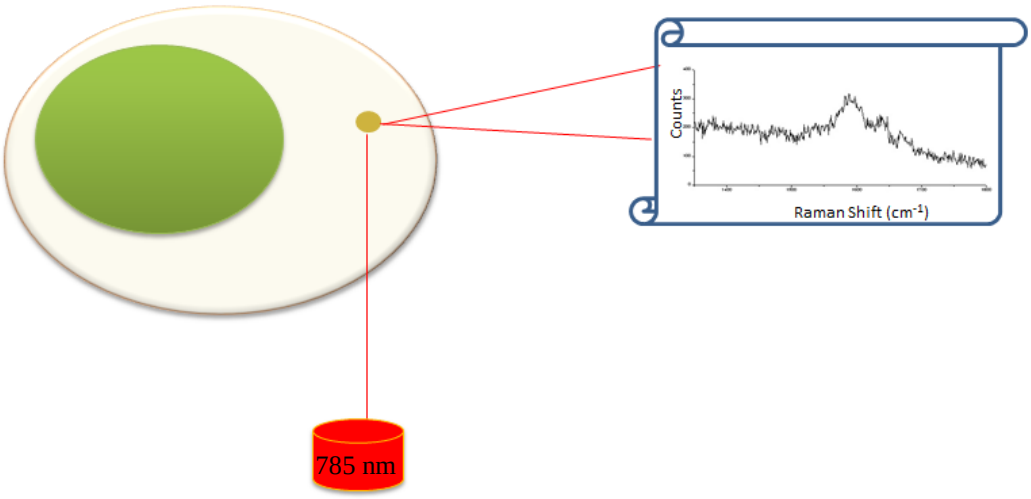

Figure 5.5 showing a principle of SERS measurements of intracellular redox potential with redox responsive nanosensors. Cell with nucleus (green) and localised to the cytoplasm nanosensor (gold) and detected using 785 nm laser diode.

As previously published by Auchinvole *et al.* the generation of ROS and the upregulation of oxidative stress levels was not detected when nanosensors were introduced to the cells, therefore it was concluded that they do not cause toxic effects or imbalance the redox status of the cell [99, 159].

5.1.2.4 MBA-NS - pH responsive sensor

pH measurements were performed in order to establish a true value of redox potential at a particular stage of apoptosis. This is important as the increase in one pH unit corresponds to a shift of approximately -59.1mV in potential.

4-mercaptobenzoic acid (MBA) which is a well-established SERS pH sensor was used for this purpose [157]. The SERS spectra of MBA-NS has two signals at 1080 cm^{-1} and 1590 cm^{-1} which are assigned to pH-independent aromatic ring vibration and thus can be used as a reference to changing pH signal intensities which are two peaks, the first at 1400 cm^{-1} (COO- stretching) and the second at 1700 cm^{-1} (C=O stretching). The 1400 cm^{-1} peak increases with increasing pH, and 1700 cm^{-1} peak decreases with increasing pH. The range of the sensor is between pH 6 and pH 9, making it well suited for reporting the cellular pH [100, 157].

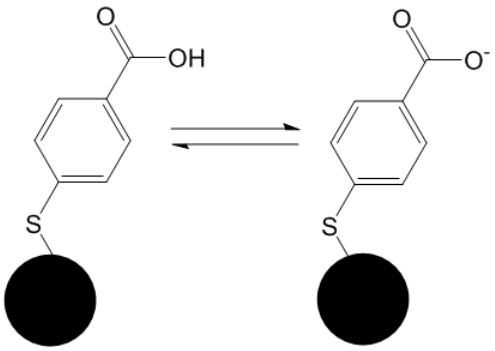

Figure 5.6 Structure of reporter molecule (MBA) in reduced and oxidised forms, assembled on gold nanoshell. A. The plot represents the calibration curve indicating the useful pH reporting range between pH 6 and pH 8 [17] and (B) an example spectrum of MBA reporter.

A.

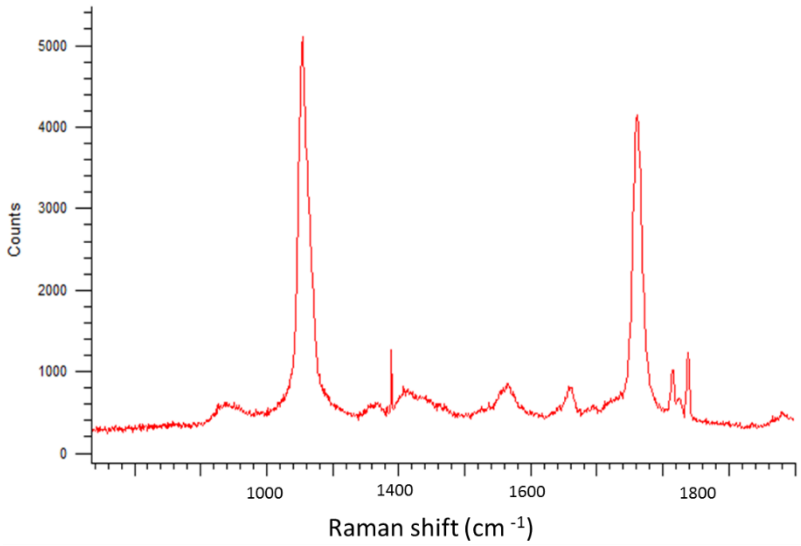

B.

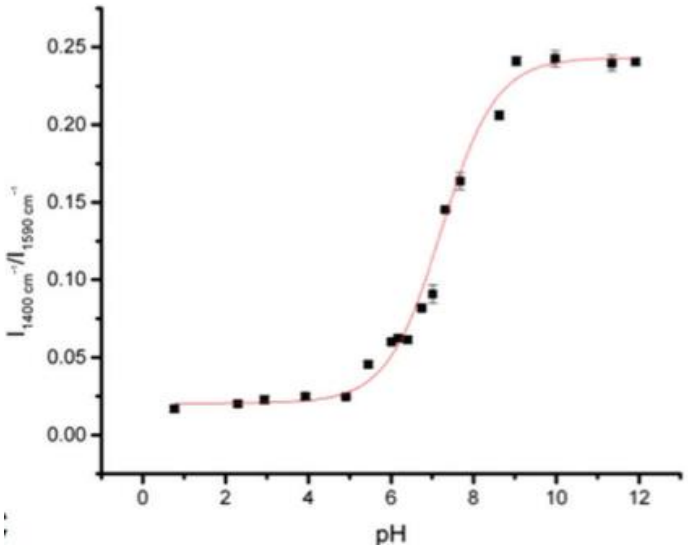

FIGURE 5.6 continued Structure of reporter molecule (MBA) in reduced (left) and oxidised (right) forms, assembled on a gold nanoshell. A. an example spectrum of MBA reporter and (B) The plot represents the calibration curve indicating the useful pH reporting range between pH 6 and pH 8 [157].

5.2 Results

5.2.1 Nanosensors do not alter the viability of cells

It was important to establish, whether the AQ-NS and MBA-NS sensors influence the cells rate of progression through apoptosis. TEM results have shown that while some cells are undergoing autophagy or are apoptotic this is normal in the population of cells and also seen in untreated controls.

Nuclear fragmentation measured by DAPI staining was used to track apoptosis progression. Results showed no significant change in progression of cells through apoptosis (condensation of chromatin and fragmentation) at any time point between the cells treated with nanoparticles and untreated controls (Figure 5.7). These results suggested that the sensors are suitable for measuring redox potential in HeLa cells undergoing programmed cell death.

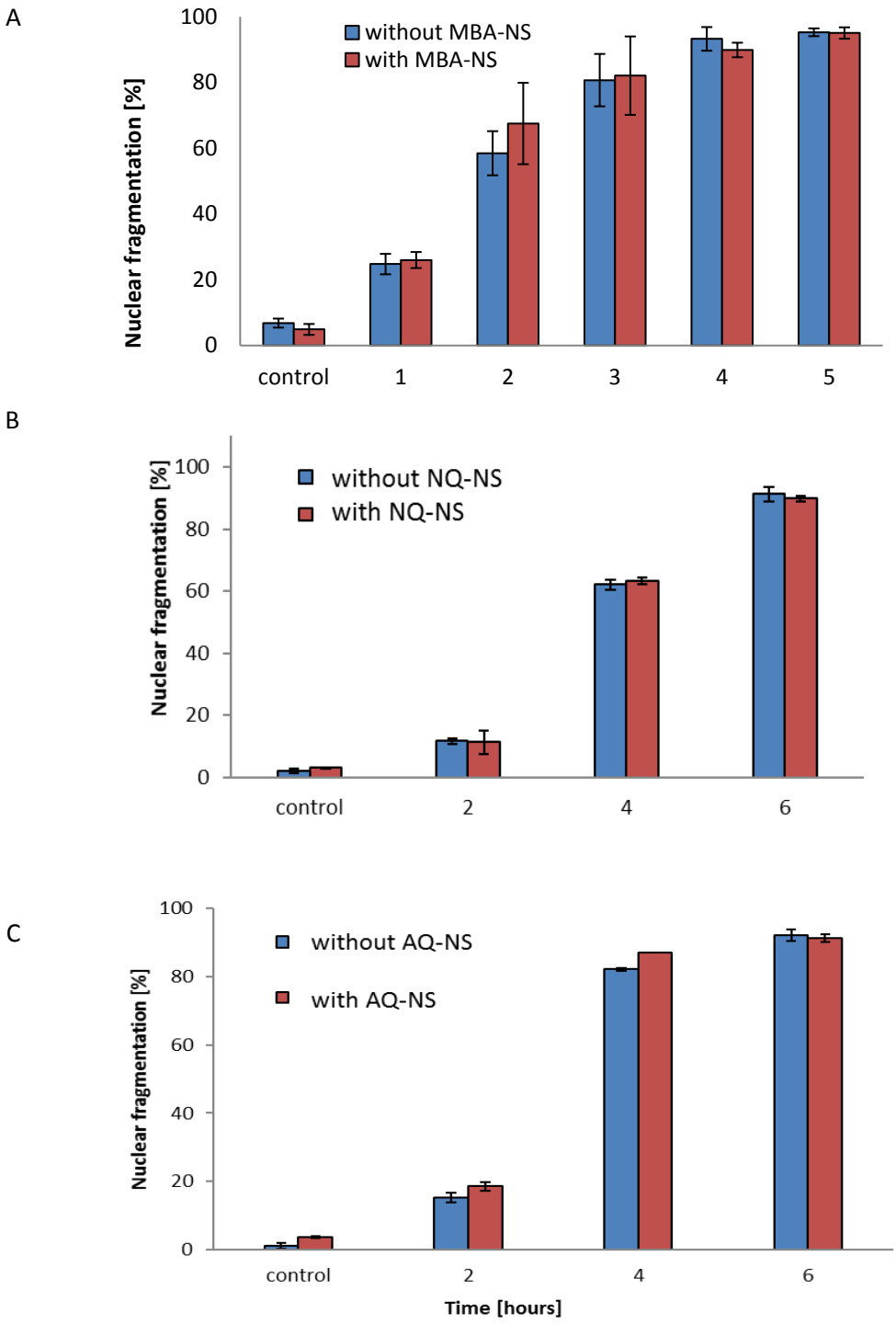

Figure 5.7 Influence of MBA-NS (A), NQ-NS (B), and AQ-NS (C) on apoptosis progression rate following induction of apoptosis with 1µM staurosporine. Condensation of chromatin and nuclear fragmentation were assessed by DAPI staining and were shown not to be significantly different between the cells treated with nanoparticles. Data shows a summary of three. Error bars represent the standard deviation of three independent experiments. Student t-test was carried out between without and with nanosensor samples.

5.2.2 Uptake and localisation of nanosensors

The uptake of nanosensors by HeLa cells was confirmed by transmission electron microscopy (TEM) (Figure 5.8).

TEM allows an electron beam to pass though the ultra-thin sample and interact with materials in the sample. This high resolution technique provides an opportunity to distinguish between organelles and establish which compartments of the cell the nanosensors are localised to.

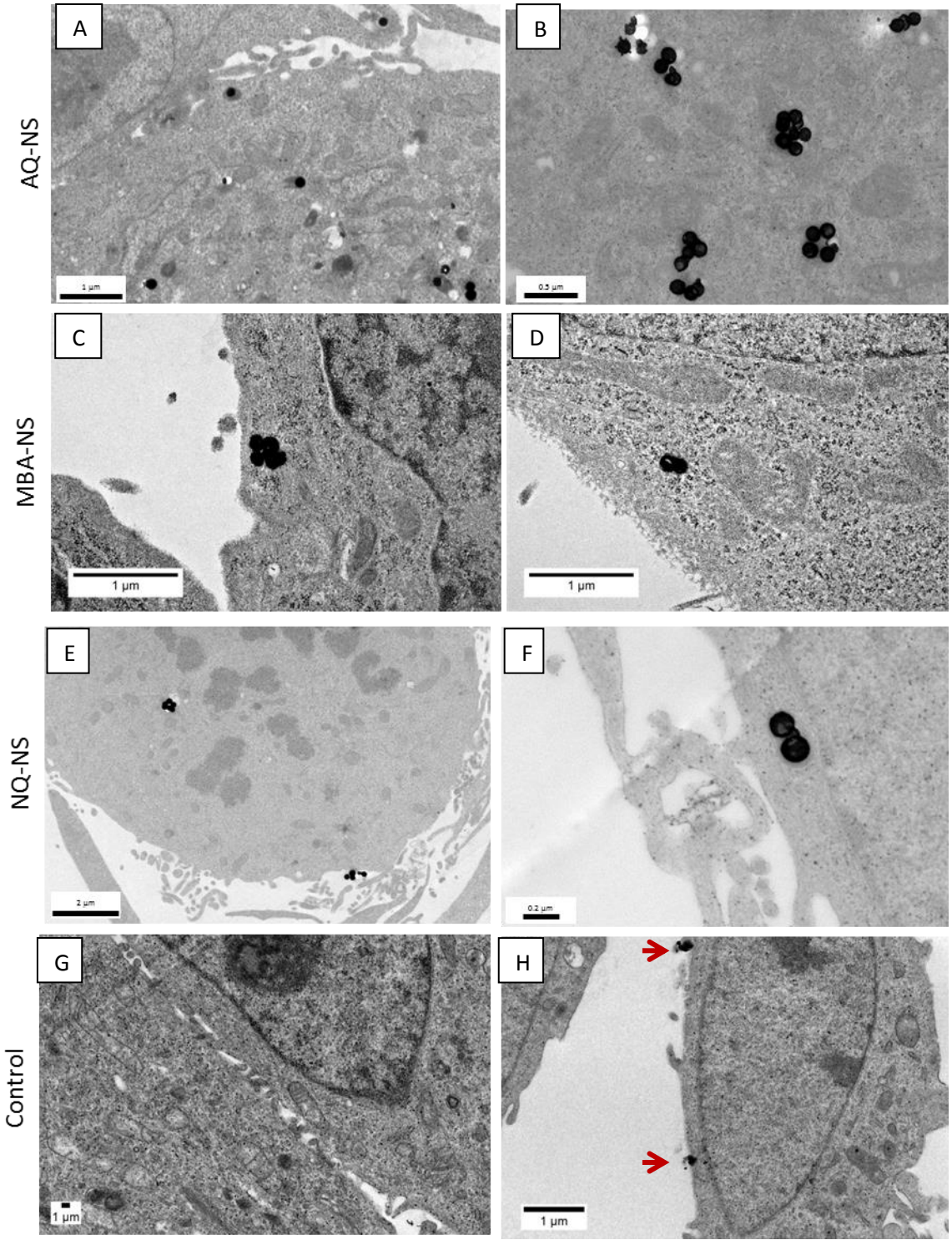

Figure 5.8. Transmission electron micrographs showing localisation of nanoparticles after uptake of AQ-NS, MBA-NS, NQ-NS by HeLa cells. Nanoparticles were identified mainly in the cytoplasm. Cells were exposed to AQ-NS (A,B), MBA-NS (C,D) and NQ-NS (E, F) nanoparticles at 10 fM overnight; Untreated control (G, H) arrows are pointing at an artefact of TEM. Nanoparticles are revealed as black electron-dense circles.

Figure 5.8 shows that NQ-NS, AQ-NS and MBA-NS were taken up by the cells and were localised to the cytoplasm. These results indicated that sensors can be translocated to the cytoplasm as single particles or aggregates. Of a particular interest is the fact that the individual nanoparticles are residing mainly in the cytoplasm while some aggregates and alike are encapsulated by some form of vesicle.

Artefacts of TEM staining which superficially resembled the sensors were sometimes seen. Examples are indicated by arrows in Figure 5.8H. These electron-dense structures were distinguished the nanoparticles by their irregular shape.

In order to establish the percentage of cells which had taken up the nanosensors, 126 and 47 TEM sections were analysed for uptake of AQ-NS and NQ-NS, respectively. 68.3% of sections included AQ-NS and 58.8% of sections included NQ-NS (Figure 5.9).

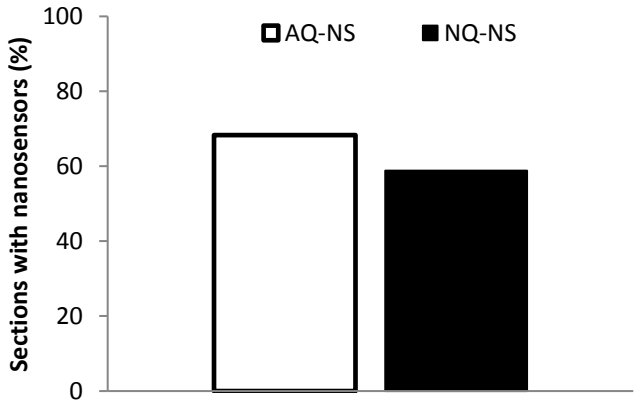

Figure 5.9 Uptake of nanosensors (AQ-NS and NQ-NS). The bar-chart depicts the percent of sections with uptake of nanosensors (126 sections were counted for AQ-NS and 47 for NQ-NS).

These data are in agreement with previously published work in Campbell's lab that the incubation of cells with nanosensors using media without serum resulted in sensors being taken up by NIH/3T3 fibroblasts [99], A549 [98], and MCF-7 cells [157].

5.2.3 pH measurements in HeLa cells by MBA-NS

From the selection of nanosensors used in this study, a unique feature of the MBA-NS was its ability to track changes at the intracellular environment's prevailing pH, with a detection range between pH 6 and pH 9. Therefore the sensitivity of this method allows the detection of pH changes at a single cell level with three orders of magnitude resolution.

The relationship between pH and apoptosis has been measured [160, 161] and the measurement of an accurate redox potential requires the measurement of pH (this is often overlooked, or a steady-state pH is assumed) [102]. Here, the MBA-NS was used to gain precise understanding of the actual intracellular pH values and provide accurate redox potential values during apoptosis progression.

Figure 5.10 shows a detailed scan of three cells in the field performed with 1 mm by 5 mm steps in y and x axis, respectively. MBA-NS SERS spectra were acquired over 10 seconds with 50% laser power. The intensity at 1500 cm^{-1} corresponding to high intensity pH-independent aromatic ring vibration allowed localisation of pH sensor within the field. Following the localisation of the pH sensor within the field quantification heat-maps were generated (Figure 5.10 and Figure 5.11) to allow mapping of pH changes at a single cell level.

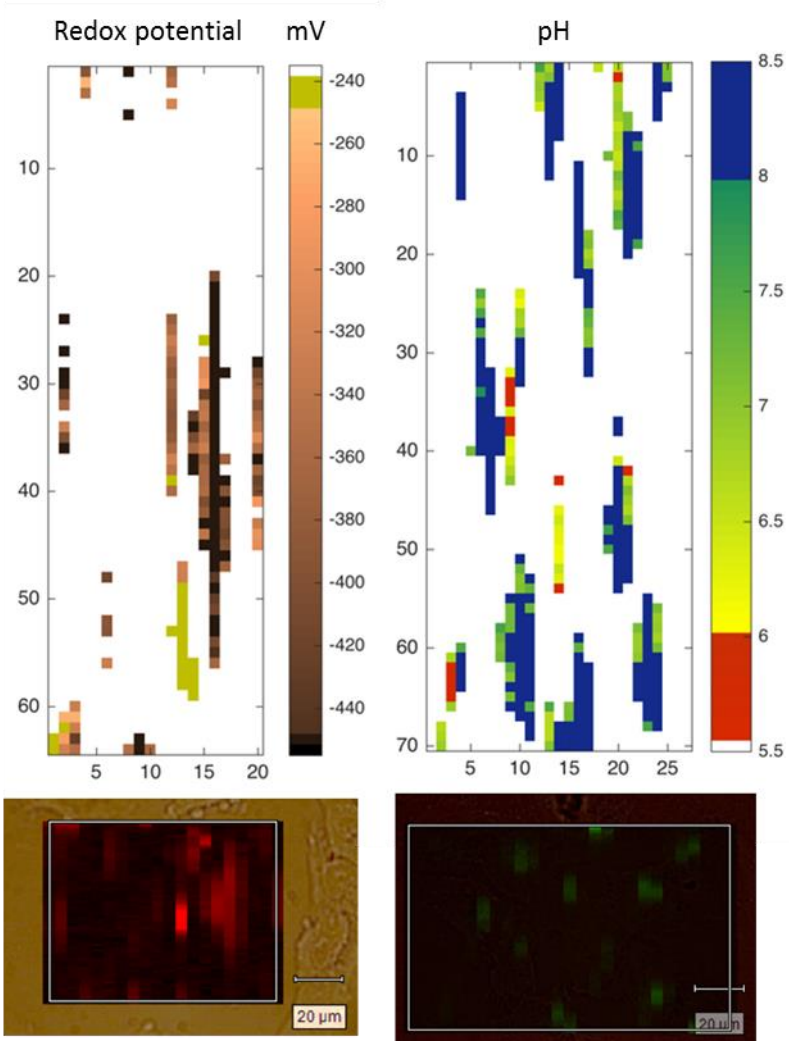

Figure 5.10A Example of maps of redox potential (AQ-NS) and pH (MBA-NS) measurements in untreated control. A detail scan was performed with 1 mm by 5 mm steps in y and x axis respectively. Colour maps for redox potential measurements and pH were generated with MatLab script written by Dr Kate Fisher (Campbell Lab). The corresponding fields on the pictures below the colour maps indicate the field analysed. The shape of two windows differ due to x and y step size width and depth. SERS spectra were acquired over 10 s with 50% laser power.

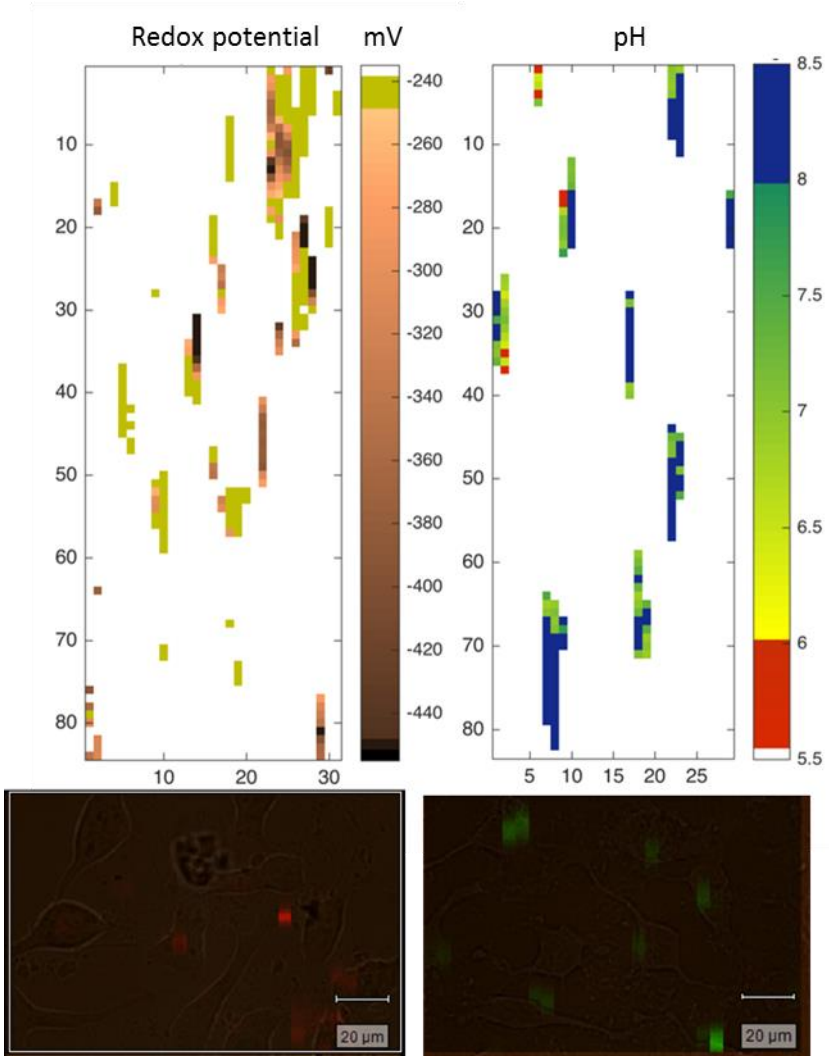

Figure 5.10B Example of maps of pH measurements with MBA-NS and redox potential measurements with AQ-NS in HeLa cells treated with staurosporine for 120 minutes. A detail scan was performed with 1 mm by 5 mm steps in y and x axis respectively. Colour maps for redox potential measurements and pH were generated with MatLab script written by Dr Kate Fisher (Campbell Lab). The corresponding fields on the pictures below the colour maps indicate the field analysed. The shape of two windows differ due to x and y step size width and depth. SERS spectra were acquired over 10 s with 50% laser power. SERS spectra were acquired over 10 s with 50% laser power.

Measurements of the intracellular pH via MBA-NS after induction of apoptosis with STS and unstimulated controls provided values which could be used for pH-adjusted redox potential calculations. The pH for each parameter was obtained from the relevant calibration curve and the associated error determined from the error in both the Lorentzian fit and the calibration curve [162]. As determined from the calibration curve

the working range of the pH sensor is between pH 6.0 to pH 9.0. The curve fitting analysis took a weighted mean of the seven parameters using inverse weighting. This was done to minimise the effect of parameters with a large error. If 4 out of 7 parameters of spectra were within the range, the spectra was taken further for analysis. The overall pH values then combined into a weighted average for each map.

No significant difference in intracellular pH was observed between apoptotic cells and controls: the mean values were 7.406 and 7.412 , respectively (Figure 5.12). In previous calculations of the redox potential, a constant value of 7.2 for pH was used, since this is considered to be a representative physiological pH.

Mitochondria are critical facilitators of a apoptosis as a result apoptosis as a result of mitochondrial permeabilisation and cytochrome-c translocation [161]. To investigate the relationship between permeabilisation, pH and redox potential, Bongkrekic acid which inhibits mitochondrial permeability transition pore opening was used. Depolarisation of mitochondria following the treatment of staurosporine was again confirmed using TMRM (Figure 5.11).

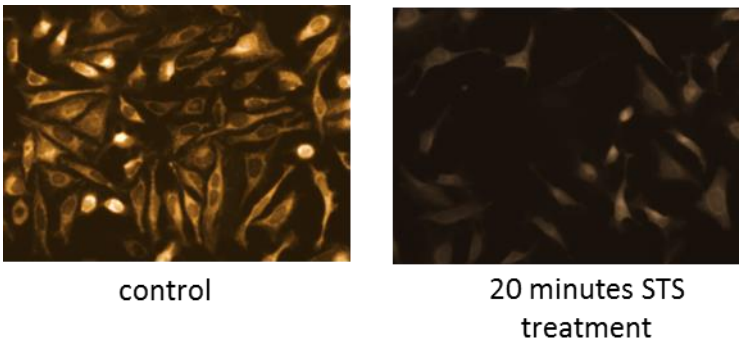

Figure 5.11 Mitochondrial membrane depolarisation measured with TMRM in HeLa cells untreated control and 20 minutes after triggering cell death by staurosporine.

After pre-treatment of cells with BKA for 1 hour, a pH of 8.085 was recorded in non-apoptotic samples (Figure 5.12), a significantly higher pH than BKA-free controls. However, following induction of apoptosis by STS in BKA treated cells for 30 minutes up to 59 minutes, a pH of 7.266 was observed, demonstrating a significant difference to

STS-free BKA treated control and suggesting a delay in apoptosis due to mitochondrial exclusion from the process. After this time point the discrepancy in the pH was minimal and not significant and allowed cells to progress further in apoptosis (Figure 5.12).

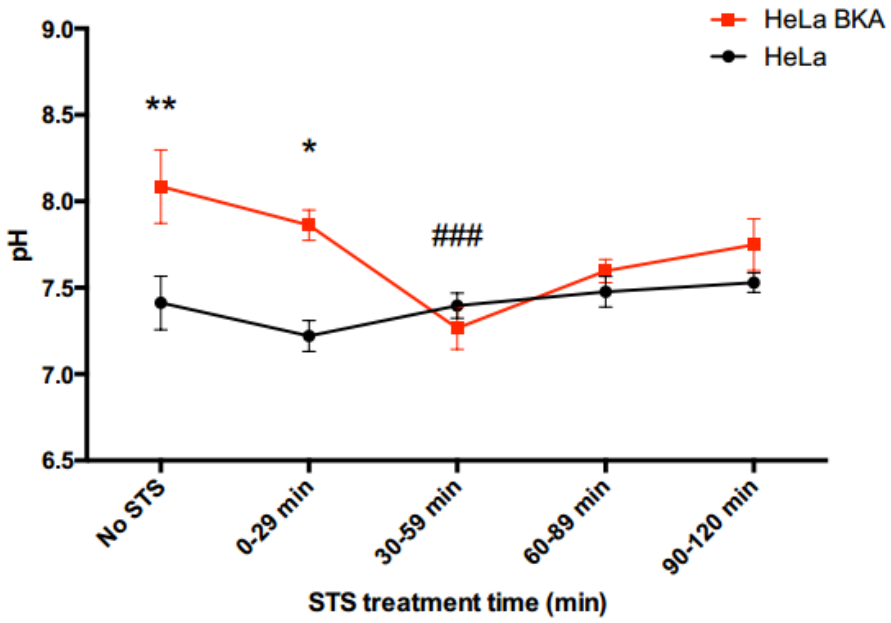

Figure 5.12 Analysis of resting cytoplasmic pH in HeLa cells and change in pH throughout apoptosis measured by MBA-NS. ** indicates significant difference of BKA treatment between samples measured by ANOVA (p=0.0016). # indicates significant difference between BKA only versus no STS treatment for all time points. *p>0.01 being statistically significant.

Data from the pH that was stated as outwith the range of the sensor and marked acidic or basic, as appropriate showed an interesting trend. Individual maps showed that the percentage of basic spectra that were out of range, were higher in HeLa cells pretreated with Bongkrekic acid. Statistical sample size (*n*) was taken to be the number of independent maps for each experimental condition.

5.2.4 Redox potential change in apoptotic HeLa cells

Each nanosensor has its own range that it can measure within. The first sensor used in this study was NQ-NS, the half-wave potential of which is -283 mV and covers a range within normal physiological redox potentials from -344 mV to -194 mV. However, SERS spectra from NQ-NS in the cytoplasm of HeLa cells were fully reduced values of the sensor and it was difficult to depict the C=O stretch signal, thus preventing determination of the resting potential in the cytoplasm.

As previously mentioned, pH values are important for the sensors since they involve proton exchange, so to accurately measure the redox potential, a value of the redox potential has to be pH adjusted. The Nernst equation shown below demonstrates the influence of pH change on the half-wave potential of the AQ-NS sensor, where *m* is the number of protons in the reaction.

$$E = E^0 + \frac{RT}{nF} ln \frac{[AQox]}{[AQred]} + \frac{RT}{F} ln[H^+]^m$$

$$E = E^0 + 29.6\ log \frac{[AQox]}{[AQred]} + 59.2\ log[H^+]^2$$

$$E = E^0 + 29.6\ log \frac{[AQox]}{[AQred]} - 59.2\ mV\ \text{pH}$$

The MBA-NS pH probe allowed a table of reference time-resolved pH values to be calculated, allowing adjustment of the Nernst and subsequent redox potential values for the intracellular pH. The redox potential within HeLa cells, during the early stages (first two hours) of apoptosis, was measured by AQ-NS (Figure 5.13).

Staurosporine time course	HeLa		HeLa BKA	
	pH	Correction [mV]	pH	Correction [mV]
No STS	7.412	-24.3492	8.085	-64.1235
0-30 min	7.221	-13.0611	7.862	-50.9442
30-60 min	7.396	-23.4036	7.266	-15.7206
60-90 min	7.477	-28.1907	7.597	-35.2827
90-120 min	7.529	-31.2639	7.749	-44.2659

Table 5.1 shows pH values measured with MBA-NS for each time point measured with and without BKA pre-treatment. Correction values for each time point are shown in mV.

The spectra of AQ-NS show signals both at 1666 cm^{-1} (C=O stretching in oxidised conditions) and 1606cm^{-1} (constant C=C stretching in reduced and oxidised forms). It showed that the redox potential reported by AQ-NS in untreated HeLa cells is

-362.8±8.7 mV at pH 7.412±0.27.

After correcting for pH, no significant difference in redox potential was observed during the early timeframe of the apoptotic process (Figure 5.13). Whereas HeLa pre-treatment with BKA had a profound effect on the redox potential at the beginning of the process (FIGURE 5.13; HeLa BKA).

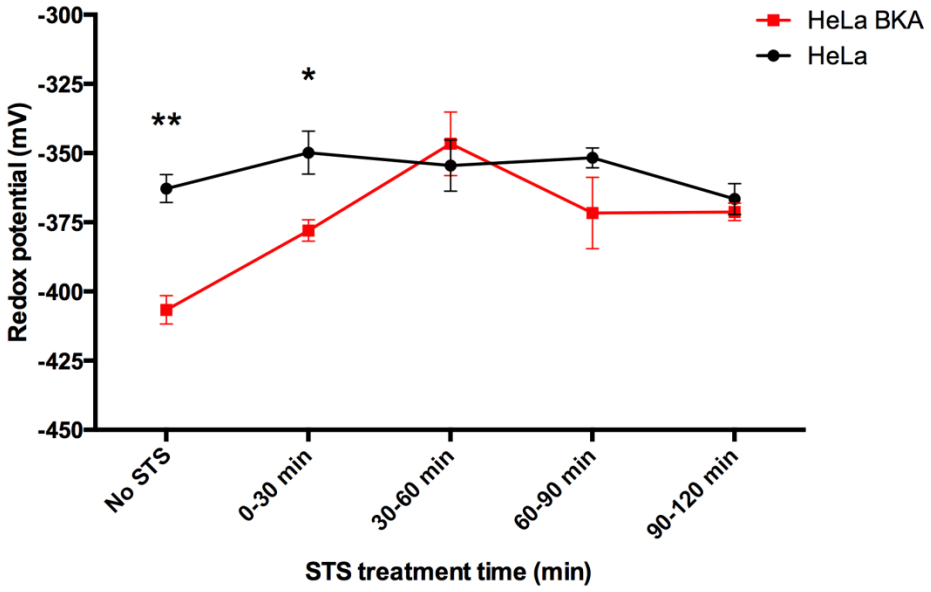

Figure 5.13 Analysis of the resting cytoplasmic redox potential in HeLa cells and change in redox potential throughout apoptosis measured by AQ-NS. * indicates significant difference of BKA treatment between samples measured by ANOVA.

Non-apoptotic BKA pre-treated samples demonstrated a mean value of -406.65±8.87 mV. This value of the redox potential is covered by the detection range of the AQ-NS, with the lower limit of -450 mV. This observation confirms continuous dependence between pH and redox potential within the intracellular space. Initiation of apoptosis through STS causes prompt and significant transition of the redox potential towards a more oxidative state and reflects the importance of mitochondria in regulating the redox state. It is also important to note that BKA treatment promotes transient inhibitory effects on mitochondria, mirroring the data trends in Figure 5.12.

Adjustment for pH provides a clearer insight into the redox potential dynamics, with consideration of the surrounding environment, and accurate quantitative assessment of redox at early stages of apoptosis.

5.3 Discussion

This chapter investigated the correlation between redox potential and apoptosis in the single cell. For this purpose, a novel method established by the Campbell lab employing redox-responsive quinone-based nanosensors was used. The method offers a potentially more reliable alternative to fluorescence-based techniques, especially for the early events of apoptosis, due to more rapid response time and greater sensitivity.

The results of this section can be summarised as follows:

- Cytotoxicity studies were performed by introducing the NQ-NS, AQ-NS, and MBA-NS and monitoring the rate of apoptotic progression using previously established techniques. No significant difference was seen between the apoptotic progression at specific time points between nanosensor-treated and untreated cells.
- Throughout the study on nanosensors it became apparent that the pH status of the compartment highly influences the redox status of the molecules and the Nernst equation parameters, and as a result the redox potential value is skewed. In this study the potential was initially calculated at a pH value of 7.2 which might not be correct for the apoptotic process as it was reported previously by other groups to change throughout the process.
- Bongkrekic acid showed that changes of pH to more alkaline is crucial for protection of the cells from apoptosis. These changes happen prior to mitochondrial depolarisation. Upon mitochondrial depolarisation the pH becomes more acidic thus contributing towards a more oxidative environment and a rise in overall redox potential.

AQ-NS with half-wave potential of -317 mV and the useful reporting range window is from -410 mV to -240 mV at pH 7.2 according to spectroelectrochemical investigation presented by Jiang *et al.* [98][138]. The AQ-NS half-wave potential is more negative than NQ-NS and is similar to NADPH which is -327 mV. Spectra from AQ-NS indicated that the resting cytoplasmic potential is approximately -362.8 mV (±8.7mV) after pH adjustment. Which is more reduced than values measured by GSH/GSSG

responsive GFP in HeLa cells, reported previously by Dooley et al [98] as their system showed basal redox potential of roGFP2 as -325mV.

In the previous chapter, the redox potential of apoptotic cells was shown to be more oxidative when compared to untreated cells therefore the change in oxidation of reporter molecules after cells were stimulated with 1µM STS was investigated. Two simultaneous measurements were taken in parallel, the pH and the redox potential, using pH and redox nanosensors since this gives more insight into the processes that are measured as opposed to the redox potential measured only by roGFP. Thus measuring both the pH and redox potential quantitatively allows advancement towards understanding of the apoptotic process.

Bongkrekic acid showed that changes of pH to more alkaline are crucial for the protection of cells from apoptosis. These changes happen prior to mitochondrial depolarisation. Upon mitochondrial depolarisation the pH becomes more acidic thus contributing towards a more oxidative environment and a rise in overall redox potential.

In some forms of cancer, the increase in reactive oxygen species triggers the production of reducing equivalents, thus cancer cells may maintain a more reducing intracellular environment in general and a more alkaline intracellular pH (pH_i) [21, 163, 164]. This may be consistent with the data from this study showing the potential measured by AQ-NS nanosensors was at the reductive range of the nanosensor giving a value of steady state potential of -386.2 mV (Figure 5.13). This value indicates that the intracellular redox potential in the cytoplasm of HeLa cells is much more reducing than the ones reported previously for GSH/GSSG ratio measured by roGFP for these cells [101].

Gutscher *et al.* reported that a five-fold increase in HeLa cell density contributes to a more reductive potential of GSH/GSSG measured by roGFP from -280 mV ($1.6x10^4$ cells/cm^2) to -320mV (when density $8x10^4$ cells/cm^2). The oxidative change in redox potential measured by the same roGFP was reported to shift from -290 mV (at ground state) to > -240mV after 3-4 hours of apoptosis. In the current study cells were kept at a constant density of approximately $1.5x10^4$ cells/cm^2.

The second aim of this chapter was to investigate whether single cell measurements are more accurate than the population level measurements made by flow cytometry. Indeed, this study shows that nanosensors are capable of indicating the redox potential and pH with subcellular resolution.

One can argue that the limitation of this method is the uptake of the sensors by cells and their subsequent localisation within the cells. However, from a single cell analysis perspective this form of sensing the redox potential gives a high resolution, point approach to analysis in different regions of the cell. Previous data from the lab showed that nanosensors can be safely delivered to the cytoplasm, did not affect the viability nor cause an imbalance in the redox status of the cell. In serum-free conditioned media these sensors were reported to be taken up without capture in the endosomes by NIH-3T3 fibroblasts [159]. Transmission Electron Micrographs of HeLa cells showed that nanosensors are not encapsulated in the vesicles. However, some of the micrographs are faint and typical cellular structures are not seen due to NS being very electron dense.

Despite the observed oxidative change in potential in some of the experiments, it is very important to have a consistency in nanosensor delivery to make sure that they are in cellular structures desired and not entrapped in vesicles. Endosomal pH is much lower than the resting cytoplasmic pH, being 5 and 7.2, respectively. Some, but not all of the nanosensors were observed to be in endosomal structures; however this did not influence the readout of the values from cells. This might be of interest as maybe upon acidification of the cytoplasm sensors were taken up by vesicles. Therefore, it is important to incubate the cells in serum-free medium as this has been shown that serum-free conditions does not promote the encapsulation of sensors in endosomal structures [99].

With recent technological advancements, single cell analysis has become a point of interest as heterogeneity is common between individual cells within the homogeneous tissue being it understanding of gene expression studies [165], or cell to cell communication [147]. Single cell analysis is viewed as an attractive means to better understand responses and communication between cells and then apply this to the population level [147]. One such example is cancer, where understanding of cell

diversity is crucial for targeted therapies against development, progression, and metastasis of the tumour mass.

In summary, this chapter shows quantitative measurements of biomarkers, redox potential and pH, in live cells using SERS nanosensors. Moreover, redox potential was characterised at a single cell level with localised specificity at different time points of apoptotic process. This chapter demonstrates that the pH remains fairly stable throughout apoptosis triggered with staurosporine.

Finally, the SERS method might represent an attractive monitoring of therapeutic intervention and could also be used in monitoring of the success of therapy progression in different tissue pathologies. This approach shows a possibility that deserves further exploration.

Chapter 6

Discussion and future work

6.1 Summary of objectives and findings

The intracellular redox potential plays important roles in determining cellular function and therefore its disruption may have adverse effects on cell function. The main objective of this thesis was to understand and measure redox potential change at the commencement and at the end of the apoptotic process and correlate these findings with biomarkers of programmed cell death to better understand the role of redox potential in programmed cell death.

The aim was achieved as this work shows the importance of the redox potential change in apoptosis both at the high throughput cell by cell level (cell population) and low throughput (single cell) levels and correlates it with apoptotic events, particularly mitochondrial outer membrane permeabilisation as this event is considered a point of no return. However, the mechanisms such as ATP hydrolysis can promote mitochondrial membrane potential maintenance even after cytochrome c is released from the intermembrane space. Encompassed in these investigations is the determination of whether the redox potential changes are the cause or a consequence of the apoptotic process. It has been hypothesised that accumulation of harmful radicals and the consequent rise of redox potential above a critical threshold triggers apoptotic pathways [5].

The first objective of this thesis was to generate a cell line that would enable redox potential to be investigated at a population level. HeLa cells were transfected with redox responsive green fluorescent protein (roGFP2) and selected on the basis of stable expression to create a monoclonal population. Apoptosis was triggered with a non-oxidant, protein kinase inhibitor, staurosporine.

The roGFP2 has been previously used in studies concerning measurements of intracellular redox status of GSH/GSSG [101, 109, 166]; however it was used for the

first time here to study redox potential in apoptotic cells. HeLa cells stably transfected with roGFP2, showed progression through apoptosis that was not significantly different from the process in non-transfected HeLa cells as measured by: nuclear fragmentation, mitochondrial depolarisation, and caspase-3 activity, highlighting the stability of the transfection. This demonstrated no significant alterations in the apoptosis machinery, and validated the in-house developed HeLa-roGFP2 cell line as a reliable model for studying the redox dynamics of HeLa cells.

The high throughput flow cytometry multiparameter experiments described in Chapter 4 depicted an overall trend in redox potential change in individual cells at the population level in the context of established apoptotic events. The data shows that cells undergoing staurosporine-induced cell death first expose phosphatidylserine, followed by mitochondrial depolarisation, caspase -3 and -7 activity and finally nuclear fragmentation.

The role of reactive oxygen species in induction and apoptotic signalling has been a main focus of research when considering oxidative stress. This current study focused mainly on quantitative changes in redox potential, rather than levels of reactive oxygen species in the cells. Redox potential measured at the population level with HeLa-roGFP2 showed that in cells undergoing apoptosis a significant change was observed after six hours post-induction. This suggested that the redox potential measured by roGFP2 changes after the depolarisation of mitochondria.

Similarly, in Chapter 5 single cell level studies using quinone-based redox reactive molecules mounted onto gold nanospheres and spectra collected by SERS, showed that the redox potential change in the early stages of apoptosis was similar to changes observed in high-throughput studies.

6.2 Correlation of environmental redox potential change and oxidative status of apoptosis

The work in this thesis showed that the redox potential change in the light of stress response is a consequence of apoptotic events. Redox potential, measured by roGFP2, was found to be significantly different only after 6 hours of apoptosis (Chapter 4, Table

4.1). Furthermore, redox tracking via roGFP2 showed that phosphatidyl serine exposure precedes changes in redox potential. While roGFP2 is responsive to Grx1 activity and glutathione status in the cell, AQ-NS responds to the overall redox potential. Moreover, the correction for pH might have been substantial for the overall redox potential reported by AQ-NS, as 1 pH unit changes the redox by 59.1 mV [8]. Redox potential at 1 hour of induced apoptosis was -300.1 mV as reported by roGFP2 at the population level and -353.5 mV reported from single cell analysis reported by AQ-NS sensors. The discrepancy of these findings might be due to the specificity of the two sensors, as they are measuring different parameters of the redox system.

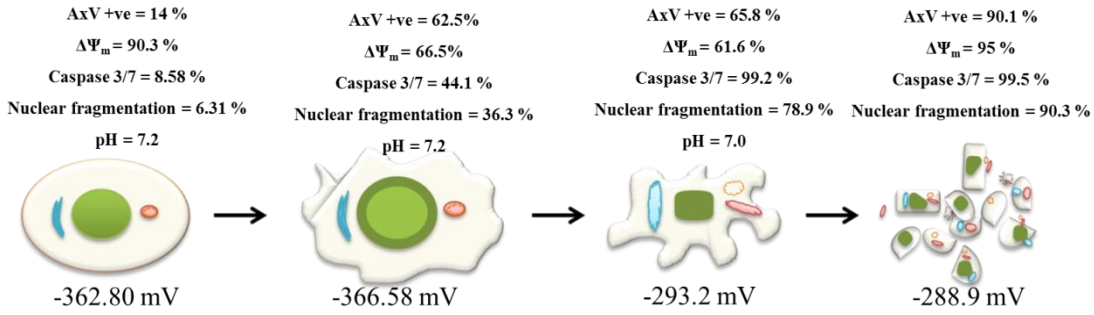

Figure 6.1 Summary view of key apoptotic events in HeLa cells and correlation with redox potential and pH. Events are ordered from left to right as they occur in the cell. Displayed are percent of cells at each stage of apoptosis with exposed phospohatidylserine (AxV +ve), polarised mitochondria ($\Delta\Psi_m$), activity of caspases 3 and 7 (caspase 3/7), fragmented nucleus (nuclear fragmentation) and pH at given redox potential. Redox potential was measured by roGFP2 and AQ-NS. pH was measured by MBA-NS.

As shown in the study by [76] Circu et al. the efflux of reduced glutathione from the adenocarcinoma epithelial cell line HT29 may play a significant role in driving apoptotic events, even though cells maintain a stable GSH/GSSG redox environment throughout apoptosis. Therefore, roGFP2, employed in the current study addressed the needs of the present experimental design. The roGFP2-Grx1 protein may be considered for future kinetic studies of redox potential once the signal quality problem in the oxidising range of potentials is resolved [140].

In Chapter 5, where surface enhanced Raman spectroscopy and nanosensors were used to provide an analysis of redox and pH at a single cell level, every analysed cell was treated as an individual experiment. The SERS method enabled the measurement of the local properties of the cytoplasm of single living cells in the physiological milieu, by tracking nanoparticles within the cell with high spatial and temporal resolution, the local redox potential properties of the intracellular environment were measured in different locations within the cell. The signal acquired from SERS can be translated to reflect the redox potential of the cytoplasm in the vicinity of the nanosensor. The map of the redox potential and pH showed a diverse distribution of redox potential in a single cell. The pH-sensitive nanosensors, MBA-NS, have identified location-specific variation of the pH at a single cell level. This suggests that the intracellular milieu inside of the cell may differ dependent on the location. On the other hand it can also be assumed that the sensors have been distributed to the endosomal structures for transportation outside of the cell. As shown in Chapter 5, the data from TEM showed that the majority of sensors were in the cytoplasm, however a fraction of the cells showed encapsulation of the sensors in the endosomal structures (Chapter 5, Figure 5.8).

6.3 Alkalisation causes reductive redox potential resulting in delay in apoptosis

Due to the role of mitochondrial function in cellular metabolism and function, these structures have been of interest for a long time. Two of the key events in apoptosis that are connected to the mitochondria are: the release of cytochrome c and mitochondrial membrane depolarisation. Even though these two events were considered to be inseparable, some evidence exists that mitochondrial depolarisation does not immediately follow cytochrome c release.

The results from the single cell experiments, presented in Chapter 5, showed that alkalisation of the cytoplasmic pH by bongkrekic acid resulted in a delay in the apoptotic processes, which is in line with the literature. Gottlieb et al. [134] showed that buffering with imidazole made the cytoplasmic pH more alkaline and protected Jurkat cells from cell death. This effect was achieved 60 minutes after induction of cell death by Fas ligand [145]. Meinsenholder et al. reported that the change in pH is linked to

Bcl-2 and the induction of caspase cascade and that both events preceded the acidification of the cytoplasm [145]. This study was conducted in CEM cells and cell death was induced by Fas antibody. Overexpression of Bcl-2 protected cells from acidification and halted phosphatidyl serine exposure. The same study showed that acidification is preceded by activation of the caspase cascade, since Z-VAD.fmk inhibited Fas-mediated acidification.

Cellular apoptosis is a sequential process, in which biochemical events underlie morphological changes and allow progression of the cells through the apoptotic process. Chiu and Oleinick showed that in photodynamic therapy-induced apoptosis cytochrome c release into the cytosol precedes mitochondrial depolarisation, and somehow occurs independently of it [160]. However, the described study used JC-1 as a reporting tool for mitochondrial polarisation. This might be misleading as JC-1 has a long equilibration time. It would be interesting to measure the loss of the mitochondrial membrane potential ($\Delta\Psi m$) with TMRM along with cytochrome c release from mitochondria. Such study showed that indeed the mitochondrial depolarisation is not an immediate consequence of cytochrome c release [167]. It would be of benefit to monitor cytochrome c redox status as this event has been reported to be one of the major hallmarks of early apoptosis preceding mitochondrial depolarisation, but it is not crucial for being a point of no return in the apoptotic process. However, the mechanism is not clearly understood [167, 168].

Cytochrome c release has been shown to be dependent on the depletion of reduced glutathione even in the occasion when the apoptosis was not an ultimate consequence of such event [56]. Similarly, Goldstein *et al.* showed that the release of cytochrome c from mitochondria precedes annexin V binding to the cell membrane [167]. This study also showed that the loss of mitochondrial membrane potential is a consequence of cytochrome c release however it is delayed and not immediate. In addition, the loss of $\Delta\Psi m$, but not the cytochrome c release, has been shown to be dependent on caspase activity [167]. Both of these studies provide a mechanistic view of the critical events in apoptosis, but they do not consider the four key events at the same time in the same cell population. The work presented in Chapters 4 and 5 tracked of four key progression markers of apoptosis (PS exposure, Caspase-3/-7 activation, loss of $\Delta\Psi_m$ and nuclear

fragmentation) along with simultaneous measurements of redox potential and pH change. Furthermore, this informative data set was further enriched with intra-cellular pH measurement at a single cell resolution.

Hence, this body of work provides a comprehensive reference list of redox potential values for the apoptosis stages and defines the sequence of events (Figure 6.1). Holistic understanding of the apoptotic process builds a solid foundation for the novel, i.e. redox-driven, development of therapies in cancer studies [169]. One of the hallmarks of cancer is the evasion of apoptosis, and thus cancer cells oscillate in a more reductive redox potential range together with more alkaline intracellular conditions, even though the extracellular environment is more acidic. Moreover, the microenvironment (including pH and pO_2) has been shown to control proliferation, invasion, viability and metabolism of tumour cells [170]. This has been shown to promote cell survival and metastasis [171]. Such an approach of using redox cancer chemotherapeutics, together with knowledge of the redox potential in the tumour environment would prove beneficial in personalised, more effective treatment of cancer. Many used chemitherapeutics use s-glycosylation already as one of the redox target to induce cell death in cancer cells. Some of the available therapeutics prevent s-glycosylation of proteins thus inhibiting the production of reduced glutathione in the cell and in consequence inhibiting growth of cells and contributing to cell death.

6.4 Loss of mitochondrial membrane polarisation and change in redox potential

Chapters 3 and 4 focused on a kinetic analysis of key markers of progression through apoptosis. roGFP2 specifically senses changes in the Grx1-dependent redox status of the GSH/GSSG redox couple [101]. It also has significantly different electrochemical properties from those of NADPH and therefore it may not give a representative indication of the general intracellular redox potential. Similarly, SERS enables quantitative measures of redox potential and pH. This gives more insight into processes that are being measured. Thus, measuring both pH and redox potential allows a greater understanding of apoptosis in quantitaive terms.

A study by Brauchle et al. studied Raman spectra and principal component analysis (PCA) to distinguish between necrosis and programmed cell death modalities. These studies could depict dynamic nuclear changes throughout apoptosis [150]. SERS was also employed in studies to distinguish early stages of apoptosis by using silver nanoparticles attached to the cell membrane [72].

It would be interesting to investigate other forms of cell death, such as recently emerging and described ferroptosis [83]. As mentioned in the Chapter 1, section 1.4.2, ferroptosis is triggered by accumulation of ferrous ions that cause oxidative stress. This in turn triggers detoxification systems such as the glutathione redox cycle. However, not much is currently known about the redox status of the environment during this form of cell death.

6.5 Single cell analysis and cell death delay by bongkrekic acid

It has been shown that single cell measurements give a more accurate temporal and spatial resolution while these parameters might be lost at the population level. Single cell studies are more accurate for tracking of rapid, localised changes in the cell [172].

Lagadic-Gossman *et al.* showed that overexpression of Bcl-2 leads to inhibition of acidification [173], this was inhibited with cyclosporine and bongkrekic acid. Alkalisation of the cytoplasm, using bongkrekic acid, delays Bax translocation and its binding to the mitochondrial membrane through change in conformation of the Bax protein [174]. Clarification of the interaction mechanism between bongkrekic acid and Bax binding to mitochondria may explain why the delay in apoptosis occurs. The study of Khaled et al. showed that staurosporine induces alkalisation of pH and Bax activation upon withdrawal of IL-7 in T lymphocytes and in consequence apoptosis [175]. This might be due to the competitive activity of anti-apoptotic protein Bcl-2, which more alkaline conditions promote activity over Bax. It is reported that Bax oligomerisation forms a pore in the mitochondrial outer membrane [176][170]. Hence, Bax binding is considered as a mechanism for creating a gradient that is going to contribute towards depolarisation of the mitochondria. In addition, it has been reported that the pH in cancer cells is more alkaline, which promotes regulation of cancer hallmarks, including higher proliferation rate and evasion of apoptosis [171]. In addition, extracellular

acidosis is one of the emerging hallmarks of cancer, and it is typical that a tumour has a reversed pH gradient ($pH_i > pH_e$) compared to healthy tissues [171, 177].

6.6 Redox potential change in apoptotic cells and correlation with metabolic disease

During preliminary experiments investigating the redox potential in HeLa cells NQ-based nanosensors were employed. Review of the results clearly showed that HeLa cells have a more reducing environment than the A549 cells and MCF-7 cell lines, which were originally used in Campbell's lab to design NQ-based nanosensors. To ensure accurate detection of the redox status in HeLa cells AQ-based nanosensors were used, also developed in Campbell's lab. The AQ-NS are able to detect changes in the redox status in more reducing environments, compared to NQ-NS. A difference in the default redox status between these cell-lines may be attributed to the fact that HeLa cells proliferate much faster than the A549 and MCF-7 cells as shown by other members of Campbell's group. However, there might be other characteristics contributing to this difference, such as type of tumour and the proteome expression (MCF-7 cells lack caspase -3). This is in line with the literature, as the data from this thesis shows that HeLa cells treated with BKA showed delayed onset of apoptosis due to alkalisation of pH_i. As shown in previously reported data, alkalisation of pH contributes to a higher rate of proliferation, result in a more reducing environment [171].

By comparing the effects of bongkrekic acid on the mitochondrial depolarisation this study has shown that alkaline conditions protect cells from undergoing apoptosis. These findings are consistent with the literature, for example, Gottlieb et al. [178] demonstrated that acidification in Jurkat cells, a common model for acute T cell leukaemia, corresponds to an early feature of the apoptotic process. The same group has also shown that the acidification precedes DNA fragmentation.

The current understanding of redox potential holds that it is one of the mediators of cellular behaviour and fate and acts by regulating cysteine switches of proteins [41]. However, it has also been suggested that even though a change in the redox potential is a consequence of apoptotic events it is irreversibly changing the cellular fate [179, 180]. This is consistent with the electrochemical theory of redox potential, where proteins

change their conformation at various redox potentials and are only activated when the environment is more oxidising [41]. For example, the endonuclease that is responsible for DNA digestion, DNase II, is reported to be activated at pH 6.8 in many cell lines and it can be switched on by more acidic pH [170].

Acceleration of apoptosis in an oxidising environment was indirectly confirmed by the present study. Mitochondrial membrane depolarisation was inhibited by bongkrekic acid and then treated with staurosporine. HeLa-roGFP2 cells showed alkalinisation of the cytoplasm after being pretreated with bongkrekic acid prior to staurosporine treatment. This alkalinisation of pH has shown a delayed effect on the progression of apoptosis in these cells when compared to non-BKA pretreated control. These findings are in line with the literature, where BKA can be used to inhibit various agents inducing mitochondria-driven apoptosis [181].

Analysis of mitochondrial depolarisation and nuclear fragmentation, as markers of apoptosis, demonstrated a delay in apoptosis upon exposure to an alkaline environment. Therefore, findings from this study are supporting the electrochemical theory described above.

6.7 Possible chemotherapeutic strategies based on redox potential measurements

Staurosporine is a non-oxidant agent and it caused all apoptotic events but did not cause a significant increase in redox potential. It would be of benefit to look at the cells treated with other apoptosis inducing agents, to show whether or not the redox potential is affected by the stimulus itself. Future work might include the induction of apoptosis with appropriate concentrations of other agents such as NEM or a right concentration and time of exposure to H_2O_2 to analyse any differences between stimuli.

Another well-known source of free radical generation used in cancer treatment is the use of radiation therapy. Furthermore, the SERS method has been used in 3D culture models, which enables the investigation of processes in different cellular and tissue contexts [182].

The redox potential has been shown to increase during apoptosis induced by H_2O_2 and this might be due to the oxidising nature of H_2O_2 and its ability to elevate ROS generation. A recent report by Thurlow *et al.* [183] described a new method of investigating protein disulfide formation. This methodology can be used to investigate the protein disulfide status of redox potential in the apoptosis process. In addition, in current study, the overall redox potential of the cell did not significantly change as the cells underwent apoptosis. This might indicate that the oxidation of proteins at different potentials is independent of the oxidation status of the proteins within the cell. The results from this current study suggest that the oxidation of redox molecules might be due to the escape of electrons from the overall system of regulation of redox potential.

It would be of interest to determine whether the rise in redox potential with apoptotic stimuli such as NEM would give the same effect as staurosporine. If so, this may suggest that the apoptotic process is dependent on the oxidation status as well as on several post-translational modifications of proteins involved in apoptosis including addition of a haem group to cytochrome c for example might be mutually important for the apoptotic activity of cytochrome c [183].

The AQ-NS half-wave potential is more negative than NQ-NS and is similar to NADPH which is -327 mV. Spectra from AQ-NS indicated that the resting cytoplasmic potential is approximately -362.8 mV (±8.7mV) after pH adjustment. This is more reduced than values measured by GSH/GSSG responsive GFP in HeLa cells, reported previously by Dooley et al [98] as the system they reported showed a basal redox potential of roGFP2 as -325mV, however this study assumed a pH value of 7.2.

Since the redox potential in apoptotic cells was shown to be more oxidative when compared to untreated cells (Chapter 4 and Chapter 5), the change in oxidation of reporter molecules after cells were stimulated with staurosporine was investigated. The results showed that the pH has a tremendous effect on the redox potential change. Thus, measuring both pH and redox potential quantitatively improves understanding of the apoptotic process.

In some forms of cancer, the increase in reactive oxygen species triggers the production of reducing equivalents, thus cancer cells may maintain a more reducing intracellular environment in general[21, 163, 164]. This is consistent with the data from this study showing the potential measured by nanosensors was established by AQ-NS was at the reductive range of the nanosensor giving a value of steady state potential of -386.2 mV. This value indicates that the intracellular redox potential in the HeLa cells' cytoplasm is much more reducing than the ones reported previously by roGFP for these cells.
Work in this thesis also attempted to determine whether single cell measurements provide a valid tool for representation of the whole cell population. This has been achieved. The understanding of diversity of cells in a population may contribute towards elucidating disease development at a single cell level, potentially providing effective treatment approaches for diseases, such as metastatic cancer and aberrant development of diseases [147].

Intracellular measurements with SERS methodologies including SERS-reporter as well as reporter-free SERS are of particular interest as new drug targets and delivery to pathogenic cells will be of crucial target to the pharmaceutical industry. This technique would allow localisation at the sub cellular level resolution.

6.8 Points of consideration for future work

In conclusion, the work in this thesis answered the fundamental question of redox status of the environment at different stages of apoptosis and correlated these findings with biomarkers of apoptosis in high throughput studies where a population of cells was measured, as well as in single cell analysis.

Certain diseases such as cancer and neurodegenerative diseases suffer from alterations in metabolism, aberrant apoptosis as well as out of control pH and possibly redox potential, thus finding a link between those parameters would be an asset for further development of diagnostic tools. It is postulated that cancer cells maintain a more reducing environment due to their higher metabolic rate. This could affect the redox potential of the cell, making it more reducing.

Similarly, cell death processes, such as apoptosis or ferroptosis, and the status of redox are of interest and thus further investigation would be advantageous.

Although one of the fundamental hallmarks of cancer is the evasion of cell death [77, 78] in particular apoptosis it has been reported that ferroptosis, an emerging form of cell death, might play a crucial role in studies on cancer and lipid metabolism. One of the characteristic of ferroptosis is shrinkage of mitochondria as well as ROS generation [83] which might be of interest in further studies on redox potential. To date, this form of cell death has been vaguely characterised, however to date little is known about the exact values of redox potential in this type of cell death. While the ROS serve as mediators of signalling cascades and activation of proteins by oxidation, the redox potential status of the cell has been significantly neglected due to a lack of appropriate tools to measure this parameter. Moreover, as seen from this study, pH measurements are crucial for the redox potential measurements.

Furthermore, shorter time points might be of benefit since observations of redox potential change in apoptotic cells might happen prior to the time scale that was used in this study. Investigation of redox potential at the 2 hour time point and addition of a reducing agent such as GSH or DTT to ‘rescue’ cells from programmed cell death and observe redox potential change would be of interest. Correlation of these changes with oxidation status of Bax, cytochrome c or caspases as well as knock out of those proteins would reveal possible correlations of redox status of those proteins at different stages of apoptosis.

As for the use of nanosensors in further research, it would be of advantage to simultaneously determine the pH and redox potential, possible number or concentration of isolated exosomes in suspension or extracellular vesicles released from apoptotic cells. This would allow for real time monitoring and analysis of the sample on a particle by particle basis, and as such would allow the redox potential and pH to be monitored in those structures.

Bibliography

1. Reuter, S., et al., *Oxidative stress, inflammation, and cancer: how are they linked?* Free Radic Biol Med, 2010. **49**(11): p. 1603-16.

2. Jungas, T., et al., *Glutathione levels and BAX activation during apoptosis due to oxidative stress in cells expressing wild-type and mutant cystic fibrosis transmembrane conductance regulator.* J Biol Chem, 2002. **277**(31): p. 27912-8.

3. Dorighello, G.G., et al., *Correlation between Mitochondrial Reactive Oxygen and Severity of Atherosclerosis.* Oxid Med Cell Longev, 2016. **2016**: p. 7843685.

4. Leichtweis, S. and L.L. Ji, *Glutathione deficiency intensifies ischaemia-reperfusion induced cardiac dysfunction and oxidative stress.* Acta Physiol Scand, 2001. **172**(1): p. 1-10.

5. Sarsour, E.H., et al., *Redox control of the cell cycle in health and disease.* Antioxid Redox Signal, 2009. **11**(12): p. 2985-3011.

6. Liou, G.Y. and P. Storz, *Reactive oxygen species in cancer.* Free Radic Res, 2010. **44**(5): p. 479-96.

7. Arner, E.S. and A. Holmgren, *Physiological functions of thioredoxin and thioredoxin reductase.* Eur J Biochem, 2000. **267**(20): p. 6102-9.

8. Schafer, F.Q. and G.R. Buettner, *Redox environment of the cell as viewed through the redox state of the glutathione disulfide/glutathione couple.* Free Radic Biol Med, 2001. **30**(11): p. 1191-212.

9. Ezerina, D., B. Morgan, and T.P. Dick, *Imaging dynamic redox processes with genetically encoded probes.* J Mol Cell Cardiol, 2014. **73**: p. 43-9.

10. Schwarzlander, M., et al., *Dissecting Redox Biology Using Fluorescent Protein Sensors.* Antioxid Redox Signal, 2016. **24**(13): p. 680-712.

11. Gough, D.R. and T.G. Cotter, *Hydrogen peroxide: a Jekyll and Hyde signalling molecule.* Cell Death Dis, 2011. **2**: p. e213.

12. Watson, W.P., T. Munter, and B.T. Golding, *A new role for glutathione: protection of vitamin B12 from depletion by xenobiotics.* Chem Res Toxicol, 2004. **17**(12): p. 1562-7.

13. Diaz-Hernandez, J.I., et al., *Knockdown of glutamate-cysteine ligase by small hairpin RNA reveals that both catalytic and modulatory subunits are essential for the survival of primary neurons.* J Biol Chem, 2005. **280**(47): p. 38992-9001.

14. Friesen, C., Y. Kiess, and K.M. Debatin, *A critical role of glutathione in determining apoptosis sensitivity and resistance in leukemia cells.* Cell Death Differ, 2004. **11 Suppl 1**: p. S73-85.

15. Armstrong, J.S., et al., *Role of glutathione depletion and reactive oxygen species generation in apoptotic signaling in a human B lymphoma cell line.* Cell Death Differ, 2002. **9**(3): p. 252-63.

16. Cazanave, S., et al., *High hepatic glutathione stores alleviate Fas-induced apoptosis in mice.* J Hepatol, 2007. **46**(5): p. 858-68.

17. Franco, R. and J.A. Cidlowski, *Glutathione efflux and cell death.* Antioxid Redox Signal, 2012. **17**(12): p. 1694-713.

18. Smith, C.V., et al., *Compartmentation of glutathione: implications for the study of toxicity and disease.* Toxicol Appl Pharmacol, 1996. **140**(1): p. 1-12.

19. Lushchak, V.I., *Glutathione homeostasis and functions: potential targets for medical interventions.* J Amino Acids, 2012. **2012**: p. 736837.

20. Sies, H., *Glutathione and its role in cellular functions.* Free Radic Biol Med, 1999. **27**(9-10): p. 916-21.

21. Calvert, P., et al., *Clinical studies of reversal of drug resistance based on glutathione.* Chem Biol Interact, 1998. **111-112**: p. 213-24.

22. Kumar, C., et al., *Glutathione revisited: a vital function in iron metabolism and ancillary role in thiol-redox control.* EMBO J, 2011. **30**(10): p. 2044-56.

23. Go, Y.M. and D.P. Jones, *Redox compartmentalization in eukaryotic cells.* Biochim Biophys Acta, 2008. **1780**(11): p. 1273-90.

24. Watson, W.H., et al., *Redox potential of human thioredoxin 1 and identification of a second dithiol/disulfide motif.* J Biol Chem, 2003. **278**(35): p. 33408-15.

25. Schultz, L.W., P.T. Chivers, and R.T. Raines, *The CXXC motif: crystal structure of an active-site variant of Escherichia coli thioredoxin.* Acta Crystallogr D Biol Crystallogr, 1999. **55**(Pt 9): p. 1533-8.

26. Kemp, M., Y.M. Go, and D.P. Jones, *Nonequilibrium thermodynamics of thiol/disulfide redox systems: a perspective on redox systems biology.* Free Radic Biol Med, 2008. **44**(6): p. 921-37.

27. Stowe, D.F. and A.K. Camara, *Mitochondrial reactive oxygen species production in excitable cells: modulators of mitochondrial and cell function.* Antioxid Redox Signal, 2009. **11**(6): p. 1373-414.

28. Banerjee, R., *Redox outside the box: linking extracellular redox remodeling with intracellular redox metabolism.* J Biol Chem, 2012. **287**(7): p. 4397-402.

29. Bulleid, N.J. and M. van Lith, *Redox regulation in the endoplasmic reticulum.* Biochem Soc Trans, 2014. **42**(4): p. 905-8.

30. Melino, G., *The Sirens' song.* Nature, 2001. **412**(6842): p. 23.

31. Curtin, J.F., M. Donovan, and T.G. Cotter, *Regulation and measurement of oxidative stress in apoptosis.* J Immunol Methods, 2002. **265**(1-2): p. 49-72.

32. Nkabyo, Y.S., et al., *Glutathione and thioredoxin redox during differentiation in human colon epithelial (Caco-2) cells.* Am J Physiol Gastrointest Liver Physiol, 2002. **283**(6): p. G1352-9.

33. Carreau, A., et al., *Why is the partial oxygen pressure of human tissues a crucial parameter? Small molecules and hypoxia.* J Cell Mol Med, 2011. **15**(6): p. 1239-53.

34. Maccarrone, M. and V. Ullrich, *Redox regulation in disease and ageing.* Cell Death Differ, 2004. **11**(8): p. 949-51.

35. Li, F., et al., *Regulation of HIF-1alpha stability through S-nitrosylation.* Mol Cell, 2007. **26**(1): p. 63-74.

36. Kerr, J.F., A.H. Wyllie, and A.R. Currie, *Apoptosis: a basic biological phenomenon with wide-ranging implications in tissue kinetics.* Br J Cancer, 1972. **26**(4): p. 239-57.

37. Elmore, S., *Apoptosis: a review of programmed cell death.* Toxicol Pathol, 2007. **35**(4): p. 495-516.

38. Gregory, C.D. and J.D. Pound, *Cell death in the neighbourhood: direct microenvironmental effects of apoptosis in normal and neoplastic tissues.* J Pathol, 2011. **223**(2): p. 177-94.

39. Bortner, C.D. and J.A. Cidlowski, *Uncoupling cell shrinkage from apoptosis reveals that Na+ influx is required for volume loss during programmed cell death.* J Biol Chem, 2003. **278**(40): p. 39176-84.

40. Truman, L.A., et al., *CX3CL1/fractalkine is released from apoptotic lymphocytes to stimulate macrophage chemotaxis.* Blood, 2008. **112**(13): p. 5026-36.

41. Mallikarjun, V., D.J. Clarke, and C.J. Campbell, *Cellular redox potential and the biomolecular electrochemical series: a systems hypothesis.* Free Radic Biol Med, 2012. **53**(2): p. 280-8.

42. Franco, R. and J.A. Cidlowski, *Apoptosis and glutathione: beyond an antioxidant.* Cell Death Differ, 2009. **16**(10): p. 1303-14.

43. Di Stefano, D.A., et al., *Immediately loaded blade implant retrieved from a after a 20-year loading period: a histologic and histomorphometric case report.* J Oral Implantol, 2006. **32**(4): p. 171-6.

44. Fernandes, R.S. and T.G. Cotter, *Apoptosis or necrosis: intracellular levels of glutathione influence mode of cell death.* Biochem Pharmacol, 1994. **48**(4): p. 675-81.

45. Leist, M. and M. Jaattela, *Four deaths and a funeral: from caspases to alternative mechanisms.* Nat Rev Mol Cell Biol, 2001. **2**(8): p. 589-98.

46. Igney, F.H. and P.H. Krammer, *Death and anti-death: tumour resistance to apoptosis.* Nat Rev Cancer, 2002. **2**(4): p. 277-88.

47. Baud, V. and M. Karin, *Signal transduction by tumor necrosis factor and its relatives.* Trends Cell Biol, 2001. **11**(9): p. 372-7.

48. Chiba, T., et al., *Fas-mediated apoptosis is modulated by intracellular glutathione in human T cells.* Eur J Immunol, 1996. **26**(5): p. 1164-9.

49. Movassagh, M. and R.S. Foo, *Simplified apoptotic cascades.* Heart Fail Rev, 2008. **13**(2): p. 111-9.

50. Liu, Z.G., et al., *Dissection of TNF receptor 1 effector functions: JNK activation is not linked to apoptosis while NF-kappaB activation prevents cell death.* Cell, 1996. **87**(3): p. 565-76.

51. Jin, Z. and W.S. El-Deiry, *Overview of cell death signaling pathways.* Cancer Biol Ther, 2005. **4**(2): p. 139-63.

52. Green, D.R. and G.I. Evan, *A matter of life and death.* Cancer Cell, 2002. **1**(1): p. 19-30.

53. Martinou, J.C. and R.J. Youle, *Mitochondria in apoptosis: Bcl-2 family members and mitochondrial dynamics.* Dev Cell, 2011. **21**(1): p. 92-101.

54. Kroemer, G. and J.C. Reed, *Mitochondrial control of cell death.* Nat Med, 2000. **6**(5): p. 513-9.

55. Kroemer, G., L. Galluzzi, and C. Brenner, *Mitochondrial membrane permeabilization in cell death.* Physiol Rev, 2007. **87**(1): p. 99-163.

56. Ghibelli, L., et al., *Glutathione depletion causes cytochrome c release even in the absence of cell commitment to apoptosis.* FASEB J, 1999. **13**(14): p. 2031-6.

57. Danial, N.N., *BCL-2 family proteins: critical checkpoints of apoptotic cell death.* Clin Cancer Res, 2007. **13**(24): p. 7254-63.

58. Almawi, W.Y., O.K. Melemedjian, and M.M. Jaoude, *On the link between Bcl-2 family proteins and glucocorticoid-induced apoptosis.* J Leukoc Biol, 2004. **76**(1): p. 7-14.

59. Vaux, D.L., S. Cory, and J.M. Adams, *Bcl-2 gene promotes haemopoietic cell survival and cooperates with c-myc to immortalize pre-B cells.* Nature, 1988. **335**(6189): p. 440-2.

60. Gross, A., J.M. McDonnell, and S.J. Korsmeyer, *BCL-2 family members and the mitochondria in apoptosis.* Genes Dev, 1999. **13**(15): p. 1899-911.

61. Veech, G.A., et al., *Disrupted mitochondrial electron transport function increases expression of anti-apoptotic bcl-2 and bcl-X(L) proteins in SH-SY5Y neuroblastoma and in Parkinson disease cybrid cells through oxidative stress.* J Neurosci Res, 2000. **61**(6): p. 693-700.

62. Degterev, A. and J. Yuan, *Expansion and evolution of cell death programmes.* Nat Rev Mol Cell Biol, 2008. **9**(5): p. 378-90.

63. Hockenbery, D.M., et al., *Bcl-2 functions in an antioxidant pathway to prevent apoptosis.* Cell, 1993. **75**(2): p. 241-51.

64. Collins, G.W., et al., *Measurements of the equation of state of deuterium at the fluid insulator-metal transition.* Science, 1998. **281**(5380): p. 1178-81.

65. Zimmermann, A.K., et al., *Glutathione binding to the Bcl-2 homology-3 domain groove: a molecular basis for Bcl-2 antioxidant function at mitochondria.* J Biol Chem, 2007. **282**(40): p. 29296-304.

66. Hengartner, M.O., *The biochemistry of apoptosis.* Nature, 2000. **407**(6805): p. 770-6.

67. Voehringer, D.W., et al., *Bcl-2 expression causes redistribution of glutathione to the nucleus.* Proc Natl Acad Sci U S A, 1998. **95**(6): p. 2956-60.

68. Suzuki, H., et al., *Characterization of rat TOM40, a central component of the preprotein translocase of the mitochondrial outer membrane.* J Biol Chem, 2000. **275**(48): p. 37930-6.

69. Skulachev, V.P., *Cytochrome c in the apoptotic and antioxidant cascades.* FEBS Lett, 1998. **423**(3): p. 275-80.

70. Brown, G.C. and V. Borutaite, *Regulation of apoptosis by the redox state of cytochrome c.* Biochim Biophys Acta, 2008. **1777**(7-8): p. 877-81.

71. San Francisco, B., E.C. Bretsnyder, and R.G. Kranz, *Human mitochondrial holocytochrome c synthase's heme binding, maturation determinants, and complex formation with cytochrome c.* Proc Natl Acad Sci U S A, 2013. **110**(9): p. E788-97.

72. Zhou, H., et al., *Early apoptosis real-time detection by label-free SERS based on externalized phosphatidylserine.* Analyst, 2016. **141**(14): p. 4293-8.

73. Cai, J. and D.P. Jones, *Superoxide in apoptosis. Mitochondrial generation triggered by cytochrome c loss.* J Biol Chem, 1998. **273**(19): p. 11401-4.

74. Sinibaldi, F., et al., *Role of lysines in cytochrome c-cardiolipin interaction.* Biochemistry, 2013. **52**(26): p. 4578-88.

75. Cohen, G.M., *Caspases: the executioners of apoptosis.* Biochem J, 1997. **326 (Pt 1)**: p. 1-16.

76. Circu, M.L., et al., *The role of GSH efflux in staurosporine-induced apoptosis in colonic epithelial cells.* Biochem Pharmacol, 2009. **77**(1): p. 76-85.

77. Hanahan, D. and R.A. Weinberg, *Hallmarks of cancer: the next generation.* Cell, 2011. **144**(5): p. 646-74.

78. Hanahan, D. and R.A. Weinberg, *The hallmarks of cancer.* Cell, 2000. **100**(1): p. 57-70.

79. Cairns, R.A., I.S. Harris, and T.W. Mak, *Regulation of cancer cell metabolism.* Nat Rev Cancer, 2011. **11**(2): p. 85-95.

80. Hirsch, T., et al., *The apoptosis-necrosis paradox. Apoptogenic proteases activated after mitochondrial permeability transition determine the mode of cell death.* Oncogene, 1997. **15**(13): p. 1573-81.

81. Zong, W.X. and C.B. Thompson, *Necrotic death as a cell fate.* Genes Dev, 2006. **20**(1): p. 1-15.

82. Ashworth, A., *A synthetic lethal therapeutic approach: poly(ADP) ribose polymerase inhibitors for the treatment of cancers deficient in DNA double-strand break repair.* J Clin Oncol, 2008. **26**(22): p. 3785-90.

83. Dixon, S.J., et al., *Ferroptosis: an iron-dependent form of nonapoptotic cell death.* Cell, 2012. **149**(5): p. 1060-72.

84. Yang, W.S., et al., *Regulation of ferroptotic cancer cell death by GPX4.* Cell, 2014. **156**(1-2): p. 317-331.

85. Doll, S., et al., *ACSL4 dictates ferroptosis sensitivity by shaping cellular lipid composition.* Nat Chem Biol, 2017. **13**(1): p. 91-98.

86. Golstein, P. and G. Kroemer, *Cell death by necrosis: towards a molecular definition.* Trends Biochem Sci, 2007. **32**(1): p. 37-43.

87. Miao, B. and A. Degterev, *Methods to analyze cellular necroptosis.* Methods Mol Biol, 2009. **559**: p. 79-93.

88. Han, W., et al., *Shikonin circumvents cancer drug resistance by induction of a necroptotic death.* Mol Cancer Ther, 2007. **6**(5): p. 1641-9.

89. Navarro-Yepes, J., et al., *Oxidative stress, redox signaling, and autophagy: cell death versus survival.* Antioxid Redox Signal, 2014. **21**(1): p. 66-85.

90. Lee, J., S. Giordano, and J. Zhang, *Autophagy, mitochondria and oxidative stress: cross-talk and redox signalling.* Biochem J, 2012. **441**(2): p. 523-40.

91. He, C. and D.J. Klionsky, *Regulation mechanisms and signaling pathways of autophagy.* Annu Rev Genet, 2009. **43**: p. 67-93.

92. Johansen, T. and T. Lamark, *Selective autophagy mediated by autophagic adapter proteins.* Autophagy, 2011. **7**(3): p. 279-96.

93. Boya, P., et al., *Endoplasmic reticulum stress-induced cell death requires mitochondrial membrane permeabilization.* Cell Death Differ, 2002. **9**(4): p. 465-7.

94. Vitale, I., et al., *Mitotic catastrophe: a mechanism for avoiding genomic instability.* Nat Rev Mol Cell Biol, 2011. **12**(6): p. 385-92.

95. Castedo, M., et al., *Apoptosis regulation in tetraploid cancer cells.* EMBO J, 2006. **25**(11): p. 2584-95.

96. Voss, J., et al., *Modulation of macrophage antitumor potential by apoptotic lymphoma cells.* Cell Death Differ, 2017. **24**(6): p. 971-983.

97. Ruprecht, J.J., et al., *Structures of yeast mitochondrial ADP/ATP carriers support a domain-based alternating-access transport mechanism.* Proc Natl Acad Sci U S A, 2014. **111**(4): p. E426-34.

98. Jiang, J., et al., *Quantitative measurement of redox potential in hypoxic cells using SERS nanosensors.* Nanoscale, 2014. **6**(20): p. 12104-10.

99. Auchinvole, C.A., et al., *Monitoring intracellular redox potential changes using SERS nanosensors.* ACS Nano, 2012. **6**(1): p. 888-96.

100. Jaworska, A., et al., *SERS-based monitoring of the intracellular pH in endothelial cells: the influence of the extracellular environment and tumour necrosis factor-alpha.* Analyst, 2015. **140**(7): p. 2321-9.

101. Dooley, C.T., et al., *Imaging dynamic redox changes in mammalian cells with green fluorescent protein indicators.* J Biol Chem, 2004. **279**(21): p. 22284-93.

102. Hanson, G.T., et al., *Investigating mitochondrial redox potential with redox-sensitive green fluorescent protein indicators.* J Biol Chem, 2004. **279**(13): p. 13044-53.

103. Rahman, I., A. Kode, and S.K. Biswas, *Assay for quantitative determination of glutathione and glutathione disulfide levels using enzymatic recycling method.* Nat Protoc, 2006. **1**(6): p. 3159-65.

104. Yano, T., et al., *A novel fluorescent sensor protein for visualization of redox states in the cytoplasm and in peroxisomes.* Mol Cell Biol, 2010. **30**(15): p. 3758-66.

105. Sporty, J.L., et al., *Single sample extraction protocol for the quantification of NAD and NADH redox states in Saccharomyces cerevisiae.* J Sep Sci, 2008. **31**(18): p. 3202-11.

106. Keese, M.A., et al., *Microinjected glutathione reductase crystals as indicators of the redox status in living cells.* FEBS Lett, 1999. **447**(2-3): p. 135-8.

107. Meyer, A.J. and T.P. Dick, *Fluorescent protein-based redox probes.* Antioxid Redox Signal, 2010. **13**(5): p. 621-50.

108. Birk, J., et al., *Endoplasmic reticulum: reduced and oxidized glutathione revisited.* J Cell Sci, 2013. **126**(Pt 7): p. 1604-17.

109. van Lith, M., et al., *Real-time monitoring of redox changes in the mammalian endoplasmic reticulum.* J Cell Sci, 2011. **124**(Pt 14): p. 2349-56.

110. Nicolier, M., et al., *Spatiotemporal activation of caspase-dependent and -independent pathways in staurosporine-induced apoptosis of p53wt and p53mt human cervical carcinoma cells.* Biol Cell, 2009. **101**(8): p. 455-67.

111. Remington, S.J., *Green fluorescent protein: a perspective.* Protein Sci, 2011. **20**(9): p. 1509-19.

112. Masters, J.R., *HeLa cells 50 years on: the good, the bad and the ugly.* Nat Rev Cancer, 2002. **2**(4): p. 315-9.

113. Saraste, A. and K. Pulkki, *Morphologic and biochemical hallmarks of apoptosis.* Cardiovasc Res, 2000. **45**(3): p. 528-37.

114. Cleland, W.W., *Dithiothreitol, a New Protective Reagent for Sh Groups.* Biochemistry, 1964. **3**: p. 480-2.

115. Jocelyn, P.C., *The standard redox potential of cysteine-cystine from the thiol-disulphide exchange reaction with glutathione and lipoic acid.* Eur J Biochem, 1967. **2**(3): p. 327-31.

116. Rost, J. and S. Rapoport, *Reduction-Potential of Glutathione.* Nature, 1964. **201**: p. 185.

117. Dalton, T.P., et al., *Genetically altered mice to evaluate glutathione homeostasis in health and disease.* Free Radic Biol Med, 2004. **37**(10): p. 1511-26.

118. Lu, S.C., *Regulation of glutathione synthesis.* Mol Aspects Med, 2009. **30**(1-2): p. 42-59.

119. Garcia-Ruiz, C. and J.C. Fernandez-Checa, *Redox regulation of hepatocyte apoptosis.* J Gastroenterol Hepatol, 2007. **22 Suppl 1**: p. S38-42.

120. Renna, M., et al., *Nitric oxide-induced endoplasmic reticulum stress activates the expression of cargo receptor proteins and alters the glycoprotein transport to the Golgi complex.* Int J Biochem Cell Biol, 2006. **38**(12): p. 2040-8.

121. Celli, A., et al., *Glutathione depletion is associated with decreased Bcl-2 expression and increased apoptosis in cholangiocytes.* Am J Physiol, 1998. **275**(4 Pt 1): p. G749-57.

122. Dunkern, T.R., G. Fritz, and B. Kaina, *Ultraviolet light-induced DNA damage triggers apoptosis in nucleotide excision repair-deficient cells via Bcl-2 decline and caspase-3/-8 activation.* Oncogene, 2001. **20**(42): p. 6026-38.

123. Morgan, B., M.C. Sobotta, and T.P. Dick, *Measuring E(GSH) and H2O2 with roGFP2-based redox probes.* Free Radic Biol Med, 2011. **51**(11): p. 1943-51.

124. Kolossov, V.L., et al., *Transient light-induced intracellular oxidation revealed by redox biosensor.* Biochem Biophys Res Commun, 2013. **439**(4): p. 517-21.

125. Yoon, J.M., et al., *Low concentrations of doxycycline attenuates FasL-induced apoptosis in HeLa cells.* Biol Res, 2015. **48**: p. 38.

126. Tawa, P., et al., *Catalytic activity of caspase-3 is required for its degradation: stabilization of the active complex by synthetic inhibitors.* Cell Death Differ, 2004. **11**(4): p. 439-47.

127. Kilic, M., et al., *Formation of noncanonical high molecular weight caspase-3 and -6 complexes and activation of caspase-12 during serum starvation induced apoptosis in AKR-2B mouse fibroblasts.* Cell Death Differ, 2002. **9**(2): p. 125-37.

128. Descamps, S., et al., *Nerve growth factor stimulates proliferation and survival of human breast cancer cells through two distinct signaling pathways.* J Biol Chem, 2001. **276**(21): p. 17864-70.

129. Kurosaka, K. and Y. Kobayashi, *[Macrophage responses during phagocytosis of apoptotic cells and their regulatory mechanism].* Seikagaku, 2003. **75**(1): p. 59-62.

130. Bratton, D.L., et al., *Appearance of phosphatidylserine on apoptotic cells requires calcium-mediated nonspecific flip-flop and is enhanced by loss of the aminophospholipid translocase.* J Biol Chem, 1997. **272**(42): p. 26159-65.

131. Chang, L.K., et al., *Mitochondrial involvement in the point of no return in neuronal apoptosis.* Biochimie, 2002. **84**(2-3): p. 223-31.

132. Di Lisa, F., et al., *Mitochondrial membrane potential in single living adult rat cardiac myocytes exposed to anoxia or metabolic inhibition.* J Physiol, 1995. **486 (Pt 1)**: p. 1-13.

133. Smiley, S.T., et al., *Intracellular heterogeneity in mitochondrial membrane potentials revealed by a J-aggregate-forming lipophilic cation JC-1.* Proc Natl Acad Sci U S A, 1991. **88**(9): p. 3671-5.

134. Perry, S.W., et al., *Mitochondrial membrane potential probes and the proton gradient: a practical usage guide.* Biotechniques, 2011. **50**(2): p. 98-115.

135. Scaduto, R.C., Jr. and L.W. Grotyohann, *Measurement of mitochondrial membrane potential using fluorescent rhodamine derivatives.* Biophys J, 1999. **76**(1 Pt 1): p. 469-77.

136. Scarlett, J.L., et al., *Changes in mitochondrial membrane potential during staurosporine-induced apoptosis in Jurkat cells.* FEBS Lett, 2000. **475**(3): p. 267-72.

137. Seervi, M., et al., *Essential requirement of cytochrome c release for caspase activation by procaspase-activating compound defined by cellular models.* Cell Death Dis, 2011. **2**: p. e207.

138. Marino, G. and G. Kroemer, *Mechanisms of apoptotic phosphatidylserine exposure.* Cell Res, 2013. **23**(11): p. 1247-8.

139. Whiteman, M., et al., *Hypochlorous acid-mediated mitochondrial dysfunction and apoptosis in human hepatoma HepG2 and human fetal liver cells: role of mitochondrial permeability transition.* Free Radic Biol Med, 2005. **38**(12): p. 1571-84.

140. Lukyanov, K.A. and V.V. Belousov, *Genetically encoded fluorescent redox sensors.* Biochim Biophys Acta, 2014. **1840**(2): p. 745-56.

141. Zhang, X.D., S.K. Gillespie, and P. Hersey, *Staurosporine induces apoptosis of melanoma by both caspase-dependent and -independent apoptotic pathways.* Mol Cancer Ther, 2004. **3**(2): p. 187-97.

142. Thuret, G., et al., *Mechanisms of staurosporine induced apoptosis in a human corneal endothelial cell line.* Br J Ophthalmol, 2003. **87**(3): p. 346-52.

143. Zamzami, N., et al., *Mitochondrial control of nuclear apoptosis.* J Exp Med, 1996. **183**(4): p. 1533-44.

144. Barry, M.A., J.E. Reynolds, and A. Eastman, *Etoposide-induced apoptosis in human HL-60 cells is associated with intracellular acidification.* Cancer Res, 1993. **53**(10 Suppl): p. 2349-57.

145. Meisenholder, G.W., et al., *Events in apoptosis. Acidification is downstream of protease activation and BCL-2 protection.* J Biol Chem, 1996. **271**(27): p. 16260-2.

146. Vigne, P., et al., *Dual control of the intracellular pH in aortic smooth muscle cells by a cAMP-sensitive HCO3-/Cl- antiporter and a protein kinase C-sensitive Na+/H+ antiporter.* J Biol Chem, 1988. **263**(34): p. 18023-9.

147. Hodzic, E., *Single-cell analysis: Advances and future perspectives.* Bosn J Basic Med Sci, 2016.

148. Lidstrom, M.E. and M.C. Konopka, *The role of physiological heterogeneity in microbial population behavior.* Nat Chem Biol, 2010. **6**(10): p. 705-12.

149. Schie, I.W. and T. Huser, *Methods and applications of Raman microspectroscopy to single-cell analysis.* Appl Spectrosc, 2013. **67**(8): p. 813-28.

150. Brauchle, E., et al., *Cell death stages in single apoptotic and necrotic cells monitored by Raman microspectroscopy.* Sci Rep, 2014. **4**: p. 4698.

151. Stiles, P.L., et al., *Surface-enhanced Raman spectroscopy.* Annu Rev Anal Chem (Palo Alto Calif), 2008. **1**: p. 601-26.

152. Wachsmann-Hogiu, S., T. Weeks, and T. Huser, *Chemical analysis in vivo and in vitro by Raman spectroscopy--from single cells to humans.* Curr Opin Biotechnol, 2009. **20**(1): p. 63-73.

153. Andreou, C., S.A. Kishore, and M.F. Kircher, *Surface-Enhanced Raman Spectroscopy: A New Modality for Cancer Imaging.* J Nucl Med, 2015. **56**(9): p. 1295-9.

154. Vo-Dinh, T., H.N. Wang, and J. Scaffidi, *Plasmonic nanoprobes for SERS biosensing and bioimaging.* J Biophotonics, 2010. **3**(1-2): p. 89-102.

155. Willets, K.A., *Surface-enhanced Raman scattering (SERS) for probing internal cellular structure and dynamics.* Anal Bioanal Chem, 2009. **394**(1): p. 85-94.

156. Alkilany, A.M., et al., *Cellular uptake and cytotoxicity of gold nanorods: molecular origin of cytotoxicity and surface effects.* Small, 2009. **5**(6): p. 701-8.

157. Jamieson, L.E., et al., *Simultaneous intracellular redox potential and pH measurements in live cells using SERS nanosensors.* Analyst, 2015. **140**(7): p. 2330-5.

158. Thomson, P.I., et al., *Series of quinone-containing nanosensors for biologically relevant redox potential determination by surface-enhanced Raman spectroscopy.* Anal Chem, 2015. **87**(9): p. 4719-25.

159. Ochsenkuhn, M.A., et al., *Redox potential dependence of peptide structure studied using surface enhanced Raman spectroscopy.* Nano Lett, 2011. **11**(7): p. 2684-8.

160. Lemarie, A., et al., *Specific disintegration of complex II succinate:ubiquinone oxidoreductase links pH changes to oxidative stress for apoptosis induction.* Cell Death Differ, 2011. **18**(2): p. 338-49.

161. Matsuyama, S., et al., *Changes in intramitochondrial and cytosolic pH: early events that modulate caspase activation during apoptosis.* Nat Cell Biol, 2000. **2**(6): p. 318-25.

162. Fisher, K.M., et al., *SERS as a tool for in vitro toxicology.* Faraday Discuss, 2016. **187**: p. 501-20.

163. Traverso, N., et al., *Role of glutathione in cancer progression and chemoresistance.* Oxid Med Cell Longev, 2013. **2013**: p. 972913.

164. Estrela, J.M., A. Ortega, and E. Obrador, *Glutathione in cancer biology and therapy.* Crit Rev Clin Lab Sci, 2006. **43**(2): p. 143-81.

165. Wang, D. and S. Bodovitz, *Single cell analysis: the new frontier in 'omics'.* Trends Biotechnol, 2010. **28**(6): p. 281-90.

166. Schwarzlander, M., et al., *Confocal imaging of glutathione redox potential in living plant cells.* J Microsc, 2008. **231**(2): p. 299-316.

167. Goldstein, J.C., et al., *The coordinate release of cytochrome c during apoptosis is rapid, complete and kinetically invariant.* Nat Cell Biol, 2000. **2**(3): p. 156-62.

168. Rego, A.C., S. Vesce, and D.G. Nicholls, *The mechanism of mitochondrial membrane potential retention following release of cytochrome c in apoptotic GT1-7 neural cells.* Cell Death Differ, 2001. **8**(10): p. 995-1003.

169. Wondrak, G.T., *Redox-directed cancer therapeutics: molecular mechanisms and opportunities.* Antioxid Redox Signal, 2009. **11**(12): p. 3013-69.

170. Matsubara, T., et al., *Additive Influence of Extracellular pH, Oxygen Tension, and Pressure on Invasiveness and Survival of Human Osteosarcoma Cells.* Front Oncol, 2013. **3**: p. 199.

171. Webb, B.A., et al., *Dysregulated pH: a perfect storm for cancer progression.* Nat Rev Cancer, 2011. **11**(9): p. 671-7.

172. Ward, M.W., et al., *Real time single cell analysis of Bid cleavage and Bid translocation during caspase-dependent and neuronal caspase-independent apoptosis.* J Biol Chem, 2006. **281**(9): p. 5837-44.

173. Lagadic-Gossmann, D., L. Huc, and V. Lecureur, *Alterations of intracellular pH homeostasis in apoptosis: origins and roles.* Cell Death Differ, 2004. **11**(9): p. 953-61.

174. Tafani, M., et al., *Regulation of intracellular pH mediates Bax activation in HeLa cells treated with staurosporine or tumor necrosis factor-alpha.* J Biol Chem, 2002. **277**(51): p. 49569-76.

175. Khaled, A.R., et al., *Withdrawal of IL-7 induces Bax translocation from cytosol to mitochondria through a rise in intracellular pH.* Proc Natl Acad Sci U S A, 1999. **96**(25): p. 14476-81.

176. Kuwana, T., et al., *Pro-apoptotic Bax molecules densely populate the edges of membrane pores.* Sci Rep, 2016. **6**: p. 27299.

177. Damaghi, M., J.W. Wojtkowiak, and R.J. Gillies, *pH sensing and regulation in cancer.* Front Physiol, 2013. **4**: p. 370.

178. Gottlieb, R.A., et al., *Apoptosis induced in Jurkat cells by several agents is preceded by intracellular acidification.* Proc Natl Acad Sci U S A, 1996. **93**(2): p. 654-8.

179. Circu, M.L., et al., *Contribution of mitochondrial GSH transport to matrix GSH status and colonic epithelial cell apoptosis.* Free Radic Biol Med, 2008. **44**(5): p. 768-78.

180. Circu, M.L. and T.Y. Aw, *Glutathione and apoptosis.* Free Radic Res, 2008. **42**(8): p. 689-706.

181. Zamzami, N., et al., *Inhibitors of permeability transition interfere with the disruption of the mitochondrial transmembrane potential during apoptosis.* FEBS Lett, 1996. **384**(1): p. 53-7.

182. Camus, V.L., et al., *Measuring the effects of fractionated radiation therapy in a 3D prostate cancer model system using SERS nanosensors.* Analyst, 2016. **141**(17): p. 5056-61.

183. Thurlow, S.E., et al., *Determination of Protein Thiol Reduction Potential by Isotope Labeling and Intact Mass Measurement.* Anal Chem, 2016. **88**(5): p. 2727-33.